HILLSLOPE REDISTRIBUTION OF SOIL ORGANIC CARBON IN THE DEPRESSIONAL LANDSCAPE IN MINNESOTA

A DISSERTATION
SUBMITTED TO THE FACULTY OF
UNIVERSITY OF MINNESOTA
BY

AN-MIN WU

IN PARTIAL FULFILLMENT OF THE REQUIREMENTS
FOR THE DEGREE OF
DOCTOR OF PHILOSOPHY

DR. EDWARD A. NATER, CO-ADVISER
DR. JAMES C. BELL, CO-ADVISER

JULY 2014

© An-Min Wu 2014

Acknowledgements

I would like to express my deepest appreciation to my PhD co-advisors Dr. Jay Bell and Dr. Ed Nater, who have inspired me to look at the big picture and to grow as an independent scientist. I am very grateful for Dr. Bell's insightful guidance in developing research in my areas of interest as well as Dr. Nater's extensive mentoring during the entire process. I would also like to thank my committee members Dr. Carrie Jennings, Dr. Joe Knight, and Dr. John Lamb for their encouragement and support on my dissertation research.

My special thanks go to Three Rivers Park District, Minnesota Board of Water and Soil Resources, and several farmers who allowed me to conduct field research on their land. Without their kind support, my research would not have been possible. I would also like to thank Dr. Robert DelMas, whose invaluable statistical advice has been tremendously helpful. In addition, Dr. DelMas introduced me to the world of Shotokan karate, a sport that has trained me to stay strong and dedicated throughout my PhD study.

Words cannot express how grateful I am for all the support from friends and family. My heartfelt appreciation goes to my parents in my hometown Taichung, Taiwan. Their liberal upbringing and unreserved love has made me who I am today. Last but not least, I would like to thank my lifelong partner and husband Deepansh Kathuria for his unconditional support while I pursued my PhD thousands of miles away. You sustained me through the hardships, and continue to inspire me to be a better person day by day.

Abstract

Agricultural tillage has been estimated to cause a loss of 30-50% of the pre-settlement soil organic carbon (SOC) through enhanced decomposition and loss to the atmosphere or through erosion and subsequently loss to surface waters or burial in lower landscape positions. However, measures of whole landscape redistribution and fate of sediments and SOC are lacking. This research seeks to estimate change in SOC storage since agricultural settlement using soil-terrain modeling techniques in closed-depressional landscapes. The overall quantity of SOC in depressional landscapes may have not been lost to the atmosphere through enhanced decomposition but rather is redistributed downslope.

I conducted field observations and soil sampling in hillslope transects in Lake Rebecca Park Reserve in East-Central Minnesota. The thickness of re-deposited sediments (termed post-settlement alluvium, or PSA) was identified by morphological indicators in the field. The spatial distribution of PSA presence and its thickness were modeled with local and regional terrain attributes using a two-stage regression approach. The current SOC inventory (1.119 Pg) in top 1-m soil at the Lake Rebecca site was estimated by spatial predictive models of SOC contents at four soil depths (0-10 cm, 10-30 cm, 30-60 cm, 60-100 cm). I estimated pre-settlement SOC inventory for erosional uplands with spatial predictive models for an uncultivated grassland in Morristown, Minnesota; for depositional lowlands, I calculated pre-settlement SOC inventory by applying models for soil profiles below the PSA depth at the study site. Erosional losses and depositional gains were determined by subtracting current SOC inventory from pre-settlement values.

The results showed high SOC contents in surface soils at lower landscape positions, especially in wetlands near the surrounding marsh. Total SOC in the uppermost meter of this 6-ha study site was estimated as 1.528 Gg. The change in SOC density since European settlement was highly overestimated (36.7% increase). The prediction error is likely due to the lack of a mechanism to constrain the prediction of PSA under natural sedimentation patterns at the very bottom of the hillslope beyond the zone where PSA was observed. The model improvement is required to more accurately predict whole landscape SOC distribution and change over time.

Table of Contents

List of Tables

List of Figures

Chapter 1
Introduction

Human activities have greatly altered the global carbon (C) cycle. Land use change, fossil fuel combustion and other anthropogenic disturbances continue to release C and result in an unprecedented high level of carbon dioxide (CO_2) in the atmosphere (Vitousek, 1994; Foley et al., 2005; Houghton et al., 1999). Soil, as the largest terrestrial C reservoir, was estimated to have lost 30-50% of soil organic carbon (SOC) and contributed to the atmospheric CO_2 since agriculture started (Amundson, 2001; Houghton et al., 1999; Mann, 1986).

Agriculture affects SOC through biomass alteration, fertilization, and tillage (McLauchlan, 2006). Agriculture replaces natural vegetation high in biomass C (e.g. forest) with crops and removes biomass by harvest annually. Fertilization addition promotes plant growth and increases biomass C inputs to soils, but at the same time it increases C decomposition rate, which offsets SOC accumulation effect from increased C inputs (Russell et al., 2009). Tillage disturbs soil and triggers soil erosion, causing a major C loss during cultivation (Lal, 2003; Six et al., 2002). Among these agricultural disturbances to SOC loss, the effect of tillage-induced erosion on SOC has been controversial. Whether agricultural erosion has resulted in a soil C sink or source is unclear (Berhe et al., 2007; van Oost et al., 2005; van Oost et al., 2007; Lal, 2003; Houghton et al., 1999; Jacinthe et al., 2001). To understand this topic, I reviewed the literature in the following sections.

Soil organic matter and its carbon protection mechanisms

Soil organic matter (SOM) stores SOC and is a key to soil functioning in the environment. SOM positively affects soil physical, chemical, and biological properties (Brady and Weil, 2004, Six and Jastrow, 2002), and conversely relies on soil properties to protect itself from decomposition (Six et al., 2002). Based on stabilization mechanisms, Six et al. (2002) identified four SOM measurable pools: 1) unprotected pool; 2) microaggregated-protected pool; 3) silt- and clay- protected pool; and 4) biochemically-protected pool. Unlike biochemically-quantified pools (Paul et al., 1999), the four SOM pools are directly related to their potential rates of decomposition and can be easily related to agricultural disturbance issues.

Among the aforementioned SOM pools, unprotected SOM is the most easily decomposed pool (the 'active' pool), followed by microaggregated-protected and parts of silt- and clay-protected pools (the 'intermediate' pools) and biochemically-protected pool (the 'passive' pool) (Tivet et al., 2013). The unprotected pool is composed of plant residues, microbial biomass C, roots, and fungal hyphae. They are free from occlusion and are easily attacked by soil microbes. Therefore, the unprotected SOM is labile and sensitive for agricultural disturbances (Six et al., 2002; Stewart et al., 2007; von Lutzow et al., 2006; von Lutzow et al., 2007).

Microaggregate-protected SOM and silt- and clay-associated SOM have intermediate turnover time (half-life around 10 - 100 years) due to SOM occlusion and organo-mineral interactions (Tivet et al., 2013). Macroaggregates (> 250 μm) and microaggregates (53 - 250μm) protect SOM from decomposition by physically restricting the accessibility of

decomposing microorganisms and their enzymes to SOM and by limiting aerobic decomposition due to reduced oxygen diffusion (von Lutzow et al., 2006). The stabilization of SOM also strongly relies on its binding to mineral surfaces, including fine silt and clay surfaces and metal ions (von Lutzow et al., 2006). The dependence of SOM stabilization in soil aggregates and particle size distribution indicates the strong influences of soil texture and soil structure to SOC dynamics. SOM in the passive pool has very slow turnover rate (half-life over 100 years) because of its biochemical protection within clay microstructures (<20 μm) (Tivet et al., 2013; Six et al., 2002; von Lutzow et al., 2007). The passive SOM can be measured by non-hydrolyzable clay and silt fractions (Six et al., 2002).

Factors affecting soil organic carbon dynamics

Soil is a dynamic entity. Soil properties vary spatially as a function of soil forming factors 'clorpt' – climate (cl), biota (o), topography (r), parent materials (p), and time (t) (Jenny, 1941). The 'clorpt' model provides a framework for SOC dynamics -- decomposition, biomass C inputs, and turnover -- in various spatial scales (Trumbore, 2009). SOC dynamics are affected by climate, vegetation, topography, land use land cover (LULC) and land use-associated management practices (Six and Jastrow, 2002; Jenkinson and Coleman, 2008; Yadav and Malanson, 2008; Yadav and Malanson, 2009).

Climate prominently controls SOC decomposition and accumulation (Jenny et al., 1949; Brady and Weil, 2004; Fissore et al., 2008). Areas with high precipitation levels tend to

store large SOM and thus contain high SOC storage (Post et al., 1982). When moisture is not limiting, lower temperatures constrain both the rates of primary productivity and decomposition, but favors productivity over decomposition. As a result, SOC contents increase with lower mean annual temperatures (Fissore et al., 2008; Trumbore, 2009; Post et al., 1982). Soils in areas with higher temperatures not only contain lower SOC contents but also lower SOC quality, the capacity to stabilize SOC (Fissore et al., 2008). Overall, climate effects to SOC in North American's Great Plains consist of a 'North-South trend' of decreases in SOC, due to increases in mean temperature, and a 'West-East trend' of increase in SOC, due to increases in effective moisture contents (Brady and Weil, 2004).

Vegetation affects SOC because plant residues are the main C inputs in the soil (Brady and Weil, 2004). However, changes in vegetation types result in changes in SOC storage, but not SOC quality (decomposition rates) (Fissore et al., 2008). Change in cover types from grass to forest in upland positions of Aspen Parkland in Saskatchewan decreases SOC storage due to increased leaching (Fuller and Anderson, 1993). Fissore et al. (2008) investigated the relationship between SOC and change in forest stand types (from hardwood to pine); the authors agreed with the alteration of SOC storage but identified no distinct change in decomposition rates.

It can be difficult to separate the effect of vegetation from climate to SOC dynamics because climate covaries with plant biomes (Trumbore, 2009; Jenny, 1949; Schaetzl and Anderson, 2005). Jobbagy and Jackson (2000) recognized that climate is more significant to the total amount of SOC, especially in the top 20 cm of soil. Vegetation, on the other

hand, controls the vertical distribution of SOC. For example, SOC is distributed the deepest in shrubland (77% on the second and third meter of soil compared to the uppermost 1m), then in forest (56%), and the shallowest in grassland (43%) (Jobbagy and Jackson, 2000).

Topographic influences to SOC dynamics are determined by runoff and sediment transport rates on topographic positions in a catena (Schwanghart and Jarmer, 2011). In other words, soil erosion and redistribution affect the lateral movement and storage of SOC in a landscape. In Saskatchewan, Pennock and Frick (2001) showed that over the 80 years of cultivation top soils (0 – 20 cm) had lost 50% of the original SOC at shoulder positions and 30% of that at footslope positions. SOC at shoulder positions has not reached a new equilibrium due to continuous erosion. On the other hand, SOC in depressions remained constant (60 Mg C ha^{-1}) in the top 20 cm after 80 years of cultivation, but the overall profile SOC storage in depressions was an increase as a result of the depth addition of C-rich soil due to redistribution (Pennock and Frick, 2001). Specific terrain attributes that affect SOC at a local scale will be discussed separately in the 'Soil-Terrain Modeling' section in this chapter.

Land use is the most dominant anthropogenic effect on SOC. Research on this topic has been focused on the impact of historical land use change to agriculture on SOC (Yadav and Malanson, 2009; Pennock and Frick, 2001; Schulp and Verburg, 2009). At uncultivated sites, SOC loss is mainly attributed by mineralization and turnover; however, at cultivated sites, lateral movement induced by erosion is the main process that affects SOC change (Martinez et al., 2010**).** Figure 1.1 illustrates SOC change under the

influence of agricultural land use. The initial SOC loss was high when agriculture started (1840s – 1850s in the Upper Midwest); the decreasing trend of SOC slowly stabilized until 1950s (or 1980 depending on regions) (Brady and Weil, 2004; Yadav and Malanson, 2008). Some studies pointed out that change in SOC shifted to positive (increase) since conservational management practices started in 1950s, while some identified the continuous decreasing trend of SOC in the landscapes (Mann 1986; Brady and Weil, 2004; Balesdent et al., 1988).

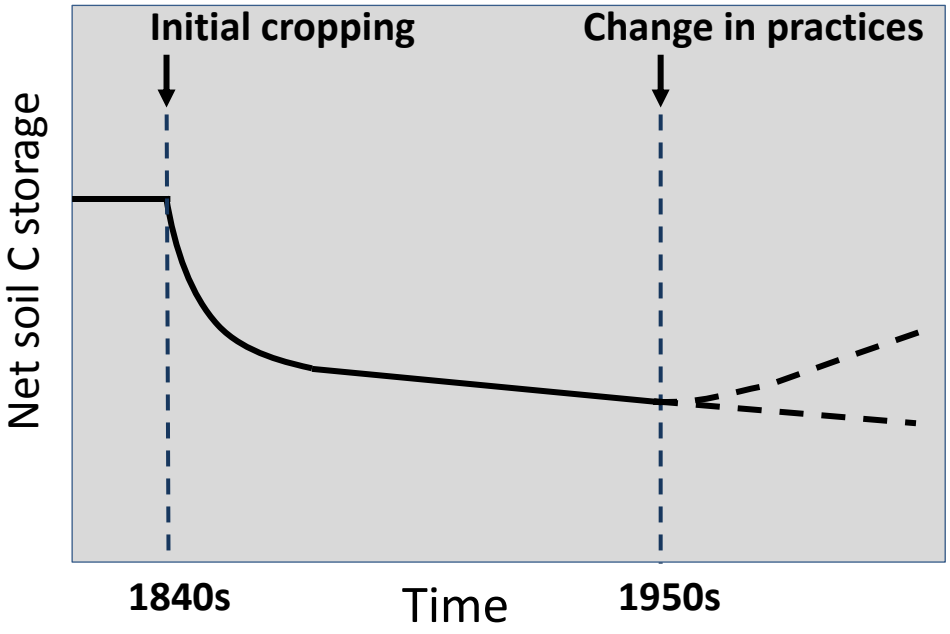

Figure 1.1 Change in soil carbon storage due to agricultural land use (adapted from Brady and Weil, 2004; Balesdent et al., 1988; Mann, 1986).

In fact, the amount of inherent SOC loss was estimated at 50% in the top soils (0 to 15 or 20 cm) since agriculture started, and it occurred mostly during the first two decades (Mann, 1986; Pennock and Frick, 2001). However, this large proportion of SOC loss (1Mg·ha^{-1}) over the 80 years of cultivation was found in upland surface soils (Pennock and Frick, 2001). Agricultural disturbances could have removed SOC from such location and translocated it vertically by mixing or horizontally by erosion. In depressions and/or wetlands, SOC has increased due to erosion-induced redistribution (Euliss et al., 2006; Pennock and Frick, 2001) of upslope sediments. Moreover, SOC loss was found to be more conservative (4 - 15% or 0.1-1.4 kg m^{-2}) when measurements were made on deeper soil profiles (0 – 30 cm) (Mann, 1986).

Nonetheless, it is difficult to explain SOC dynamics using historical land use change (Schulp and Verburg, 2009). High local variability of SOC is one of the reasons; in addition, it is possible that spatial SOC flux is controlled by processes resulting from LULC, not the spatial representation of LULC itself (Yadav and Malanson, 2008).

Management practices affect horizontal and vertical distributions of SOC in agricultural landscapes. Tillage breaks down soil structure, mixes and aerates soils at the plough layer (0 to ~25cm). Loose and broken soil particles are released from physical protection, become susceptible to decomposition and can be mobilized for lateral movement (i.e. erosion) (Grandy and Neff, 2008). Soil loss and SOC loss from surface soils (0-15cm deep) were found to be significantly less under ridge till (32 Mg·ha^{-1} and 0.7 Mg·C ha^{-1}, respectively) than in moldboard/disk plowed fields (243-292 Mg·ha^{-1} and 3.8-4.3 Mg·C ha^{-1}) (Moorman et al., 2004). Similarly, no till and shallow till resulted in less SOC losses

than moldboard plow in the top 15 cm of soil (Viaud et al., 2011). However, for the whole profile (0 – 40 cm), there was no significant differences on SOC storage between fields with these tillage practices (Viaud et al., 2011).

The effects of management practices on SOC vary among SOC physiochemically-defined pools described earlier in this chapter (Six et al., 2002). When land is cultivated, unprotected SOC can potentially decompose within a short time (Tivet et al., 2013). Mineral- (i.e. silt and clay) associated SOC is sensitive to disturbance (e.g. tillage) and would be lost upon cultivation. Microaggregates can, to a certain level, physically protect SOC from loss due to cultivation, which breaks down soil structure (Six et al., 2002; von Lützow et al., 2007). Biochemically-protected SOM is recalcitrant from decomposition and is therefore least affected by management practices in agricultural landscapes (Tivet et al., 2013; Six et al., 2002).

Agricultural soil erosion and its environmental factors

Erosion comprises three stages -- detachment, transportation, and deposition. Wind erosion and water erosion are the two types of soil erosion naturally occurred in sloping land (so-called geologic erosion). Compared to geological erosion, anthropogenic erosion triggered by tillage actions removes soil faster than soil formation, and its rates are often orders of magnitude higher than those in geologic erosion (Govers et al., 1994, Toy et al., 2002). The term ‘tillage erosion’ has been used to separate agriculture-accelerated erosion from ‘water erosion’ (Lobb et al., 1995; van Oost et al., 2000; van Oost et al., 2007). Because the accelerated erosion can be moved not only by tillage machinery and

gravity, but also by water after tillage loosens soil particles, I use a general term 'agricultural erosion' for overall agriculture-accelerated erosion in this study.

Environmental factors affecting agricultural erosion include topography, climate, vegetation, and land use (Toy et al., 2002; Follain et al., 2006). Among these factors, agricultural erosion is largely controlled by topography. Soil erosion is a function of slope steepness and slope length (distance from the surface runoff origin) (Toy et al., 2002; Govers et al., 1994). Besides these variables, curvature also appears to be significant topographic variable for accelerated agricultural erosion (Govers et al., 1994).

The knowns and unknowns of erosion effect to soil carbon

Agricultural erosion affects SOC in two aspects: 1) Erosion physically redistributes SOC; 2) Erosion biologically alters C mineralization processes in the landscape due to redistribution of soil and SOC (Gregorich et al., 1998; Lal, 2003). C mineralization is the most dominant process of SOC loss in the first year of cultivation, whereas erosion and deposition becomes dominant after the first year for many years (Gregorich et al., 1998).

Over 70-80% of erosion-induced soil redistribution may have redeposited in lower hillslope positions within the same catchment or landscape (Smith et al., 2001; Stallard, 1998; van Oost et al., 2007). The fate of SOC (C sink or source to the atmosphere) under the influence of erosion and deposition remains debatable (van Oost et al., 2005; Lal, 2003; Houghton et al., 1999; Jacinthe et al., 2001; Baker et al., 2007). The estimated net C flux due to erosion-induced redistribution ranged from C sink (van Oost et al., 2005;

van Oost et al., 2007; Berhe et al., 2007) to C source (Lal, 2003; van Hemelryck et al., 2010; Dlugoβ et al., 2012). The uncertainty lies in whether C mineralization is increased during sediment transport and at depositional sites; in addition, SOC has high spatial variability (Yadav and Malanson, 2008) and erosion-induced SOC change varies in catchments/landscape types (Berhe et al. 2007). Approaches to resolve this uncertainty issue may include the investigation of the magnitude and spatial locations of redistributed soil at the local catchment or landscape scale, as well as the prediction of SOC change in the redistributed soils (Dlugoβ et al., 2012; Yadav and Malanson, 2009).

Recent research has combined erosion and SOC models to simulate processes relating to SOC dynamics in erosion-induced redistribution (Yadav and Malanson, 2009; van Oost et al., 2007; Dlugoβ et al., 2012). The main processes relating to the fate of SOC due to erosion-induced redistribution include: 1) dynamic replacement of eroded SOC by increased biomass C inputs at erosional sites; 2) enhanced C mineralization due to detachment and transport of eroded soil particles after the breakdown of soil aggregates; and 3) SOC burial in depositional sites (van Oost et al., 2007; Harden et al., 1999; Lal, 2003; Dlugoss et al., 2012). Based on process modeling, Yadav and Malanson (2009) found that 11 – 31% of redistributed SOC remained in the same alluvial landscape (~28 ha), and net C fluxes vary with management practices. The importance of management practices to SOC flux was confirmed by Dlugoβ et al. (2012); the authors found that SOC loss in a small alluvial landscape (4.2 ha) near Cologne, Germany ranged from 0.9 g C m^{-2} a^{-1} to 7.7 g C m^{-2} a^{-1}, and much of the loss was due to SOC eroded out of the landscape. Erosion-induced C sink, on the other hand, occurs in landscapes where depositional sites

have reduced decomposition rates, and the combined SOC from dynamic replacement at erosional sites and reduced C loss in depositional sites compensates for the erosional losses of SOC (Berhe et al., 2007). The examples of these C-sink landscapes include a Tennessee Valley watershed in California, the Nelson Farm in Mississippi, and the Saeby farm in Northern Jutland in Denmark (Berhe et al., 2007; van Oost et al., 2005).

Soil-Terrain modeling

To understand local soil variability, the prediction of soil property employs the catena and toposequence concepts (which terms are often used interchangeably in modern soil studies) to connect soil properties with associated soil forming processes on a chain of hillslope (Milne, 1935; Bushnell, 1943; Jenny, 1946; Moore et al., 1993; Brown, 2006). Based on the catena and toposequence concepts, soil-terrain models predict individual soil properties by extending the relationships of point soil observations and digital terrain attributes onto a spatial surface using statistical methods (McKenzie et al., 2000). The soil-terrain relationships respond to catenary soil development, particularly for those properties relating to water movement through and over landscapes (as subsurface and overland flow) (Moore et al., 1993). Past studies have applied multiple statistical methods in soil-terrain modeling, including multiple linear regression, discriminant analysis, k-means clustering, generalized linear and addictive models, artificial neural network, and tree-based models (Bishop and Minasny, 2006; Grunwald, 2009). Each method has its own advantages and disadvantages. Methods involved in regression analysis, including multiple linear regression and regression trees, are easy to use, low cost, and

computational efficient. General linear and addictive models and tree models can handle quantitative and qualitative data. Neural network typically has better predictive power but is expensive, computational complex, and not easy to interpret (Bishop and Minasny, 2006).

Terrain attributes traditionally are grouped into primary and secondary attributes (Moore et al., 1993; Wilson and Gallant, 2000). Primary terrain attributes are slope, aspect, plan and profile curvature, flow path length, and catchment area and can be derived from a digital elevation model (DEM) (Wilson and Gallant, 2000; Gessler et al., 1995). Secondary terrain attributes are indices computed from two or more primary terrain attributes. Popular secondary terrain attributes for soil-terrain modeling include compound topographic index (CTI, or TWI as terrain wetness index) and Stream Power Index (SPI):

$$\text{CTI} = \ln(A_s / \tan\beta) \tag{1.1}$$

$$\text{SPI} = \ln(A_s \cdot \tan\beta) \tag{1.2}$$

where A_s is specific catchment area and β is slope gradient in degrees (Wilson and Gallant, 2000; Moore et al., 1993). Originated from hydrological modeling, CTI indicates soil wetness condition, and SPI is directly proportional to stream power which measures erosive power of overland flow (Moore et al., 1993).

For soil properties relating to pedogenic processes developed with material accumulation and dispersion on landscape surface, terrain attributes in upslope contributing area of any

given point location may be more significant than the location itself (Gallant and Wilson, 2000). Compared to the commonly used terrain attributes developed from local neighborhood of the location (typically in 3-by-3-cell moving window), upslope area terrain attributes can be viewed as 'regional' terrain attributes. Soil-terrain models have applied mean slope or curvature in individual cells of upslope area, but this type of 'regional' terrain attribute is still far less used than the 'local' terrain attributes (Wilson and Gallant, 2000). High computational cost (time and effort) has constrained development of regional terrain attributes.

Quantitative soil spatial modeling is not limited to using terrain attributes as predictor variables. Upgraded from Jenny's (1941) state factor model 'clorpt', McBratney et al. (2003) developed the 'scorpan' model – soil (s), climate (c), organism (o), topography (r), parent materials (p), age (a), and space (n) -- that adds relevant soil properties (s) and spatial positions for soil spatial prediction. Nevertheless, about 80% of previous studies used topographic attributes in their final model selection (McBratney et al., 2003; Bishop and Minasny, 2006).

Terrain attributes used for soil-terrain modeling depend on soil properties of interest. Table 1.1 lists the selected soil-terrain modeling studies for SOC (Bishop and Minasny, 2006; Minasny et al., 2013). Overall, elevation, slope and CTI are most used predictors for SOC prediction. Regardless of spatial resolution and areal extents, regression and regression-based approaches (e.g. regression kriging and regression trees) are the most popular and effective methods in the spatial prediction of SOC.

Table 1.1 Examples of soil carbon prediction using soil-terrain models and terrain attributes *(adapted from Table 7.3 in Bishop and Minasny, 2006 and Table 1.1 in Minasny et al., 2013).*

Reference	Terrain attribute predictors	Other predictors	Methods	Resolution (m)	Geographic Area	Area Extent (km^2)
Arrouays et al., 1995	Distance from upstream	Climate data	Linear regression	1000		5,000
Bui et al., 2009	Elevation	Climate data, lithology, moisture index, soil class	Piecewise linear decision tree	250	Australia	2,765,000
Gessler et al., 2000	Flow direction, CA, slope, profile & plan curvature, CTI		Linear regression	2, 4, 6, 8, 10	Santa Barbara, CA, USA	20.6
Grimm et al., 2008	CA, CTI, LS, slope, hillslope positions, profile/plan/mean curvatures	Parent materials, soil units, forest history	Random forest	5	Colorado Island, Panama Canal	15
Marchetti et al., 2010	Elevation, slope, plan curvature, profile curvature	Landsat TM imagery (NDVI, grain size index, clay index)	Regression kriging with principle components (PCA)	40	Teramo, Italy	100
Mendonça-Santos et al., 2010	Elevation, slope, aspect, plan and profile curvature, QWETI, slope	Landsat, land cover, lithology	Regression kriging	90	Rio de Janeiro, Brazil	44,000
McKenzie & Ryan,	Elevation, slope, aspect,	Geology map,	Regression tree,	25		500

1999	SCA, CTI, SPI, dispersal area, erosion index, flow direction	climate data, gamma radiometrics	GLM			
Miklos et al., 2010	Elevation, plan curvature	ECa, gamma radiometrics	Decision tree	5	IA Watson, Narrabri	4.6
Minasny et al., 2006	Elevation, slope, aspect, CTI	Landsat (land use), gamma radiation (^{40}K); Munsell color, soil texture (for depth profile)	Artificial Neutral Network	25, 90	Lower Namoi Valley, NSW	1,500
Mishra et al., 2010	Elevation, slope	Climate, land use, parent material (bedrock), MODIS NDVI	Geographically weighted regression	30	Midwest USA	658,168
Moore et al., 1993	Slope, CTI		Linear regression	15		0.05
Mueller and Pierce, 2003	Elevation, slope, aspect, plan/profile/tangential curvatures	X, Y	Kriging (ordinary, with trend model, with external drift, cokriging), multivariate regression	30.5, 100	Shiawassee River watershed, Michigan	0.12
Munoz and Kravchenko, 2011	Relative elevation, slope, total/profile/plan curvature, flow length, CTI, solar radiation	NIR, aerial photograph	Linear regression	1	Southeastern Michigan	0.12
Razakamanarivo et al., 2011	Elevation, slope		Boosted regression tree	30	Central Madagascar	15.9

Kempen et al., 2011	Relative elevation	Land cover, soil type, drainage, paleogeography, geomorphology	Linear regression	25	Drenth, the Netherlands	125
Simbahan et al., 2006	Relative elevation	Eca, surface reflectance (IKONOS), and soil series	Regression kriging	4	Nebraska	0.48; 0.52; 0.65
Thompson and Kolka, 2005	check	Landsat	Linear regression	30	Eastern Kentucky	15
Vasques et al., 2010	Elevation	Landsat images	Regression kriging	30	Santa Fe river watershed, Florida, USA	3,585
Zhao and Shi, 2010	Elevation, slope, CTI	AVHRR, NDVI	Regression kriging, artificial neutral network	100	Hebei, China	187,693

Description of the study

The above literature review confirmed the important linkage between erosion and SOC in agricultural landscapes and the uncertainty of SOC dynamics and storage under the influence of soil redistribution at a landscape scale. Based on this review, I challenge the widely accepted view that agricultural cultivation has led to large quantity of SOC losses (Figure 1.1). My rejection of this hypothesis is based on two assumptions. First, whole-landscape SOC accounting is essential in understanding true SOC dynamics. Previous SOC storage studies focused mostly on uplands and overlooked SOC at the bottom of hillslopes. In closed-depressional landscapes that have limited water outlets (e.g. rivers), the quantity of SOC lost in uplands may have simply re-deposited to lower hillslope positions. Soil redistribution might also have triggered dynamic C replacement in erosional uplands due to exposure of "fresh" mineral surfaces as well as buried SOC in depositional lowlands (Figure 1.2), resulting in net whole landscape SOC sequestration. Second, many SOC studies only measured surface soils (top 5 – 25 cm) and ignored possible SOC mixing and burial to deeper profiles due to plowing and agricultural erosion. When measuring whole-profile SOC, change in net SOC storage due to agriculture may be potentially more conservative than previously estimated.

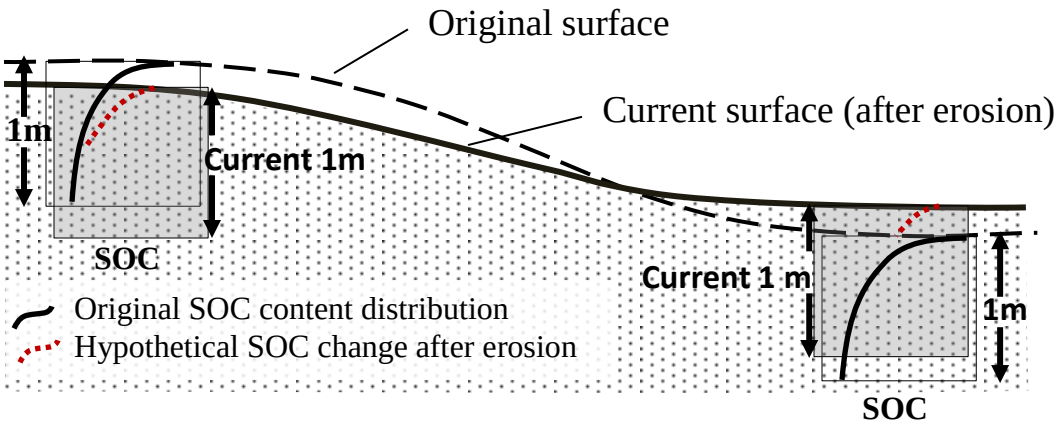

Figure 1.2 Conceptual changes in soil landscapes and soil organic carbon (SOC) contents in top 1 meter before and after agricultural erosion in closed-depressional landscapes.

My goal is to understand whether soil has a positive C feedback to agriculture-induced soil redistribution in depressional landscapes in Minnesota. To achieve this goal, I investigate the spatial relationship of SOC and erosion-induced redeposition since European settlement, termed post-settlement alluvium (PSA). Three **overall objectives** for this study are to:

1. Identify the spatial distribution and depth and volume of PSA in a closed depressional landscape at the Lake Rebecca Park Reserve, Minnesota;

2. Determine the spatial distribution of SOC storage change at the Lake Rebecca site; and

3. Assess the change of SOC storage due to erosion-induced redistribution since settlement.

Chapter 2 focuses on spatial analysis for the PSA distribution at the Lake Rebecca site using local and regional terrain attributes. I modeled spatial PSA availability and thickness based on field study data and digital terrain attributes from 1-m LiDAR-derived elevation data. In Chapter 3, I developed spatial models to predict SOC contents in four depth layers, and obtain SOC density in the top 1m of soils. Chapter 4 synthesizes PSA and SOC spatial information with pre-settlement baseline SOC to determine SOC change since European settlement in the depressional landscape of Minnesota.

I hypothesize that SOC loss since European settlement is much less than 30-50% losses observed in many other studies. With dynamic replacement and SOC burial after agricultural erosion, I expect only a small net SOC loss in a whole depressional landscape under the influence of PSA deposition compared to the pre-settlement condition.

Chapter 2

Spatial predictive models for post-settlement alluvium using local and regional terrain attributes

2.1 Introduction

Carbon (C) emission and C storage in soil, the largest terrestrial C reservoir, are closely connected with soil erosion (Pennock and Frick 2001; Van Oost et al., 2007; Van Hemelryck et al., 2010; Berhe et al., 2007). In erosive agricultural landscapes, soils have greater potentials to replenish C than in non-eroding environments (Stallard, 1998; Yadav and Malanson, 2009; McCarty and Ritchie, 2002). The consequences of agricultural soil erosion to net C feedback to the atmosphere have been an ongoing scientific debate since the last decade (van Oost et al., 2005, Lal, 2003, McCarty and Ritchie 2002, Jacinthe et al., 2001, Houghton et al., 1999). Even so, there still remains a high degree of uncertainty regarding the fate of soil organic carbon (SOC) in erosive landscapes, and the actual C source or sink term varies depending on the type of basins in the landscape (Berhe et al., 2007).

In typical dendritic hydrologic networks, the majority of eroded soil materials from uplands converge towards water channels at the bottom of hillslopes resulting in deposition in the channels or flowing out of the watershed (van Oost et al., 2005). However, in closed-depressional landscape, such as the late glacial, ice-marginal area of the Des Moines lobe in east-central Minnesota, soils eroded from land surfaces are likely to be deposited within the same landscape because of limited water outlets in this

hummocky landscape. Therefore, SOC in the eroded materials is likely to have redeposited within the depressional landscape instead of moving out of the watershed.

Understanding the re-deposited eroded soil material since settlement, termed *post-settlement alluvium (PSA)*, in closed-depressional landscapes is essential for understanding the fate of SOC in erosive agricultural landscapes (Ritchie et al., 2007; Bedard-Haughn et al., 2006). If PSA accumulates in depressional wetlands, the wetlands' high organic matter inputs and slow decomposition rates might result in SOC sequestration in PSA. Figure 2.1 illustrated the conceptual model for SOC and its relevant processes on an agricultural-influenced depressional landscape. Plant biomass input, or net primary production (NPP), is the main source of soil organic matter (SOM). The agricultural upland retains less NPP due to harvest, removal of crop residues, plant type, and less soil moisture for plant growth. While plowing aerates soils in agricultural uplands, prolonged saturation in the wetland results in little or no oxygen for microbial decomposition, leading soil to accumulate SOC. The original C-rich wetland surface soils may also be buried by PSA and preserved in the subsurface.

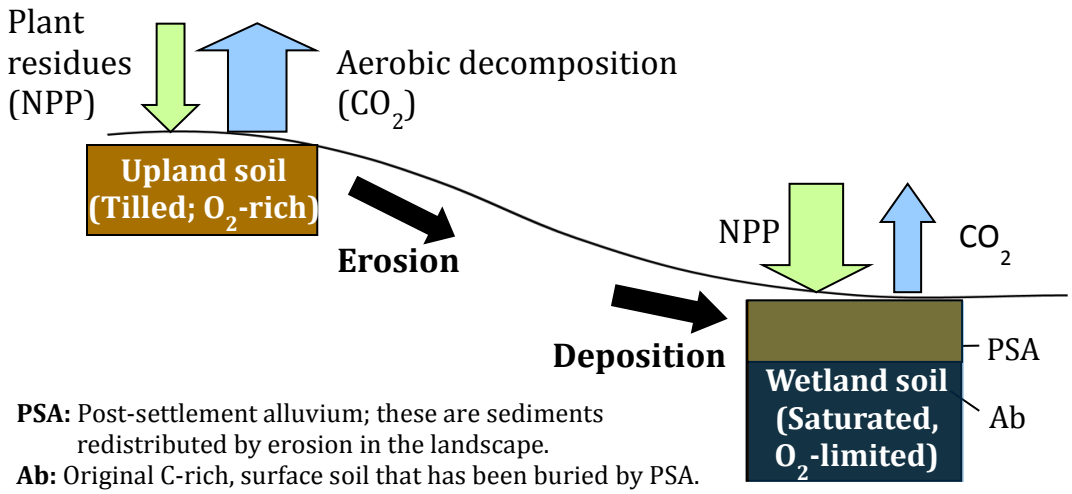

Figure 2.1 The conceptual model for soil organic carbon and its relevant processes on an agricultural-influenced depressional landscape.

Soil erosion accelerated by agriculture is orders of magnitude faster than geological erosion rates (Govers et al., 1994). Although the overall soil carbon storage is known to increase in response to geological erosion and deposition (Rosenbloom et al., 2006; Yoo et al., 2005), the effect of accelerated soil erosion on the fate of SOC remains uncertain (Van Oost et al 2005, Berhe et al 2007). Moreover, most studies on accelerated soil erosion and deposition were limited to uplands (vs. wetlands) due to the nature of the typical riverine landforms (open channels at the bottom of hillslopes) and agricultural land use (mostly in uplands) (Smith et al., 2001; Berhe et al., 2007; van Oost et al., 2007). Studies usually consider wetlands as a separate system, even where they coexist in same landscapes. One exceptional study in a hummocky till landscape in Saskatchewan, Canada investigated wetland SOC storage from agricultural erosion and found the SOC storage of 168.6 mg ha^{-1} for uncultivated wetlands within the agricultural area (Bedard-

Haughn et al. 2006). The resulting SOC storage was small, most likely due to the short flow path length, subtle topographic changes, small depressional areas, and relatively low precipitation in the study site of Bedard-Haughn et al. (2006). In southwestern Minnesota, restored wetlands were also found to play a role in carbon sequestration in small areas near the center of the wetlands (Lennon, 2009). I predict that stronger soil redistribution effects and a higher SOC accumulation are likely to occur in the central to eastern portion of the Des Moines lobe till region because of the relatively greater relief and higher precipitation.

Research has approached agricultural soil erosion and redistribution (or PSA) from various directions. Radionuclide tracing and simulation models have been applied to quantify erosion rates and their effect on SOC over time (de Alba et al., 2004; Yadav and Malason, 2009; Richie and McHenry, 1990; Dlugoβ et al., 2011; Gaspa et al., 2013). Estimation of SOC fluxes were also modeled by the simulation of soil erosion and redistribution processes (van Oost et al., 2005; Yadav and Malason, 2009). Radionuclide tracers Cs-137 and Pb-210 were widely applied to estimate soil redistribution that occurred over the past 50 and 100 years, respectively (Richie and McHenry 1990, Walling et al., 1995, McCarthy and Ritchie, 2002; Ritchie et al., 2007; Gaspa et al., 2013). A fallout radionuclide Be-7 has also been used for assessing short-term erosion events, but it is not suitable for the century-long erosion timeframe from settlement because of short half-life (53 days) (Walling et al 1999). Be-10 has also been used for sediment dating but its long half-life (1.5 million years) makes it suitable for studying geological events rather than anthropogenic disturbances (Balco et al., 2009). Although Cs-137 and

Pb-210 can successfully trace medium-term soil redistribution, the equipment cost for gamma-ray analysis is high, and data collection and processing are both resource- and time-consuming (Yoo et al., 2006).

It is cost-effective and efficient to use soil profile observations that incorporate soil pedogenic processes to understand the history of post-settlement alluvium. Dark colors in surface soils are correlated to organic matter content; in typical pedogenic development a soil has dark horizons overlying lighter-colored layers (Randall and Schaetzl, 2005). However if external materials were introduced that covered the original surface horizon, the darker horizon will be found at depth.

In the past two decades, terrain analysis has been widely applied to model soil property distributions and to understand soil-landscape functions (Moore et al., 1993; Gessler et al., 1995; Gessler et al., 2000; Thompson et al., 2006). Based on the catena concept (Milne, 1935), topographic characteristics are the primary factors that drive soil variability at hillslopes when other soil-forming factors are similar (Grunwald 2005; Thompson et al., 2006). Topographic relief and other terrain attributes can represent landscape geomorphology and flow patterns that drive surficial landscape processes like soil erosion and deposition (Ritchie and McCarty, 2003). During the last decade, more complex statistical and data-intensive models (e.g. geostatistics, regression tree models and fuzzy logic) have been used for soil-landscape modeling. However, modeling soil variability with terrain analysis allows us to understand soil-landscape processes and topographic drivers behind the dynamic changes of soil properties. Therefore, I chose to model PSA with terrain analysis using various local and regional terrain attributes.

While accepted as an effective soil-landscape modeling technique, terrain analysis is mostly limited to using 'local' terrain attributes. Local terrain attributes are spatial terrain surface characteristics derived from a digital elevation model (DEM) by a fixed, small-sized, moving window, typically 3-by-3-cell grids. Because of the small neighborhood operation, local terrain attributes such as slope and curvature consider only local topographic surface variations. These local terrain attributes capture the local variation at sample locations well but do not consider upslope contributions in the entire landscape.

The vital roles of landforms and flow patterns on surficial landscape processes (e.g. erosion) indicate that surface topography in an upslope dependence area (UA), where flow originates, has enormous influences on soil morphological development, and thus on the relevant soil properties (e.g. PSA). The importance of terrain attributes in the UA, or 'regional terrain attributes' (in contrast to local terrain attributes constructed using local neighborhoods in typically three-by-three cell-sized moving window), has been noted (Grunwald, 2005). However, perhaps due to the technical complexity, approaches to incorporating true regional terrain attributes have not been developed (Wilson and Gallant, 2000; Olaya, 2009).

In this chapter, I revisit the terrain analysis method to build a predictive model of PSA using both local and upslope terrain attributes in a depressional landscape. My research goals are to identify the spatial distribution and the quantity of PSA and to understand the controls of terrain attributes on PSA development in depressional landscapes, specifically the stagnation area of the Des Moines lobe region in Minnesota. The specific objectives underlying the project goals include:

1. Observe post-settlement alluvium in a hummocky landscape with closed depressions ;

2. Develop spatial datasets of local and regional terrain attributes for post-settlement alluvium prediction;
3. Build a soil spatial prediction model to assess the spatial distribution of post-settlement alluvium.

I hypothesize that regional terrain attributes significantly correlate to soil development relating to water movement on the landscape and therefore they have strong controls on soil re-deposition (i.e. PSA). While local terrain attributes developed by 3-by-3 moving windows explain some soil processes, the spatial variance of PSA would be better captured by combining local and upslope terrain attributes in a spatially-explicit model. I expect that regional terrain attributes control erosion in upper hillslope areas; local terrain attributes, on the other hand, drive where and how much deposition can occur.

I hypothesize that both local and regional terrain attributes can explain some of the variance in agricultural erosion and deposition, and therefore the operative processes. PSA is expected to accumulate on the lower part of catena, namely the footslope and toeslope, because slope angles decrease to nearly horizontal at these positions, and water flow becomes too slow to carry eroded materials farther. Because the UA is the source area of the eroded materials, regional slope and regional plan curvature are expected to influence the quantity of sediment eroded and therefore should be significant predictor variables for the thickness of PSA. Local terrain attributes including elevation, slope steepness, profile curvature, specific catchment areas (SCA) or compound terrain index

(CTI), and the rate change of profile curvature (representing the inflection point on a catena) are expected to be important predictor variables to PSA presence. Topographic controls for PSA thickness are expected to include stream power index (SPI), regional slope steepness and regional plan curvature.

I developed local and regional terrain attributes from a high-resolution (1-m) LiDAR (Light Detection and Ranging)-derived elevation model in a geographic information systems (GIS). A two-stage regression analysis method is used with the terrain attributes to develop spatially-explicit models. The resulting model not only predicts the spatial distribution and the quantity of PSA in this depressional landscape, but also will help soil pedologists understand the effects of topographic characteristics on soil processes relevant to PSA.

2.2 Site description

The study site is a moderate hill surrounded by depressional wetlands at Lake Rebecca Park Reserve in east-central Minnesota (45.05324, -93.7511) (Figure 2.2). The site is about 6.13 hectare in area, elevation ranges from 279m to 300m above mean sea level and slopes ranging from 0 to 28.5%. Today the Rebecca site has a typical subhumid, midcontinental climate with a mean annual precipitation of 691mm. Native vegetation at the Lake Rebecca site was a deciduous hardwood forest (Marschner, 1974). Conversion of forests to cropland started in the 1840s during European settlement (Hennepin County, 1873; Dahl, P.M. 1898).

The study area is on the Pine City moraine, an irregular terminal moraine segment of the Des Moines lobe. The Des Moines lobe retreated from this area around 11,700 radiocarbon years before present. Loamy and calcareous (unless leached) soils have formed in the unsorted till deposits and the drainage pattern is deranged with many small depressions and very limited water outlets (Tiner, 2003).

Situated in the prairie-forest transition zone, upland soils at the Rebecca site are dominated by the Lester series (Mollic Hapludalfs), a forest-based soil with a thick, black Mollic epipedon developed under prairie vegetation during the warm hypsithermal period in the mid-Holocene. The marsh on the north of the Lake Rebecca site consists of the Houghton soil (Typic Haplosaprists), and the wetland on the south to southeast belongs to the Klossner soil series (Terric Haplosaprists). Soils in the midslope to footslope

positions between Lester and wetland soils (i.e. Houghton or Klosser series) are classified as Hamel (Typic Argiaquolls) (Soil Survey Staff, 2013).

The Rebecca study area was converted from cropland to grassland in the early 1970s when the current park reserve was established (Larry Gillette, personal communication, 2009). The adjacent wetland in the north, also known as Kasma Marsh, is classified as semi-permanently flooded, and the wetland in the south-southeast is seasonally flooded (Cowardin et al., 1979). From aerial photos (the earliest dating to 1937, a period of drought), we can see that agricultural activities not only occurred on the rolling hills, but also extended into the surrounding wetlands (Figure 2.3). Row crops were the main land cover for decades indicating that tillage occurred across the entire Rebecca site. The Kasma Marsh on the north appeared to be dry enough during the drought period in the 1930s for plowing, but has been getting wetter since that time. By 1969 to 1971, the Kasma Marsh was no longer in agricultural production (Figure 2.3).

In this study we are interested in post-settlement deposition in depressional landscapes of Minnesota, particularly in the hummocky margins of the Des Moines lobe in South-Central Minnesota. The Rebecca Site represents the native environment and development history of the region.

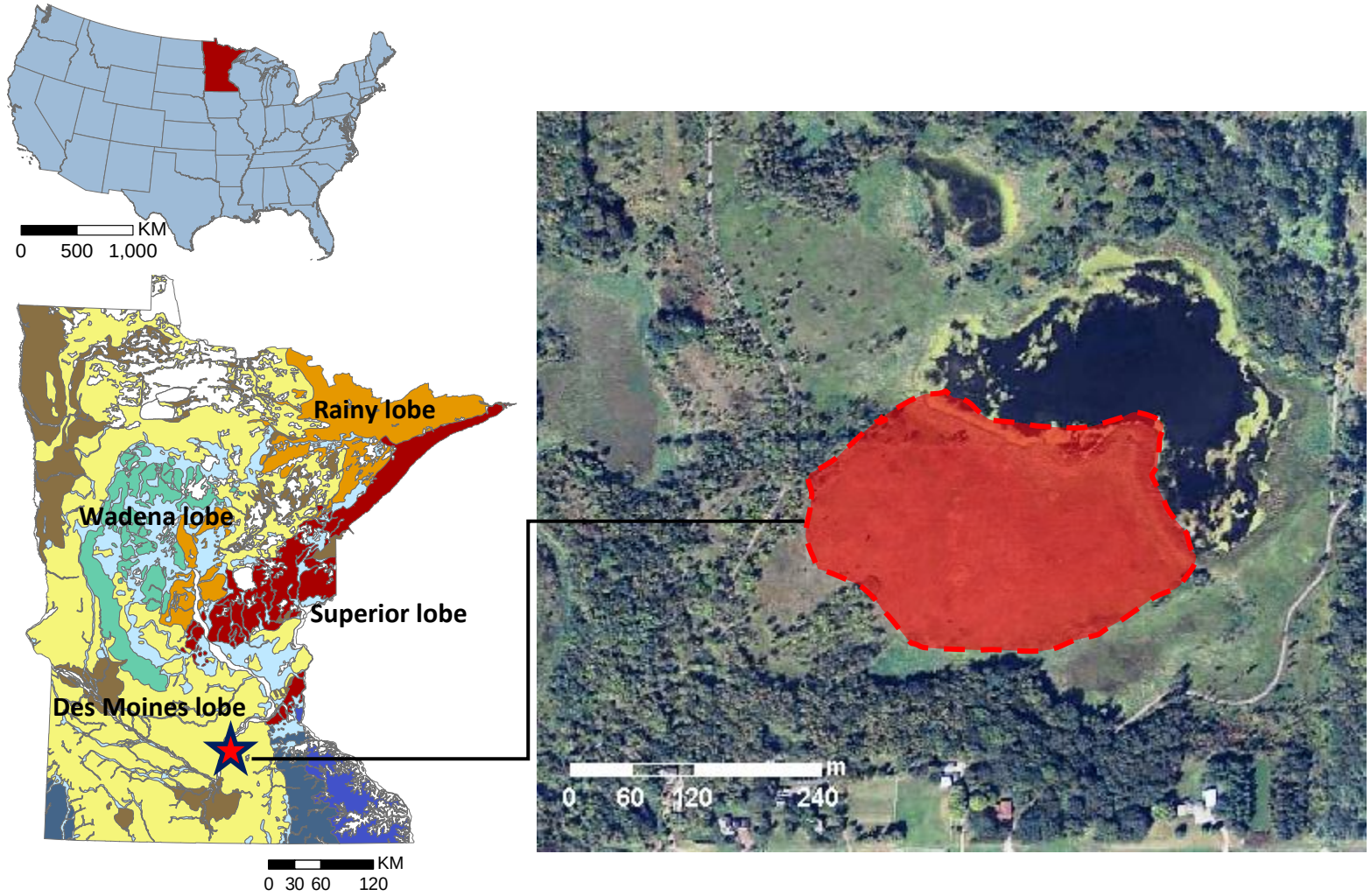

Figure 2.2 The study site in Lake Rebecca Park Reserve is located on the recently glaciated Des Moines lobe till region with rolling topography along its margins.

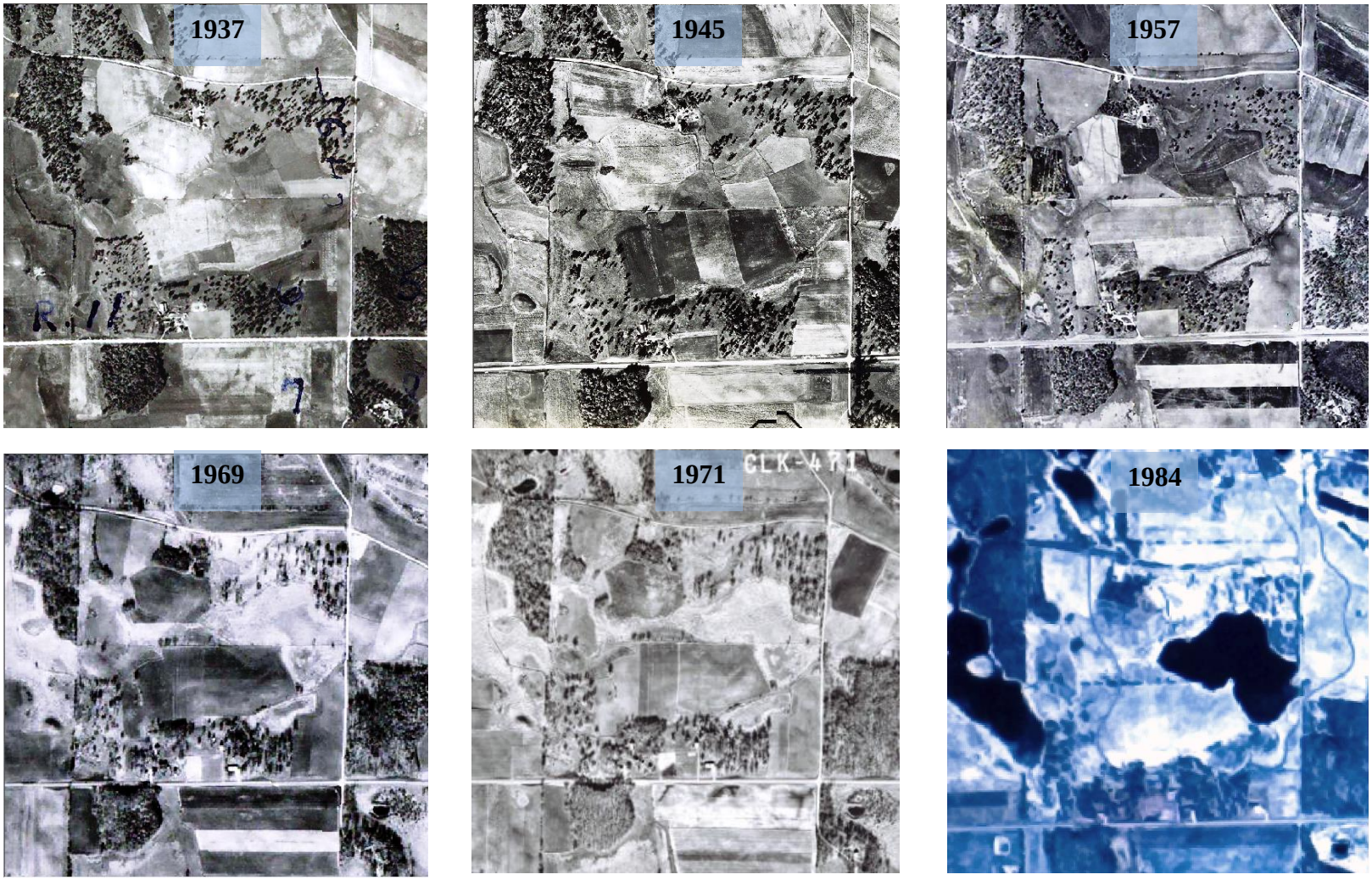

Figure 2.3 Aerial photos at the Lake Rebecca study site over the period of 1937 to 1984.

2.3 Methods and materials

The schematic diagram for the approaches and logistics used in this study can be found in Figure 2.4**.** I started with field data collection at the Rebecca study area. Terrain data development was conducted at the Soil and Land Analysis Laboratory in the Department of Soil, Water, and Climate at University of Minnesota at the same time. Terrain attributes were used as predictor variables in linear regressions to predict post-settlement alluvium data for the entire study site. The detailed method will be described in this section.

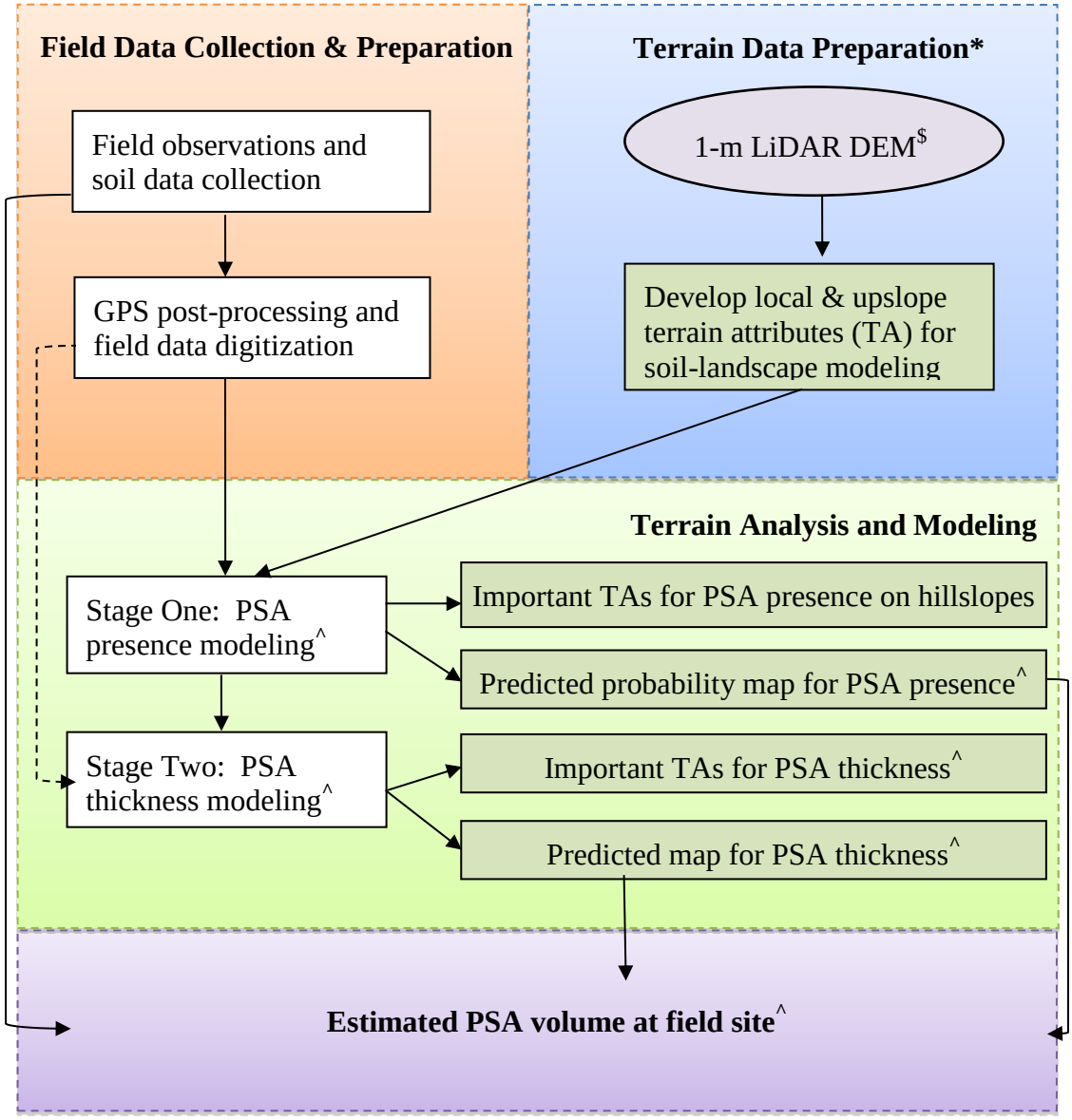

*A detailed framework for terrain attribute developed can be found in Figure 2.9

$Digital Elevationi Model derived from Light Detection and Ranging, a remote sensing method.

^PSA: Post-settlement alluvium

Figure 2.4 The schematic workflow for the spatial prediction of post-settlement alluvium.

Field data collection and post-processing

I described 61 soil profiles on the hillslopes of the Lake Rebecca study site during the growing seasons of 2009 and 2010. The sampling locations were based on preliminary observations on-site and were designed to cover a diverse range of (profile and plan) curvatures and the distances to summit. Thirty-six of the samples were located along 6 transects and followed the stratified-gradient sampling approach of hillslope positions – summit, shoulder, backslope, footslope, and toeslope/wetland (Figure 2.5). Twenty-five samples were in the lower hillslope position to capture the hypothesized location of PSA in footslope and toeslope positions. This specific sampling scheme was designed to capture important influences of terrain characteristics on PSA accumulation and to enable spatial PSA modeling. Detail geometry of sample locations is available in APPENDIX A.

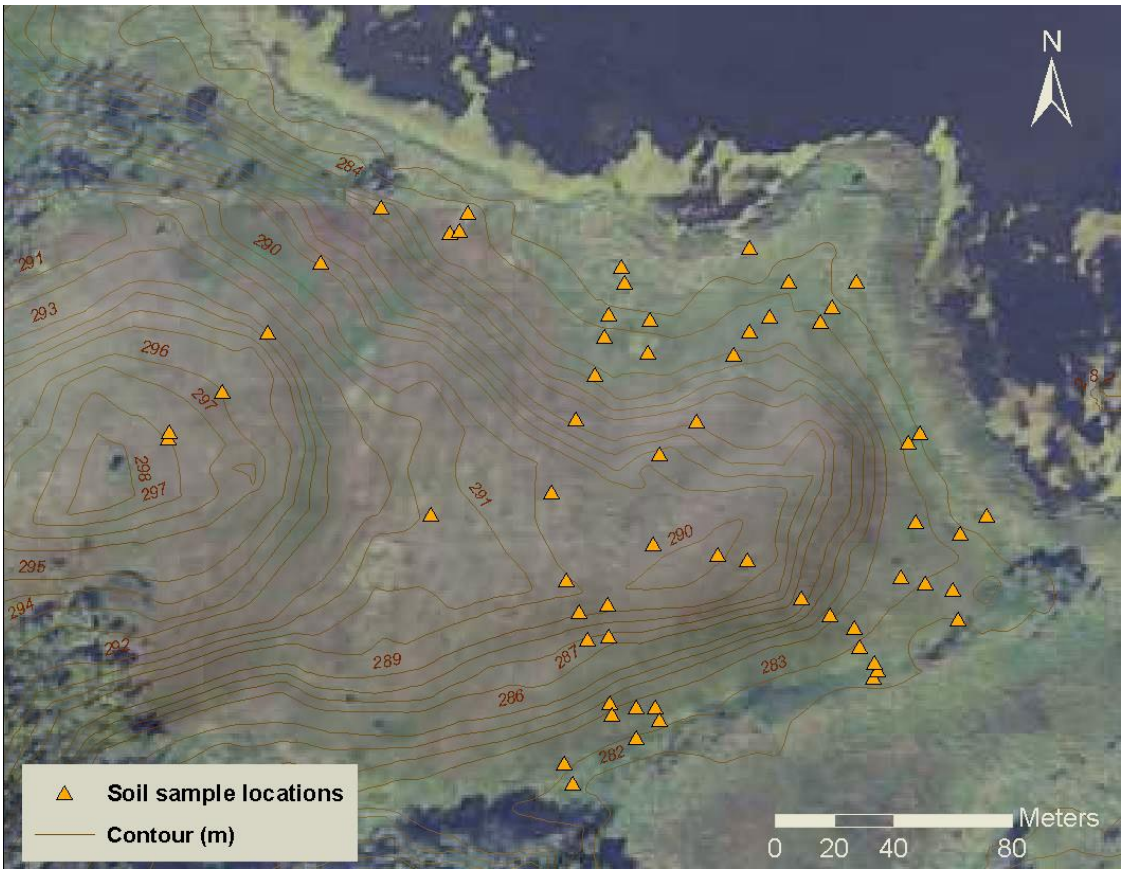

Figure 2.5 The sample locations at the Lake Rebecca study area in South-Central Minnesota.

Soil deposition (PSA) information was measured and recorded for all samples at the Rebecca site. At each sampling location, I used an 8.25cm-diameter soil auger to recover samples that were placed on clean, flat ground according to depth. In each sample location, I described the presence and thickness of PSA and described the soil profile morphology. The PSA layer can be recognized by its distinct soil morphology and color. Even after continuous surface mixing and burial for more than 150 years, the PSA and the underlying horizons are still identifiable in the field (Figure 2.6**).**

The boundary between PSA and the underlying original surface horizon was identified by differences in soil texture, structure, and Munsell color. PSA has a siltier texture because of its erosional history, a weaker structure and is lighter in color than the underlying Ab horizon. Denoted by the subscript "b" for "buried", the buried horizon normally has a darker soil color since it was developed at the surface of a lower, moister hillslope position than where the PSA sediments originated. Dark colors in surface soils are attributed to organic matter content decomposed from biomass at the surface. Regular pedogenic development does not result in darker horizons underlying the lighter layers unless external materials cover the original surface horizon. These abrupt changes of horizonation may not be easily observed if PSA is less than 20 - 25 cm in depth due to soil mixing associated with agricultural plowing.

(a) Soil profile without PSA (b) Soil profile with PSA

Figure 2.6 A comparison of soil profiles with and without post-settlement alluvium (PSA) at the Lake Rebecca site. (a) A soil profile in upland (Sample #029) with no PSA shows a typical soil color change with reduced values and hues over the depth profile; (b) A soil profile in a toeslope position (Sample #012) with PSA observed by an abrupt darkness increase as well as soil structure and/or texture changes in the buried A horizons.

I recorded latitudes and longitudes for soil sample locations in geographic coordinates with the datum of WGS 84 using a professional-level handheld differential Global

Positioning System (GPS) (Magellan® MobileMapper™ 6). The geographic information in the GPS device was uploaded and post-processed for differential corrections upon return from field data collection. Using daily geodesy data for the closest base station(s) with known GPS position(s), differential correction improves the horizontal accuracy of sample GPS locations. The base station I used is the closest reference station in the Minnesota Continuously Operating Reference Station (MnCORS) Networks -- either Hollywood (44.905833, - 93.986666) or Golden Valley (45.000555, - 93.351388), depending on availability at the time of data processing. After differential correction, the horizontal accuracy is less than a meter (Magellan Professional, 2006).

A rough vegetation survey was also conducted at Lake Rebecca site. The coordinates of various major wetland vegetation species, including cattails (*Typha angustifolia*, *Typha latifolia* or hybrids), sedges (*Cyperaceae*) and willows (*Salicaceae*), were recorded using GPS. I used the vegetation survey to estimate the spatial extent of PSA assuming that PSA deposition ended near the wetland boundary. This boundary was difficult to measure in the field; I assumed that PSA stopped at substantial plant barriers near submerged surfaces and I used vegetation boundaries as the limit of PSA in the catena. Cattails were considered to be the most effective barrier but tree species such as willows were also counted. I recorded these vegetation locations using the differential GPS device and re-digitized the boundary in ArcGIS after post-processing.

Development of digital terrain attributes

I downloaded the 1m-resolution LiDAR-derived Digital Elevation Model (DEM)

covering the spatial extent of the Lake Rebecca Park district using Filezilla, an FTP client program. The LiDAR data in this region were collected in 2011 and acquired during the Metro phase of a statewide Minnesota Elevation Mapping Project (Minnesota Geospatial Information Office, 2012). The horizontal accuracy of the LiDAR DEM meets or exceeds a RMSE of 0.6m; the vertical accuracy meets the National Digital Elevation Program guideline requirements of a RMSE of 12.5cm, and is reported by Minnesota Department of Natural Resources (DNR) as having a true accuracy level of ±5cm (Fugro Horizons, Inc. and MN-DNR, 2011).

I smoothed the 1-m DEM twice using low-pass filter in the GIS software ESRI® ArcGIS 10.0. in order to fill unrealistic pits and remove artifacts resulting from mechanical errors during data measurements and processing, Next, I used the smoothed DEM to derive the spatial databases of local terrain attributes relevant to landscape surface processes. These terrain attributes include both primary terrain attributes—slope steepness(%), flow path length (m), profile curvature, plan curvature, the rate change of profile curvature, specific catchment area (or SCA, m^2)—and secondary terrain attributes—compound topographic index (or CTI, also known as wetness index), and stream power index (or SPI).

Besides numerical attributes, profile and plan curvature datasets were also categorized into three classes—concave, convex, and straight—using thresholds suggested in ArcGIS 10 (ESRI, 2013). The classification criterion was illustrated in Table 2.1. Cell with values between -0.5 to 0.5 in both profile and plan curvature gridded data are classified in the 'straight' category. For profile curvature, values equal or less than -0.5 are classified as

‘convex’ and greater than +0.5 are ‘concave’. For plan curvature, the classification is reversed on the +/- signs, where values greater than +0.5 are classified as ‘convex’ and those equal or less than -0.5 are classified as ‘concave’ (Table 2.1).

Table 2.1 The illustration for the classification criteria of profile and plan curvature.

	Convex (*x*)	Concave (*v*)	Straight (*f*)
Profile Curvature	- (< -0.5)	+ (> 0.5)	between -0.5 & 0.5
Plan Curvature	+ (> 0.5)	- (< -0.5)	between -0.5 & 0.5

I also added a new attribute, the first derivative of the profile curvature, to identify the inflection point in a catena. This defines the rate change of profile curvature. The inflection point of a hillslope is where surface changes from convex to concave, and I expect the inflection point to be a critical location where erosion switches to deposition (Figure 2.7).

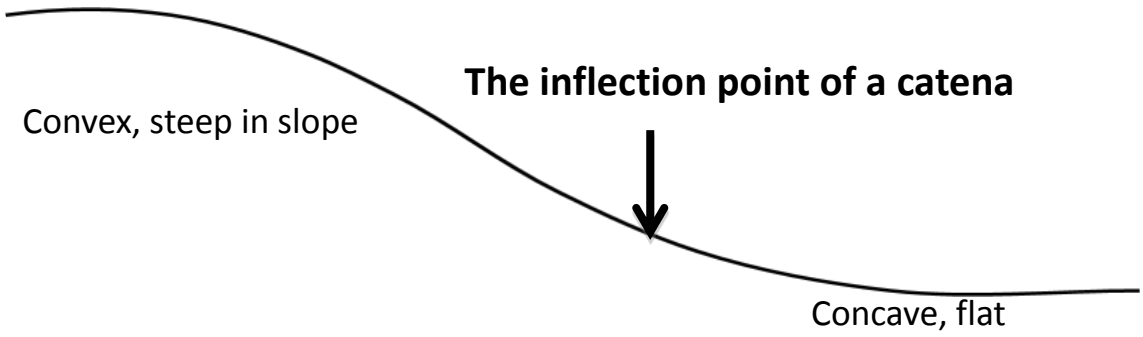

Figure 2.7 A hillslope with the hypothetical inflection point, where a soil surface changes from erosive (convex, steep) to potentially depositional (concave, mildly sloping to flat) on a catena.

Because surface landscape processes in erosive uplands control the amount and the quality of soil materials being delivered to depositional sites, topography in the UA is potentially influential in the spatial distribution and the quantity of PSA in landscapes. So, in addition to using local terrain attributes, I developed a procedure to generate the upslope dependence area terrain attributes (UDTA) for soil-landscape modeling. The raster-formatted UA, defined as the area from which water flows to a defined outlet, is commonly used in hydrologic modeling but less so in soil-landscape modeling (Eddins, 2009). The diagram in Figure 2.8 illustrates the logistics of the UDTA development. I created UA for all sample locations using a multiple flow-direction (MFD) algorithm in the open-source software SAGA-GIS (Cimmery, 2010). In order to obtain UAs for the sample locations, I defined the coordinates of my sample locations as the outlet points in this study.

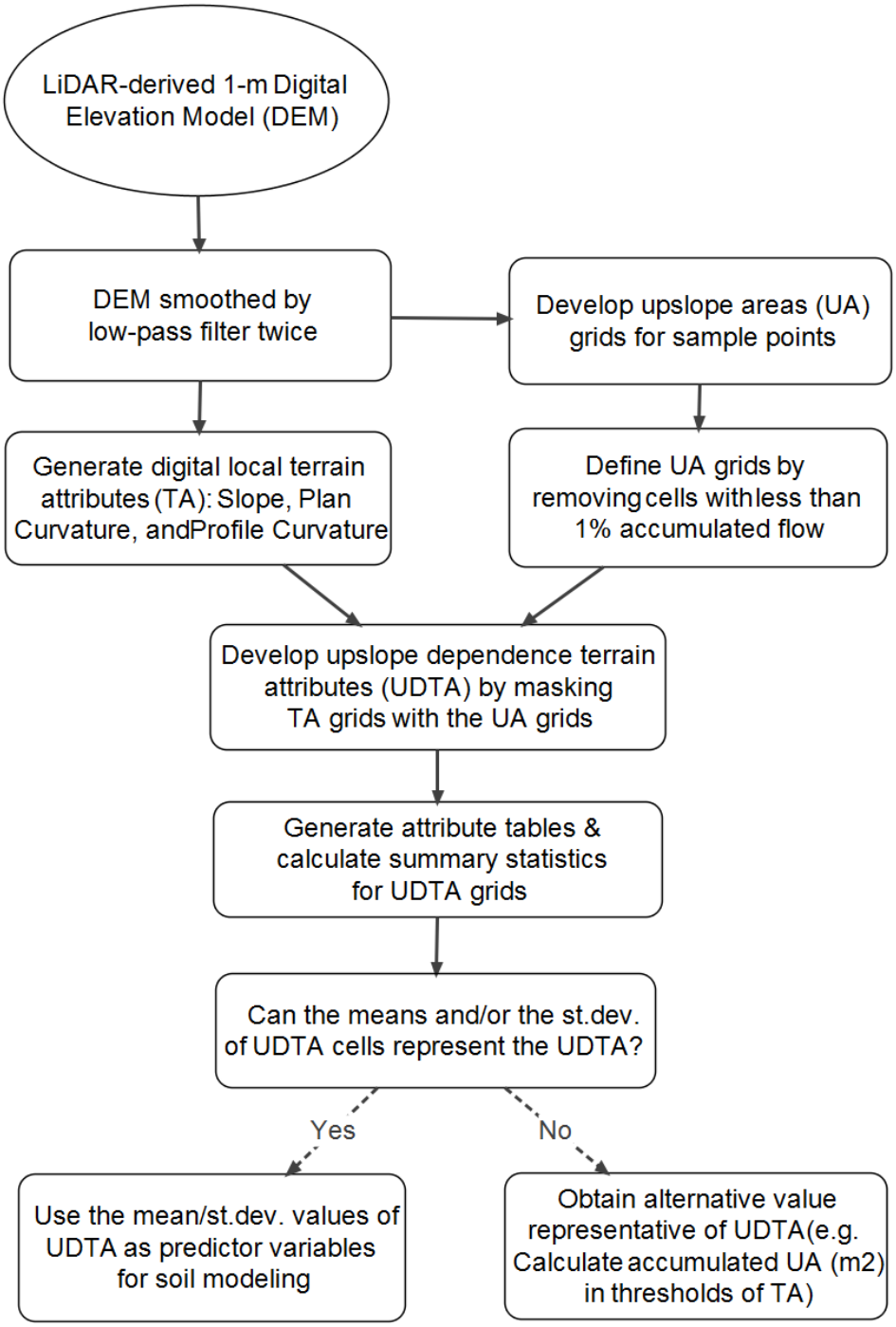

Figure 2.8 The schematic diagram for the development of upslope dependence terrain attributes (UDTA).

The MFD algorithm used for calculating spatial UA grids in SAGA-GIS is modified from the conventional single flow-direction algorithm D8. Also known as FD8, the MFD algorithm allows water to flow from processing cells in multiple directions downslope, which more closely simulates natural flow processes across landscapes than D8 (Freeman, 1991; Olaya and Conrad, 2009). I exported the MFD-based UA grids as ESRI ASCII files to ArcGIS 10 and selected only cells with greater than 1% of accumulated flow contributing to the target location for PSA modeling. The constrained UA grids were then used as masks to extract slope, profile curvature and plan curvature using the scripting language Python with Arcpy packages and Spatial Analyst extension in ArcGIS 10.

I created summary statistics and histograms of slope and curvature values at the UA cells for each sample location. In order to obtain attribute tables from these floating-point raster data, the UA slope and curvature gridded databases were converted to integer grids before generating attribute tables and descriptive statistics. Significant digits of the gridded UDTA cell values were preserved by multiplying the values in order of magnitudes (i.e. 1000) prior to integer conversion. The descriptive statistics, however, showed UA slope and curvature cells for individual sample locations were not all normally distributed. To use a digital terrain attribute as a predictor variable in regression analysis requires one representative value for each sample location. The UDTA histograms for my samples did not have consistent patterns (skewed to the right, to the left, or normally-distributed), so using the means and standard deviations of UDTA for regression modeling would not be optimal.

During this UDTA exploratory analysis, however, I observed some relationships between

PSA thickness and UDTA thresholds. My preliminary data analysis showed significant correlations between PSA thickness and area with the area (m^2) and percentage area of UA slope and UA curvature in thresholds. These were therefore used as regional terrain attributes in spatial modeling of PSA.

The idea behind using UA slope in thresholds (e.g. the area of UA in slope greater than 6%) as regional terrain attributes is the possible control of critical slope steepness to the flow-relevant soil properties in a specific landscape. I defined slope thresholds as 4%, 6%, 8%, 12%. These values were selected from the literature as well as the recommendations of field soil scientists. Slope angles of 4% and 8% had been used for soil landform classification in literature (Brabyn, 1996), and 6% of slope was suggested by the USDA-NRCS Soil Survey team as the key slope threshold in finding soil deposition on hillslopes in similar landscapes in this region (John Beck, personal communications, 2012). I added 12% as a cut-off steep slope threshold.

After splitting UA grids by the above-mentioned slope thresholds, I calculated the areal extent for each slope category (<4%, >=4%; <6%, >=6%; <8%, >=8%; <12%, and >=12%) using Python scripts. The threshold-split UA grids are also floating-point raster data without attribute information. I obtained the raster data area information (m^2) by converting the data to integer grids prior to getting attribute data and calculate statistics.

In addition to the previously mentioned slope categories, the sizes of UAs in the slope ranges between 4-8% and 8-12% were also calculated as potential predictor variables in PSA modeling. Similar steps were taken for obtaining UA in thresholds of profile

curvature and plan curvature. I used the three curvature categories as thresholds for UA profile and plan curvatures: straight, concave and convex.

As previously mentioned in Section 2.1, the development of regional terrain attributes (UDTA) is computationally challenging and thus time- and resource- consuming. While recent GIS advances in hydrological modeling simplify UA development, I was only able to create UDTA for sample locations. Without mapping UDTA for cells in the entire spatial extent of the study area, the PSA models with UDTA are limited in their use to understanding the relationships between PSA and UDTA (explanatory). I will not be able to predict the spatial distribution of PSA at the Lake Rebecca site using the UDTA-related PSA models. Further development of the UDTA automation will depend on the usefulness of the attributes tested herein.

Two-stage regression analysis method

I examined summary statistics and the frequency distribution of PSA and both local and regional terrain attributes at sample locations using the statistical language R. Since local and regional terrain attributes were all derived from a single source, the LiDAR DEM, I was aware of potential collinearity issues in this soil-landscape modeling. Predictor variables were selected carefully to avoid high collinearity issue.

Forward and backward stepwise multiple linear regression was applied to fit PSA thicknesses for all samples (n=61) at the Lake Rebecca. The best-fit models were constructed by local and regional terrain attributes together (as 'the mixed models') and

separately. All three types of regression models (local, regional, and mixed) helped identify topographic drivers and related soil processes for PSA. The high processing time involved in developing UDTA for all cells, mixed and regional models does not allow the prediction of PSA. Spatial prediction models will be built using only local terrain attributes as predictor variables (Table 2.2).

Table 2.2 The usefulness of predictor variable types in regression modeling for landscape soil processes.

Use	Terrain attribute categories	
	Local (the 3-by-3 cell neighborhood)	Regional (upslope areas)
Understanding soil processes	√	√
Predicting soil properties	√	

The best local terrain variables for modeling PSA thickness are elevation, CTI, SPI, and SlpProfile with an adjusted R^2 of 58.87%. All partial correlation coefficients in the regression model were statistically significant with the confidence interval (CI) of 90% (p-values < 0.10). However, when evaluating the residual scatterplot of the model, I found a clear linear pattern, indicating that the estimates from the regression model did not capture some predictable trend. The regression was not valid because it violates the random error requirements for linear regressions. The investigation of my data showed that several PSA-absent samples (PSA = 0) had non-zero PSA predictions in the regression model, and the large number of soil samples (29 out of the total 61 samples)

with no PSA (PSA = 0) may have destroyed the predictive power of local terrain attributes to PSA in the regression model. To remove the linear pattern in the residuals and predict PSA properly, I updated the PSA modeling to a two-stage regression analysis (See diagram in Figure 2.4).

The purposes of two-stage regression analysis method were to: 1) Identify where PSA is present, and 2) estimate PSA thickness where it occurred. At Stage 1, I used a logistic regression to predict the probability of PSA presence. The dependent variable in the logistic regression is 'PSA presence' (1= PSA present, 0=PSA absent). The binomial distribution was fitted with local and/or regional terrain attributes in a generalized linear model (the *glm()* function in R) to develop the predictive and explanatory models of PSA presence.

Logistic regression, also known as logit function, transforms the odds of PSA presence or absence (a range between 0 and 1) from an S-curve to a straight line by taking the natural logarithm of the odds:

$$\text{logit}\,(p) = \ln\,(p/(1-p)) = \beta_0 + \beta_1 X_1 + \beta_2 X_2 + \ldots + e \qquad (2.1)$$

where p is the probability of PSA presence, X_i are predictor variable with partial regression coefficients β_i, and e is the error term.

A total of 61 sample point data were used in the spatial prediction of PSA presence with local terrain attributes using logistic regression. However, I encountered problems generating reasonable UA grids at toeslope locations and could not apply all sample data

to the mixed model (using local and regional terrain attributes). The UA grids were derived from the 1-m LiDAR DEM, at several toeslope sample locations and contain unreasonably low cell numbers. Trivial elevation changes (less than 0.1m or even 0.01m) in the source data between neighboring cells were likely picked up during UA development process. Seven samples (009-DEP, 015-TOE, 020-TOE, 1E, 4E1, 4E3, and 7E) at toeslope locations with UA less than 100 cells were removed prior to the mixed model regression.

For the logistic regression models of PSA presence, I selected predictor variables based on stepwise regression and the regsubsets( ) function in the 'leaps' package in R. The regsubsets function performs an exhaustive search on independent variable combinations and returns the best subsets of independent variables based on estimated R^2 or Bayesian information criterion (BIC). By running the regression function glm( ), I confirmed best-fitted model(s) that have the lowest Akaike information criterion (AIC) with 90% of significance level (p-values < 0.10). As logistic regression is not an OLS regression but an estimator of maximum likelihood, it does not actually have a true R^2 to explain the variance captured as a linear regression. I used AIC to select best-fitted models but reported a pseudo R^2 for the common understanding. AIC, calculated as -2 * ln(likelihood) + 2K (K as the number of free parameters in the model), is a criterion that seeks a model with a good fit while considering the number of predictor variables used.

My preliminary logistic regression shows that elevation is the sole variable controlling the presence of PSA, yet the use of absolute elevation as a predictor variable limits the model transferability. Local elevation represents the relative potential energy in hillslope

positions of a catena, and therefore it is expected to be significant in landscape soil properties like soil erosion. However, absolute elevation is not a transferable variable outside of this study area. Each basin has different elevation ranges; the same absolute elevation may not represent the same hillslope positions and therefore may have different sediment accumulation capacity in different basins. To make our spatial PSA model applicable to other areas of interest in similar geological settings, I replaced absolute elevation with another variable, relative elevation. Typically calculated by subtracting local minimum elevation within a defined watershed from absolute elevation for each cell, it is difficult to define watershed boundary for closed-depressional landscapes in the GIS. With no suitable flow algorithms for depressional landscapes, I calculated local minimum elevation within a moving window of 200-m radius circular neighborhood using a focal statistics function in ArcGIS. The radius was selected by trials for the Lake Rebecca area. Local minimum elevation remains almost identical when the neighborhood processing window in the GIS has a radius greater than 200m.

Once the best-fitted PSA presence model was selected, I evaluated the model performance by calculating its prediction accuracy as well as by using a 10-fold cross-validation. Then I generated a predictive probability map for PSA presence. There are various ways to interpret logistic regression results (e.g. odds ratio, predicted probability); because I am interested in the spatial distribution of PSA, I assessed the predicted probability for PSA presence. The probability (p) of the PSA presence can be back-transformed firstly to odds ratio:

$$p/(1-p) = \text{Exp}(\beta_0 + \beta_1 X_1 + \beta_2 X_2 + \ldots) \quad (2.2)$$

then, rearranging the odds ratio Eq. (2.2) to probability as:

$$p = \text{Exp}\,(\beta_0 + \beta_1 X_1 + \beta_2 X_2 + \ldots) \,/\, [1+\text{Exp}\,(\beta_0 + \beta_1 X_1 + \beta_2 X_2 + \ldots)\,] \qquad (2.3)$$

Based on Eq. (2.3), I mapped the probability distribution of PSA presence at the Lake Rebecca site. I defined the zone of PSA presence on the map by determining the probability threshold. Using the agreement of the observed samples, a 50% probability (the area with 50% chance to contain PSA) would be the minimum threshold I would use for defining the spatial distribution of PSA presence on the map, and a higher probability is preferred.

Samples located within the PSA presence area from the result of Stage 1 analysis were selected for Stage 2 analysis. In Stage 2 analysis, I used a multiple linear regression method (MLR) to model the spatial distribution of PSA thickness. The number of samples used in this stage depends on the predicted probability map of the PSA presence and the chosen percentage probability threshold. By modeling PSA thickness without PSA-absent samples, I expected the MLR residuals to be randomly distributed with a mean of zero.

Similar to the procedure for Stage 1 logistic regression analysis, the selection of predictor variables for Stage 2 MLR used stepwise regression and the regsubsets function in R. I looked for both local and mixed models of PSA thickness with good fit. While not strictly predictive, regional terrain attributes help illuminate the pertinent soil erosion and deposition dynamics in this depressional landscape. A spatial map of PSA thickness was generated for the area predicted to have PSA present at study site.

Model performance and validation were done after the two-stage models were chosen. The model performance included root mean squared error (RMSE) and mean absolute error (MAE) for the local and mixed models of PSA presence (Stage 1) and PSA thickness (Stage 2). The residual analysis, including residual scatterplots with the locally weighted scatterplot smoothing (LOWESS) line, normalized quantile-quantile plots (qqplots), and density plot, were also used to evaluate if regression assumptions were met in these models. A 10-fold cross-validation (CV) method was also applied to validate the regression models from the two-stage regression analysis.

The k-fold CV method avoids overfitting and estimates the predicted errors for both logistic regression and multiple linear regression. This validation technique splits the total samples into 'k' equally and mutually exclusive sub-groups and trains the model k times. In each run, one sub-group is left out as the testing dataset and the rest of subgroups (k-1) are the training data for the model development. As a result, the model would be tested for 'k' times, with all of the samples being used in the training and at least once in the validation test. The k-fold CV method is beneficial to the small sample size (e.g. the PSA dataset in this project) without taking away model datasets (training) for the validation (testing) purpose. For the balance between the error variance (increase when k is large) and the estimator bias (increase when k is small), I used 10-fold cross-validation in this project. Ten has been proven to be an effective number of folds in this cross-validation technique (Borra and Di Ciaccio, 2010).

Estimate the amount of post-settlement alluvium

Estimating the volume of PSA present at study area requires the both the areal extent (X, Y) and depth (Z). The upper hillslope boundary of PSA is available from the predicted probability map of PSA presence (the result of Stage 1 analysis); the depth boundary of PSA is the PSA thickness map resulting from the Stage 2 regression analysis. In order to close the loop for calculating the spatial area (m_2) of PSA, I estimated the lower hillslope boundary of PSA as being near the wetland edge using the field vegetation survey. The volume of PSA was estimated as follows:

PSA volume (m^3) = [PSA presence area (m^2)] * [PSA thickness (m)] (2.4)

2.4 Results and discussion

Field observations of post-settlement deposition

The observed PSA at the 61 sample locations ranges from 0 to 80 cm in depth (Table 2.3; Figure 2.9). The average of PSA is 23.5 cm deep and 29 out of the 61 sample locations had no observed PSA (PSA thickness = 0). As expected, the 32 PSA-present sample locations are located at footslope and toeslope positions (Figure 2.10). The thickness of PSA is consistently greater than 25 cm except in the wetland which was 18cm deep. The depth (25cm) aligns with the common plowing depth in agricultural landscapes, suggesting that active mixing by plowing (and maybe other bioturbation) at the deposition locations has made it difficult to distinguish PSA shallower than 25cm in depth. Mean and median of the PSA thickness (23.49cm and 20cm, respectively) do not

accurately reflect the actual distribution of PSA thickness at PSA-present locations because nearly one half of the sample locations do not have PSA present (PSA=0).

Table 2.3 Descriptive statistics for the thickness of post-settlement alluvium (PSA) at Lake Rebecca study site.

Summary Statistics	**PSA Thickness (cm)**
Number of samples	61
Number of zero values	29
Min.	0
Max.	80
Range	80
Median	20
Mean	23.49
Standard deviation	25.70

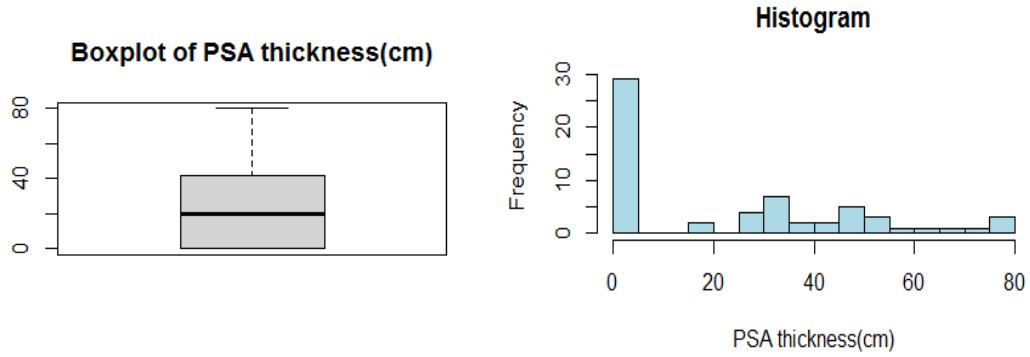

Figure 2.9 Boxplot and the frequency distribution of post-settlement alluvium (PSA) thickness.

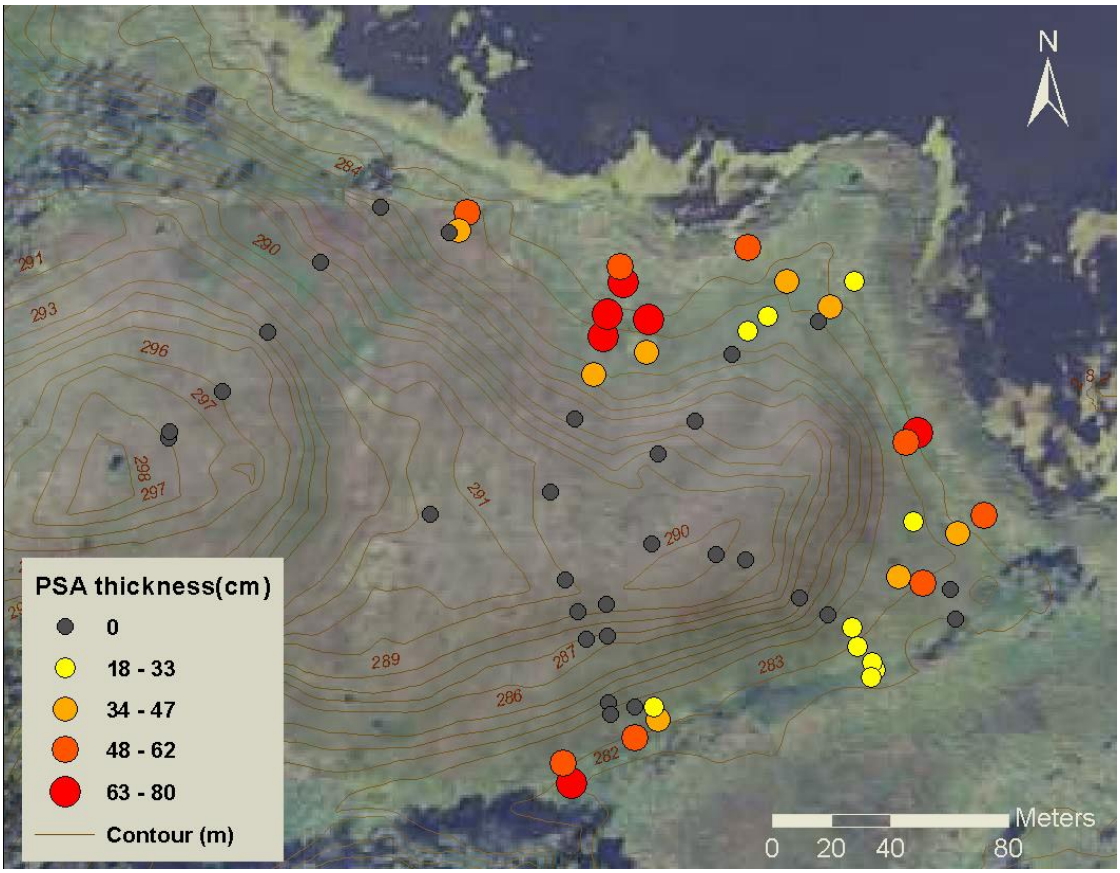

Figure 2.10 The observed post-settlement alluvium (PSA) thickness at Rebecca site. All PSA were found in footslope and toeslope positions in the landscape.

Local and regional terrain attributes

The spatial datasets of local terrain attributes at the study area are displayed in Figures 2.11-2.19. These local terrain attributes include relative elevation, slope, profile curvature, plan curvature, slope of profile (the rate change of profile curvature to capture the inflection points on catena), flow path length, specific catchment area (SCA), compound topographic index (CTI) and stream power index (SPI). All attribute data are floating-point raster datasets determined for 1-m cells. Relative elevation ranges from 0 to 17.1 m

at the Rebecca site (Figure 2.11). The values of relative elevation are highest at the ridge top in the west and decrease slightly to the ridge extended to the east before dropping quickly downhill to the surrounding wetlands (relative elevation ~ 0). In Figure 2.12, the spatial distribution of slope shows that areas with slope steeper than 15% are situated in a band on backslope positions surrounding the east-west oriented ridge across the center of the Rebecca site, and also on a small north-south band between two summits with different elevation in the west part of the ridge.

For the spatial distribution of profile curvature (Figure 2.13), convex profile curvature dominates the western ridge top and the shoulder positions. About half way downslope to the wetlands in the north, northeast, and southeast, concave profile curvature dominates. Plan curvature shows where flow converges (at concave locations) and disperses (at convex locations) across the hill (Figure 2.14). Convexity is more dominant at the east and there are two main concave lines (flowlines) north of the hill. At the bottom of the hillslope, plan curvature still displays many bumps (convexities) and dips (concavities). These are likely very small changes captured by the high resolution DEM and may not be meaningful if eroded sediment moves through them downhill by overland flow. Note that the maps of plan and profile curvature both contain some striping (Figure 2.13 and 2.14). These are likely artifacts produced during the LiDAR data collection or DEM processing. This type of error should not affect the overall analysis.

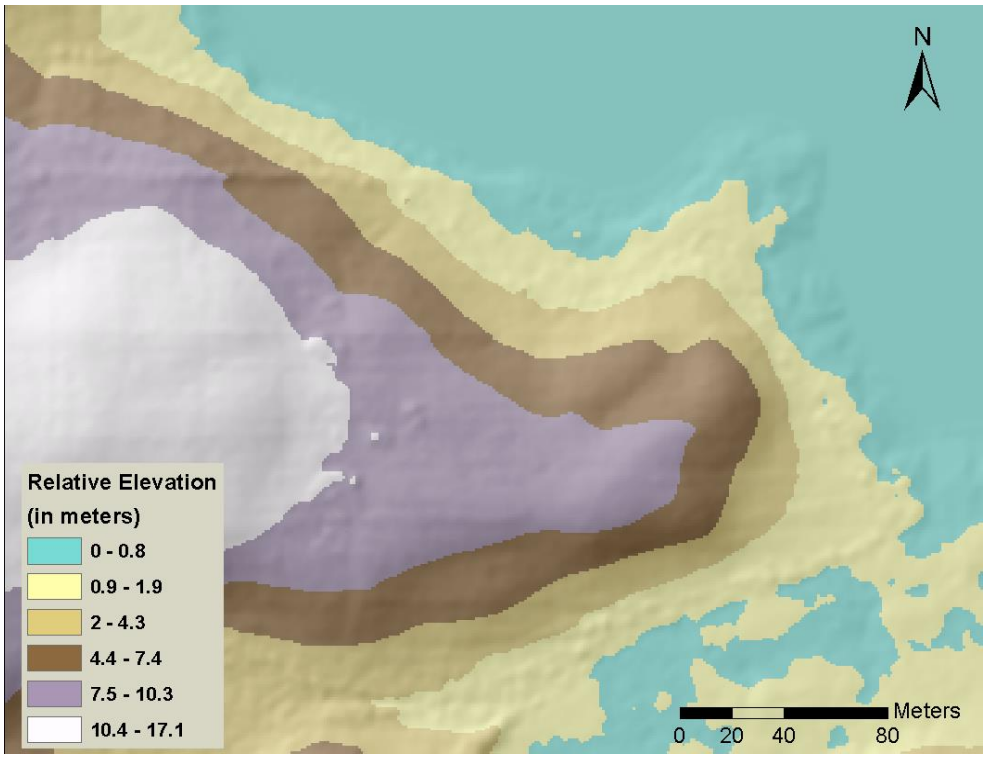

Figure 2.11 The distribution of relative elevation at the study area.

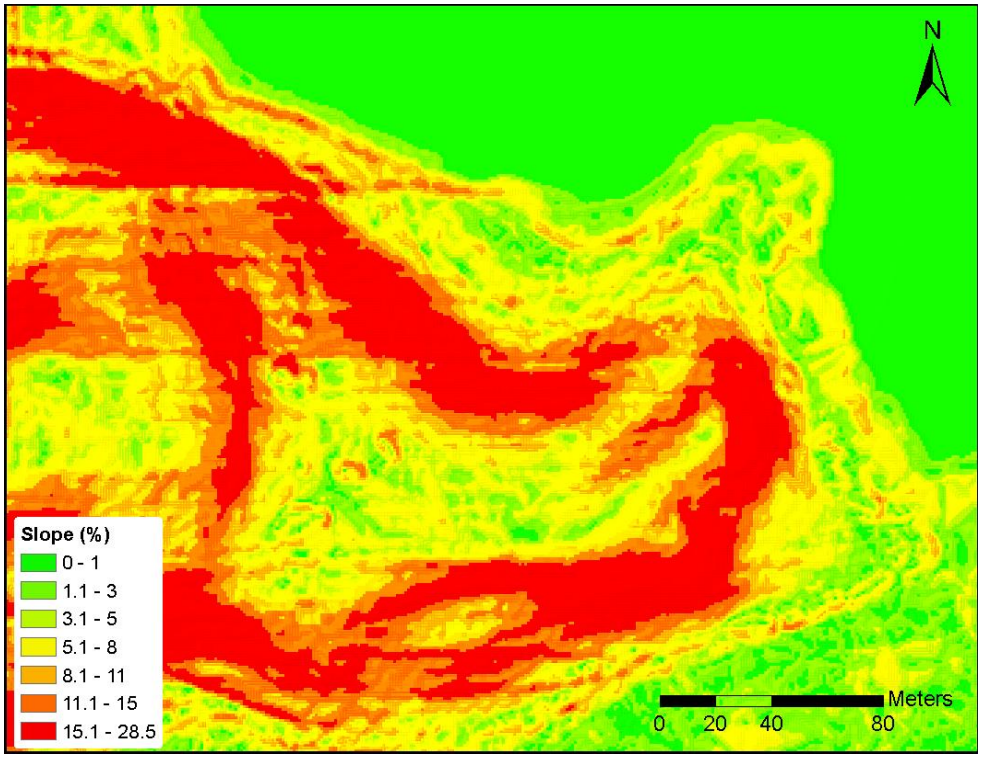

Figure 2.12 The spatial distribution of slope steepness at the study area.

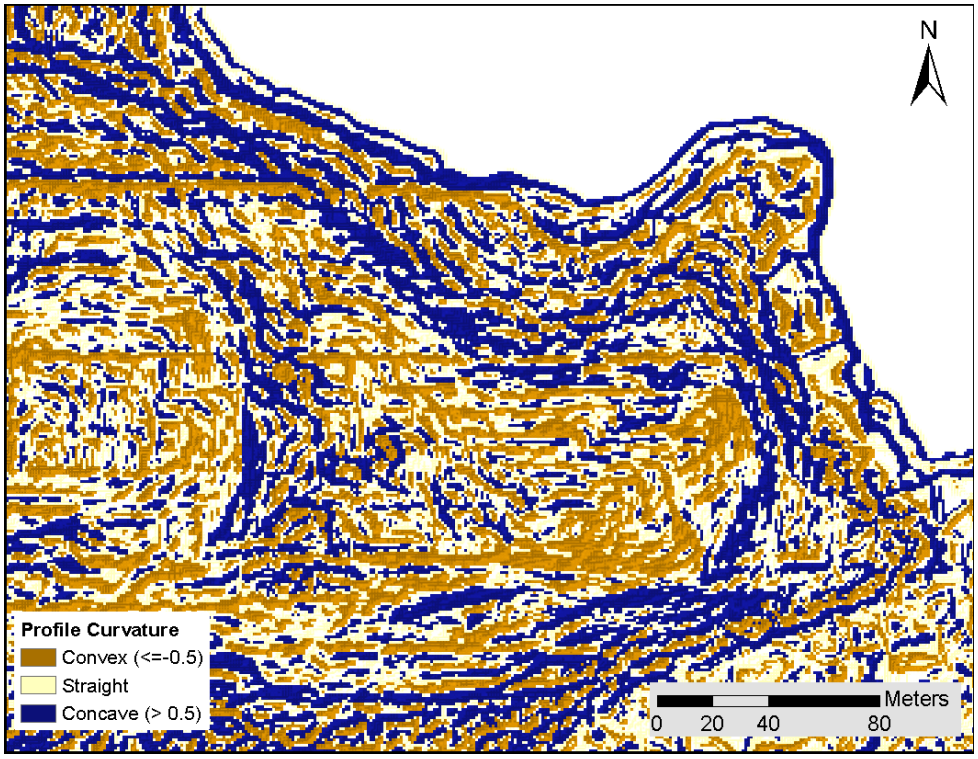

Figure 2.13 The spatial distribution of profile curvature at the study area.

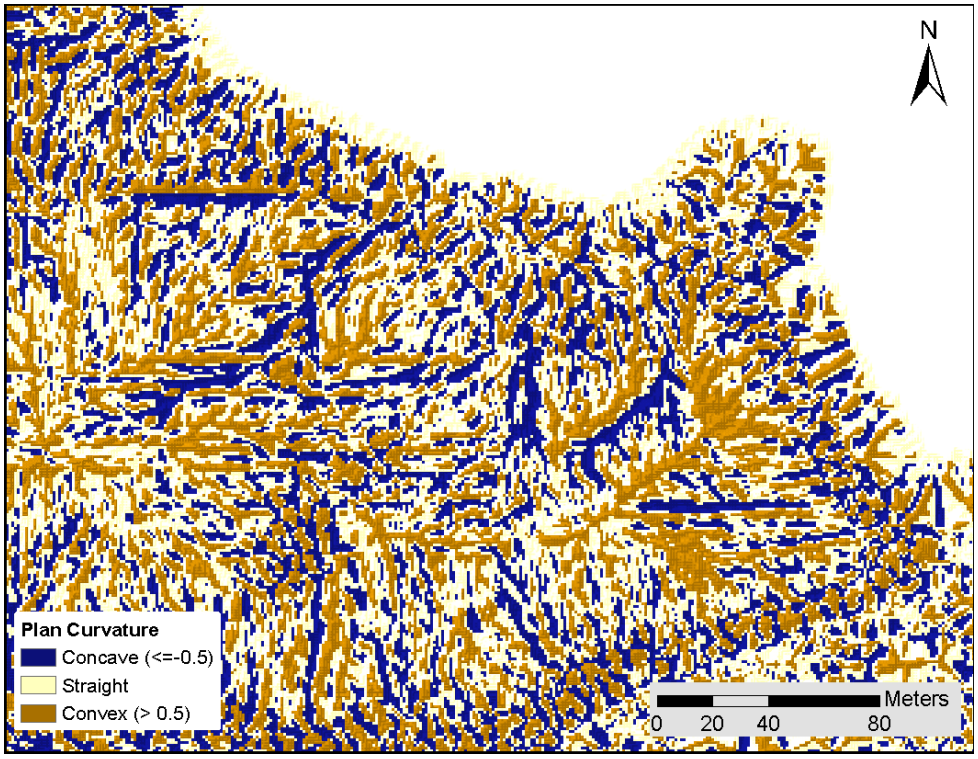

Figure 2.14 The spatial distribution of plan curvature at the study area.

The slope of profile curvature is illustrated in Figure 2.15. As expected, the patterns of this derivative of profile curvature show a change in the curvature toward the bottom of the hillslope. Some large rates of change of profile curvature can also be seen between two summits on the ridge top at the west-central part of the study area. Figure 2.16 is the flow-path-length map of the study area. The flow-path length ranges from 0 to 227 m and displays concentric circle patterns on the map. Note that flow-path length becomes random and problematic at the bottom of the hillslope where the flow disperses. The specific catchment area (SCA) in Figure 2.17 clearly illustrates the overland flow patterns. SCA ranges from 0 to 7,210 m^2. The CTI and SPI, the two indices derived from slope and SCA, are also displayed in Figure 2.18 and 2.19. The CTI, the wetness index, seems to emphasize major flow patterns similar to the SCA. The SPI map displays the stream power, which is very low in summit and toeslope positions.

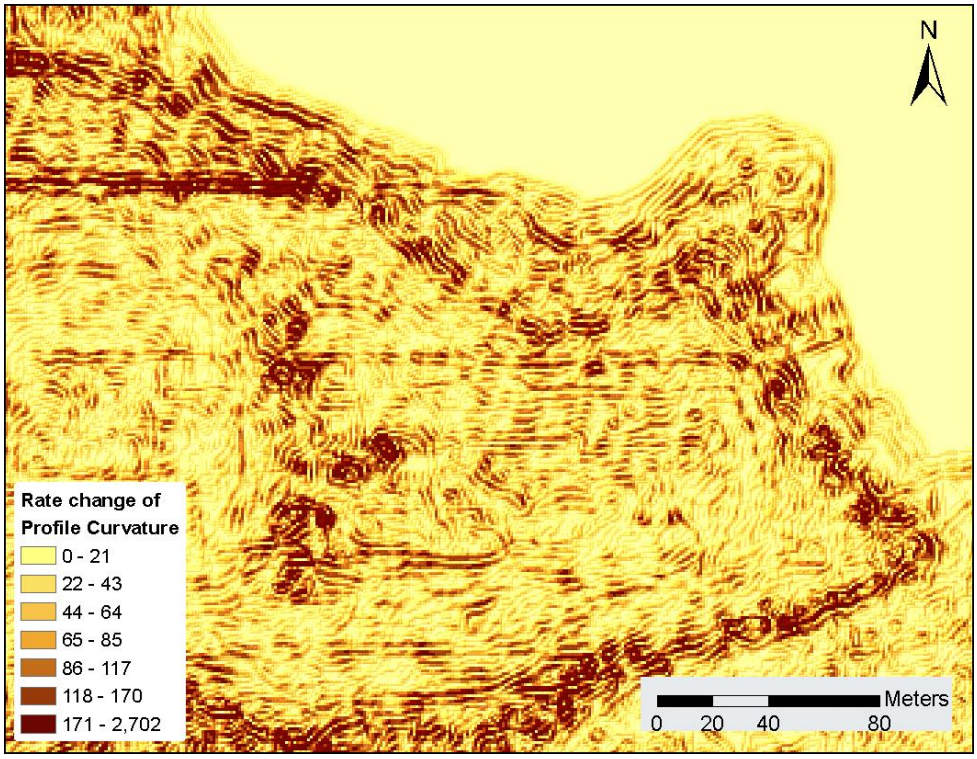

Figure 2.15 The rate change of profile curvature at the study area.

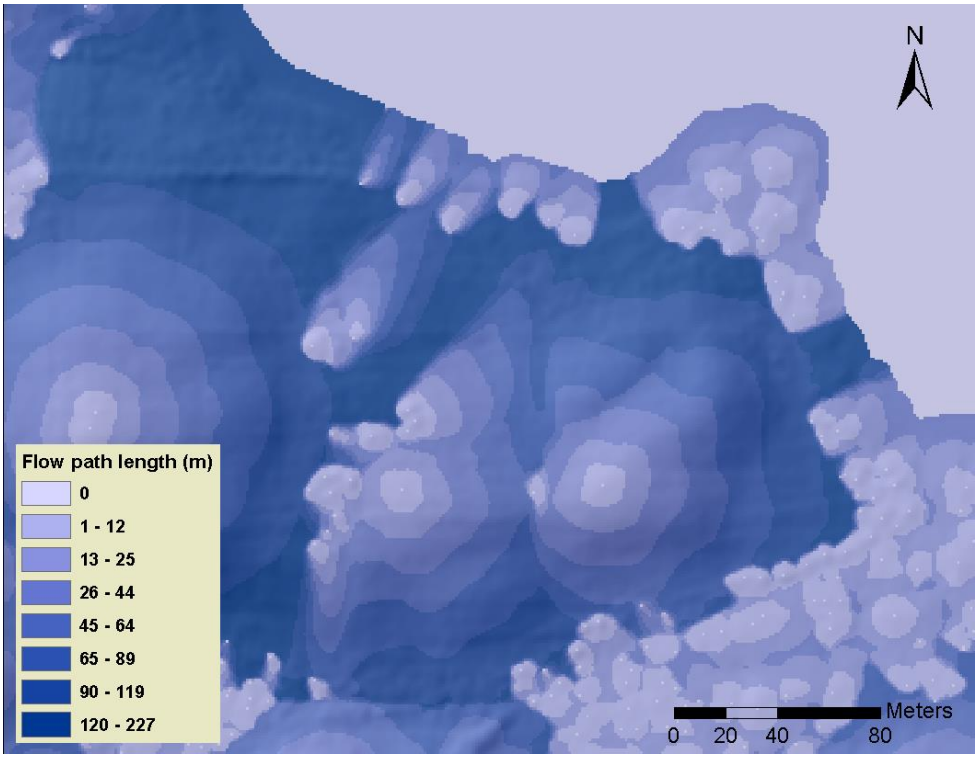

Figure 2.16 The map of flow-path length at the study area.

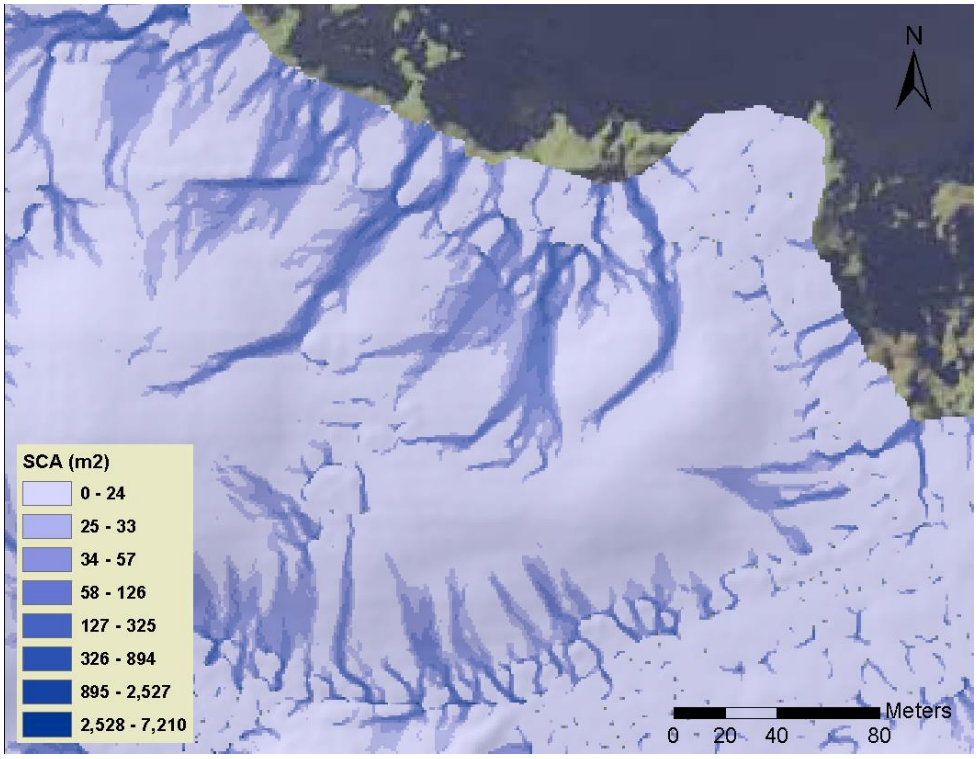

Figure 2.17 The map of specific catchment area at the study area.

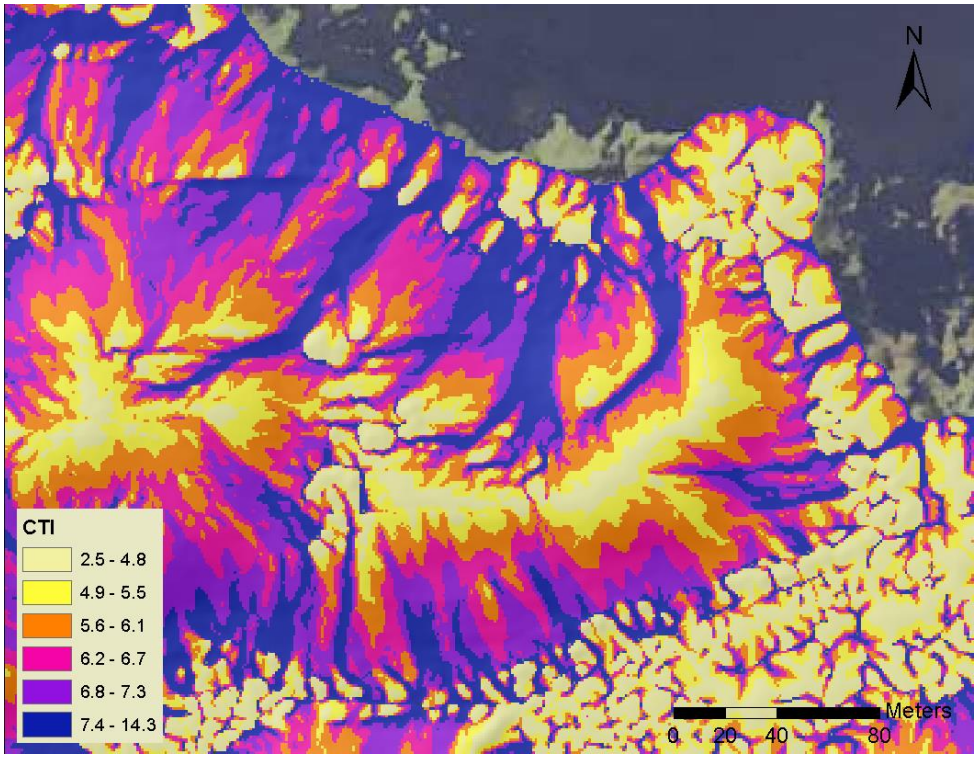

Figure 2.18 The map of compound topographic index (CTI) of the study area.

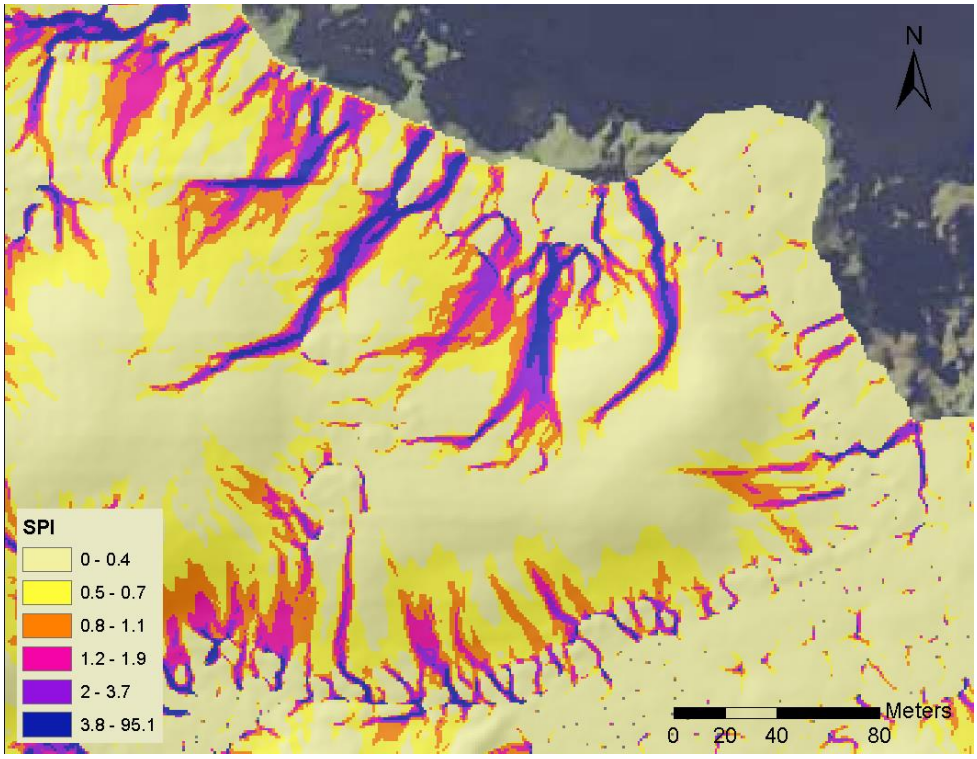

Figure 2.19 The spatial database of stream power index (SPI) at the study area.

As for regional terrain attributes, here I showcase the spatial distribution of slope and curvature at the UA for individual sample points in one transect (Figure 2.20 and Figure 2.21). Depending on samples' hillslope positions and landforms, upslope dependence areas vary in size and shape. The size of the UA increases as its elevation on the hillslope decreases. However, in Figure 2.21, the UA in a summit position is unexpectedly large. This error may have resulted from the sensitivity of the high-resolution source DEM; tiny surface changes on top of the hill were picked up during the UA processing.

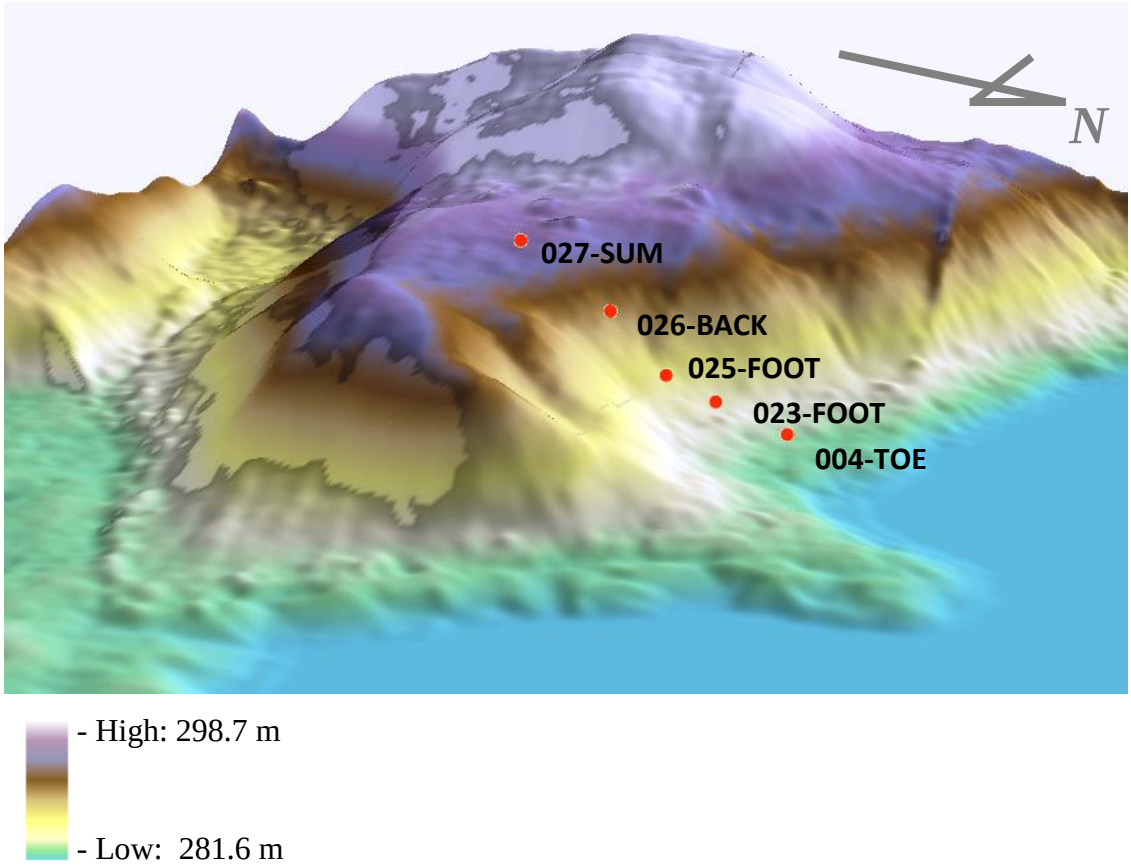

Figure 2.20 An example transect of sample locations at study site (with vertical exaggeration).

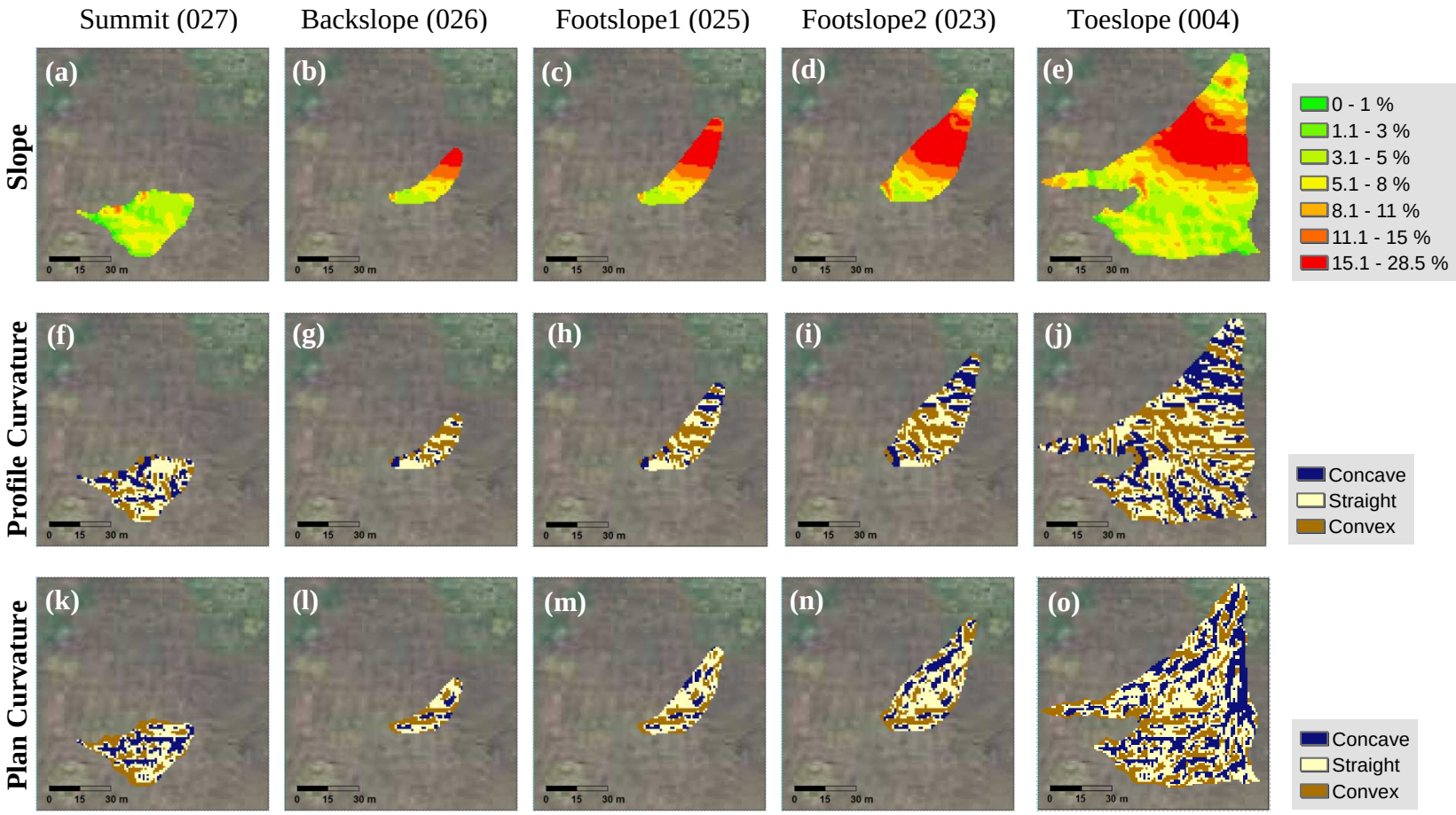

Figure 2.21 The spatial distribution of the upslope areas' slope and curvature grids at sample locations of a hillslope transect (shown in Figure 20).

As described in *Section 2.3*, the actual regional terrain attributes (UDTA) used in this study were developed using the UA terrain thresholds. The regional terrain attributes, defined by the UA slope and curvature thresholds in percentage (%) and in areas (m^2), were combined with local terrain attributes in building the explanatory PSA models.

Stage 1 analysis results: Logistic regression model for PSA presence

The best-fit logistic regression model for PSA presence prediction consists of the variables: relative elevation, flow path length, and stream power index (SPI) and can be defined with the following equation:

$$\text{logit (PSA presence)}_{\text{local}} = 17.27 - 4.39 * [\text{Relative elevation}] - 0.08 * [\text{Flow path length}] + 0.97 * [\text{SPI}] \quad (2.5)$$

This local PSA presence model has the lowest AIC of 29.6 and the highest pseudo R^2 of 85.8% compared to models built with other combination of terrain attributes. All partial regression coefficients and the logit model as a whole are significant at a confidence level of 90% (p-values < 0.10). A similar amount of variance can be explained by replacing SPI with CTI in the logistic regression model (AIC=30.342; pseudo R2 = 85.2%).

Compared to the predictive model Eq. (2.5) built with local terrain attributes, the best-fit explanatory Logit models for PSA presence increased pseudo R^2 by a mere 1.4% to 87.2%. The model for explanatory purpose is the mixed model consisting of both local and regional terrain attributes (UDTA). The mixed model has an AIC of 23.5 and consists

of two predictor variables, the relative elevation and the percentage of the upslope area with convex profile curvature:

$$\text{Logit(PSA Presence)}_{\text{mixed}} = 1.83 - 5.15 * [\text{Relative elevation}] + 0.28* [\%\text{upslope area in convex profile curvature}] \quad (2.6)$$

One of the mixed models that used three predictor variables (relative elevation, flow path length and % upslope area in concave profile curvature) performed slightly better (AIC =23.2; R^2 = 89%)**.** The mixed model in Eq. (2.6) has only two predictors so I chose it for its simplicity and the still outstanding model performance.

As for individual predictor variables, relative elevation is the single most significant terrain attribute for modeling the presence of PSA. When predicting PSA presence by relative elevation alone, I obtained the logit model results with an AIC of 37.72 and a pseudo R^2 about 75.3%. Measured by elevation difference from the minimum elevation in a 200-m radius local neighborhood, relative elevation is the quantitative measurement for hillslope positions, and thus provides information about distinct water accumulation and mass movement at each location on a catena. The negative relationship between relative elevation and PSA presence indicates that a lower hillslope position has a higher probability to contain PSA.

Besides relative elevation, flow path length and SPI are the terrain attributes controlling the presence of PSA in the landscape. Flow path length has a small and negative relationship with PSA presence. However, I hypothesized that the flow path length should have positive relationship with PSA presence. Conceptually, the longer the flow

path, the greater the overland flow accumulates at the sample location. Investigated visually on the spatial database, I found that the values of flow path lengths at toeslope locations abruptly decrease and then restart from zero (Figure 2.16). This demonstrates the inability of the current flow algorithms to handle depressional landscape properties. When water flows to the flat bottom of a hillslope the flow should be dispersed; current flow algorithms (e.g. F8, D-infinite, MFD and etc.) do not know how to assign values to flat zones. Nonetheless, flow path functions correctly in uplands and this method will still be used in the PSA modeling.

It is no surprise that SPI is one of the significant variables for predicting the spatial distribution of PSA presence. SPI displays the rate that flowing water's energy is expended in the landscape, so it represents the erosive power of overland flow (Moore et al 1993). CTI has a similar effect in combination with relative elevation and flow path length to PSA presence too. CTI categorizes the surface saturation zones and is known as the wetness index (Borough et al 1998). A site with a large CTI that accumulates surface water would be expected to be where sediments (PSA) deposit.

In terms of upslope terrain control, the mixed model Eq. (2.6) indicates that upslope profile curvature is a significant regional terrain attribute, and is a good predictor of PSA presence in a logistic regression when coupled with relative elevation. In fact, the regression analysis showed that the UA percentage in a convex profile curvature is the second most important terrain attribute (next to relative elevation) that drives PSA distribution in this landscape. Convex profile curvature in the UA is significant with a positive partial regression coefficient when coupled with relative elevation. This suggests

material is eroded where profile curvature is convex and this drives the downhill development of PSA in a catena.

This relationship can be also identified from the negative partial coefficient when choosing ‘upslope area percentage in concave profile curvature’ as the predictor variable (the model is not shown here). The UDTA-only models fit well using the variables UA with slope greater than 12% and UA with concave plan curvature. The positive partial coefficients of these predictor variables (not shown) indicate that steep slope angles and concave plan curvature in the UA drive the development of PSA. While steep slope triggering erosion is to be expected, I did not expect a positive relationship with concave plan curvature in the UA. I suspect that these areas of UA with concave plan curvature are cells right above sample locations where PSA is deposited. Further analysis is required to understand the details of UA terrain attribute distributions and their relationship to PSA development.

Based on the PSA presence model Eq. (2.5), I developed a probability map for the presence of PSA (Figure 2.22). Recall that logistic regression predicts the chance of a binary distribution (1 or 0), and the probability of the PSA presence can be predicted by converting the resulting odds ratio to the probability Eq (2.3). The probability map (Figure 2.22) clearly shows PSA being present at the bottom of the catena. The map also shows that PSA was completely absent in the uplands (0-10% probability, shown in blue). The zone with ≥ 90% probability of occurrence (shown in red) covers a broad area near the bottom of hillslopes. In comparison, the probability of PSA presence between these

extremes (10-90% probability) appears to cover a very narrow band on the hillslope. I used 90% probability as the threshold in determining where PSA is present.

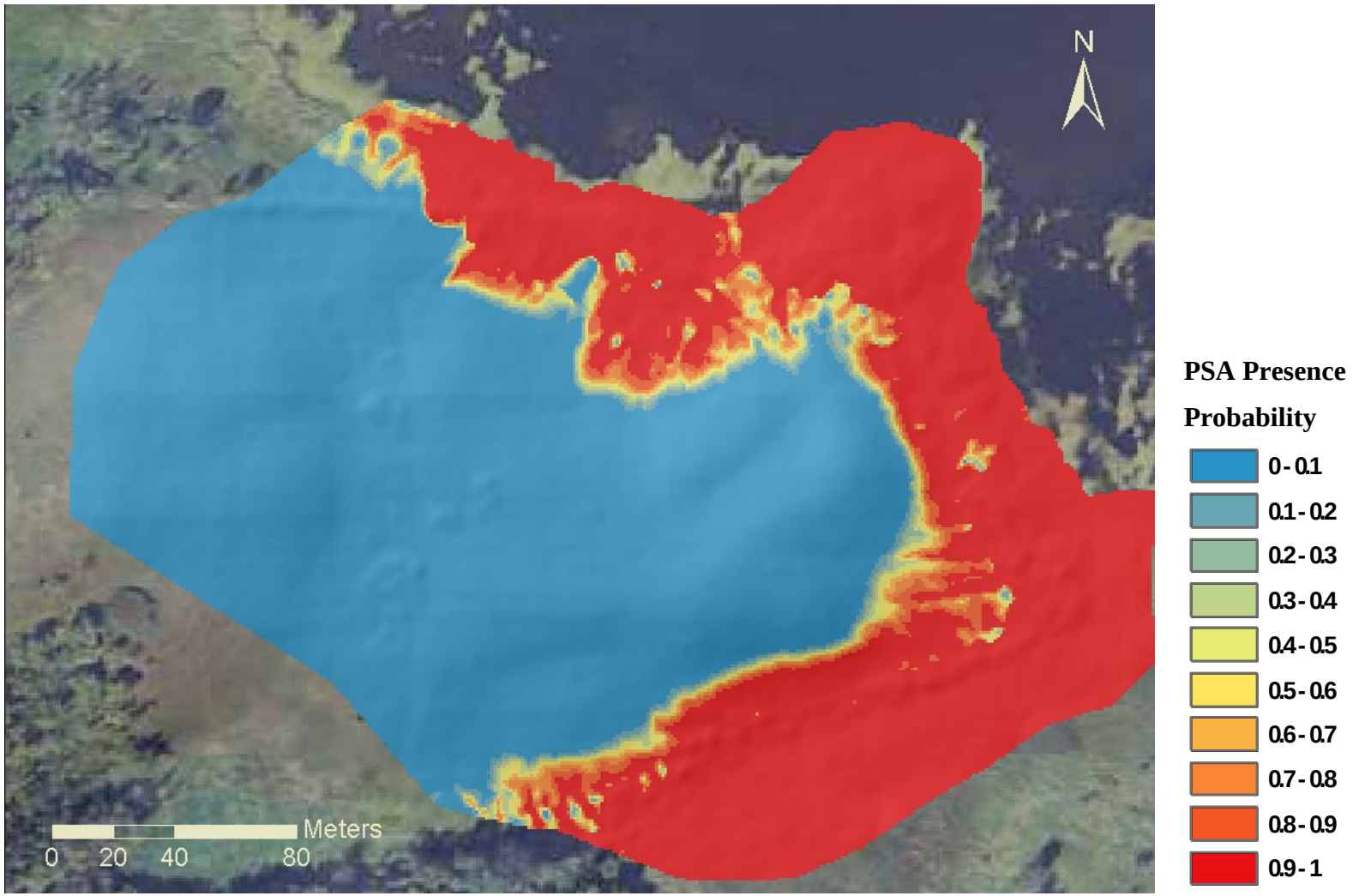

Figure 2.22 The predicted probability map for the presence of post-settlement alluvium.

During model evaluation, prediction accuracy and cross-validation both proved to be in good agreement for the PSA presence model selection (Table 2.4 and Table 2.5). Prediction accuracy was only tested for the predictive (local) model, not the explanatory one (the mixed model). Using 90% as the minimum acceptable probability to count on PSA presence, the overall correctness of the model is 86.9%, (Table 2.4). More specifically, the PSA presence model correctly predicted 96.6% of the PSA-absent samples and 78.1% of the samples with PSA present. As for the 10-fold cross-validation, the predictive and explanatory models of PSA presence both demonstrate very high estimated accuracies (88.5% and 90.7%, respectively) (Table 2.5).

Table 2.4 The percentage accuracy for the predictive model of PSA presence.

PSA presence	**Predicted (Prob. ≥ 90%)**			
Observed	**No (0)**	**Yes (1)**	**Total**	**% Correct**
No (0)	28	1	29	96.6
Yes(1)	7	25	32	78.1
Total	35	26	61	86.9

Table 2.5 The predictive and explanatory models for the PSA presence.

Stage 1 Regression Analysis	Predictor Variables	N	Pseudo R2	10-fold Cross-Validation Estimated Accuracy	
				Training	Validation
PSA Presence – Prediction (Local)	1) Relative Elevation 2) Stream Power Index 3) Flow Path Length	61	85.8%	0.918	0.885
PSA Presence – Explanatory (Mixed)	1) Relative Elevation 2) % Upslope Area with Convex Profile Curvature	54	87.2%	0.926	0.907

Stage 2 analysis results: Spatial prediction for PSA thickness

After matching sample locations with the spatial distribution of PSA presence (in the threshold of 90% probability), I reduced the sample number to 26 for Stage 2 analysis (Figure 2.23). The 26 samples, therefore, were all predicted to contain PSA (PSA thickness $\neq 0$). However, one of the selected samples (021-TOE) was not observed to have PSA (PSA thickness = 0). Overall, the PSA thickness ranges from 0 to 80 cm, with a mean of 45.81 cm and a standard deviation of 19.38 cm (Table 2.6). More than half of the samples used during Stage 1 analysis (PSA presence) were not included in Stage 2 (PSA thickness) since they fell out of the zone that has over 90% probability of PSA presence.

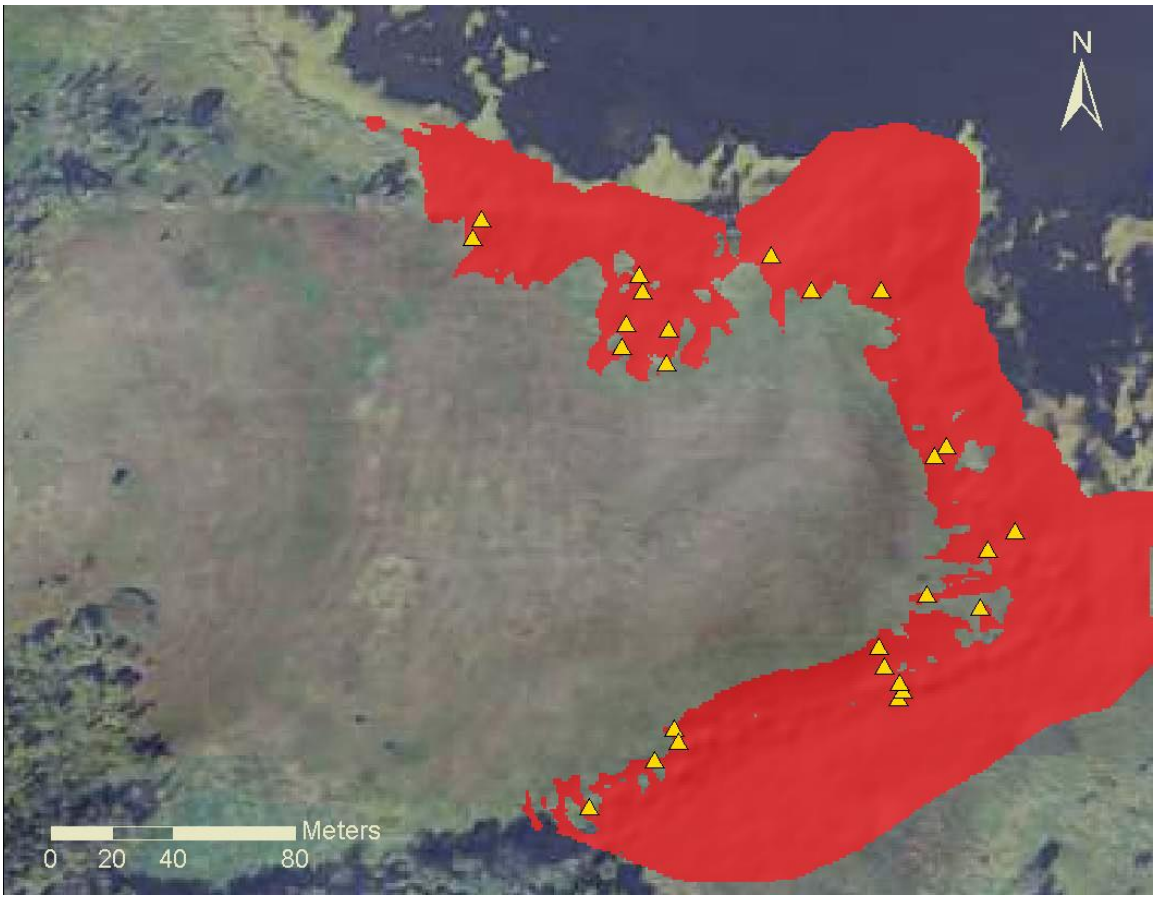

Figure 2.23 Samples contained in the area with over 90% probability of having PSA present were used for Stage 2 Analysis on PSA thickness.

Table 2.6 Summary statistics of PSA thickness for the samples spatially located within the predicted PSA-present area.

n	Mean	Standard deviation	Median	Min
26	45.81	19.38	44	0
Max	Range	Skewness	Kurtosis	Standard Error
80	0-80	0.05	-0.49	3.8

For the mixed model analysis, only 19 samples out of the 26 were used. I filtered out seven samples for Stage 2 analysis because their UA were too small (≤ 100) to be reasonable. The small UA size was likely caused by the source data (1-m LiDAR DEM) being highly sensitive to minor elevation variations in ground surface.

Using multiple linear regression, Stage 2 analysis developed the best-fit model for PSA thickness and it had two predictor variables: plan curvature in three classes, straight, concave and convex; and specific catchment area (in natural-log):

PSA thickness-local (cm) = 11.214 - 5.506 * [Concave Plan Curvature (categorical)] + 29.962 * [Convex Plan Curvature (categorical)] + 10.046* [Log-transformed Specific Catchment Area] (2.7)

This local PSA thickness model has an adjusted R^2 of 41.3% (p-value = 0.001975). This means that although plan curvature and SCA are the best variable selection among local

terrain attributes, only approximately 41% of variance in PSA thickness can be accounted for by this set of variables.

While plan curvature is a significant predictor for PSA thickness, it is only true for categorical values (convex, concave, and straight), not for numerical values. The numerical curvature data are not significant; the number distributions are not as related to PSA as when they were categorized into only three classes. A similar adjusted R^2 (41.6%) was found on another local model comprised of CTI, the rate change of profile curvature, and plan curvature. In comparison, Eq. (2.7) only uses two predictor variables, plan curvature and SCA. For simplicity, I chose the two-parameter model over the alternative.

Compared to the local model that has less than half of the variance accounted for (R^2 < 50%), the mixed and regional models do a much better job of explaining the variance in PSA thickness at the study site. The best-fit mixed models returned an adjusted R^2 of 73.8%, a 32% increase over the regional terrain attribute model. The overall best PSA thickness model is comprised of SCA (in natural log), the UA with 8-12 % slope, the percentage of the UA in flat profile curvature, and the percentage of the UA in flat plan curvature:

PSA Thickness-mixed (cm) = 52.35 + 10.11 * [Ln(SCA)] + 0.04 * [UA with 8 to 12% Slope] - 2.61 * [% UA in Flat Profile Curvature] + 1.12 * [% UA in Flat Plan Curvature] (2.8)

All partial regression coefficients in the mixed model are significant at the confidence level of 90%. As for the regional model, it returned a fairly high adjusted R^2 (67.5%)

using the predictor variables UA with medium slope steepness (6-12%), UA with straight profile curvature and UA with straight plan curvature (not shown here). While both regional and mixed models are significant and explained a high degree of the variance of PSA thickness, the sample size is small (n = 19), which could affect the model reliability.

The regression results match my expectation that the mixed model better captures the variance of PSA thickness than the local model. The adjusted R^2 increased from 41.3% in the local model to 73.8% in the mixed model. Plan curvature, both in local neighborhoods and in upslope areas, showed a strong influence in PSA accumulation.

While the UA plan curvature was expected to be significant in predicting PSA thickness, I did not expect the local plan curvature to be significant. Interestingly, the model results were contrary to this speculation based on what I know of soil morphological development. Overland flow converges where curvature is concave and I assumed that would results in soil deposition (PSA). However, the sign of the partial regression coefficient on plan curvature indicates the negative effect of concave plan curvature and the positive effect of convex plan curvature on PSA thickness. What I might have overlooked is the 'after-event' effect in the landscape. Soil deposition has already occurred, changing the shape of the landform over the past one hundred and seventy years. The positive contribution of convex plan curvature to PSA thickness reveals that convexity could be the result of, rather than the cause of, PSA accumulation. On the other hand, linearity and concavity in local plan curvature might just be indicators for where no PSA has accumulated.

It was not surprising that SCA (specific catchment area) is one of the significant predictor variables for PSA thickness. In fact, even though SCA was grouped as a local terrain attribute, it carries the characteristics of upslope topography. This is important for the purpose of PSA prediction because I cannot apply regional terrain attributes for the spatial prediction of PSA at this time. SCA involves an understanding of the amount of water flow along the UA; therefore, it is also an indication of how readily eroded materials can be collected and transported through the UA. This may also indicate that tillage erosion is not easy to separate from water erosion in the field.

The coupling of slope and CTI explained a similar amount of variance in PSA thickness as SCA coupled with plan curvature did. The wetness index CTI, which reflects deposition, was a significant predictor variable for PSA thickness as expected (not shown here). Both CTI and slope had positive partial regression coefficients and therefore positive contributions to the PSA accumulation.

The mixed model with the best goodness-of-fit for PSA thickness combined SCA as the local terrain attributes with regional terrain attributes. The model used SCA, UA with moderate slope (between 8 to 12%) and UA with flat curvatures (both profile and plan). Prior to modeling, I investigated slope steepness threshold used in literature and in field and the suggested slope, 4% or 6%, for landform changes is smaller than the resulting slope range (8-12%) (Brabyn, 1996; John Beck, personal communication, 2012). This slope difference may imply that the previous landform criteria should be limited to local neighborhood application and is not suitable for regional terrain categorization. The significance of moderately steep slope (8-12%) also suggests that slope angles in uplands

are most effective for erosion. While steeper slope increases soil loss, extreme steepness in slope (greater than 12%) may have caused eroded materials to move too fast to contribute to PSA accumulation in footslope and toeslope positions. Other significant regional terrain attributes related to PSA thickness (UA straight profile curvature and UA straight plan curvatures) were surprising. I suspect this is due to the definition of our upslope area curvature and has nothing to do with the straight surface being more important (than curved locations) in UA. As our spatial upslope curvature databases were made by clipping local curvature gridded data by the spatial extent of the UA raster database, the curvature values were simply calculated for individual grid cells in 1m-by-1m resolution, not the overall curvature of the entire upslope area. The significance of straight curvatures in UA, therefore, might simply indicate that continuous surfaces in UA are more beneficial for PSA deposition than the small curvature changes within individual cell extent.

As to model performance, the mixed model of PSA thickness has a higher accuracy and results in smaller predictive errors (Table 2.7) than the local model. The MAE and RMSE for the local model are 10.91 and 13.67, and those terms for the mixed model were 7.03 and 8.86, respectively. Residual plots, including the scatterplot and the normalized quantile-quantile plot (qqplot), can be found in Figure 2.24. The scatterplot shows the model residuals were overall randomly distributed with homoscedasticity, and qqplot shows the residuals being normally distributed. The model uncertainty may be higher than the error statistics (MAE, RMSE) discussed here due to the small sample size (n=26 for the local model, and n=19 for the mixed model). Model validation by the 10-

fold cross-validation method returned a slightly higher mean squared error (MSE) for the local model than the mixed model. The MSE of the cross-validation dataset are 261 in the local model and 132 in the mixed model (Table 2.7).

Table 2.7 Error analysis and validation for the PSA thickness models.

Stage 2 Regression Analysis	**Predictor variables**	**Variances explained**	**MAE***	**RMSE^**	**CVMSE^{+}**
PSA Thickness - Prediction	Plan curvature Ln-transformed SCA[1]	41.26%	10.91	13.67	261
PSA Thickness - Explanatory	Ln-transformed SCA UA with slope 8-12%[2] %UA with straight profile curvature %UA with straight plan curvature	72.6%	7.65	9.06	132

MAE* = mean absolute error

RMSE^= root mean squared error

CVMSE^{+}= the average of 10 mean squared errors in 10-fold cross-validation. The MSE is used as the estimated accuracy for the model.

[1] SCA = specific catchment area; [2] UA = upslope area

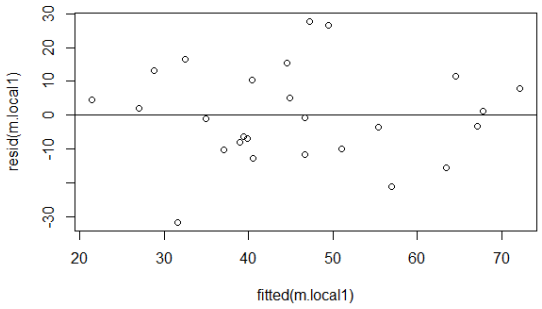

(a) Residual scatterplots, the local model

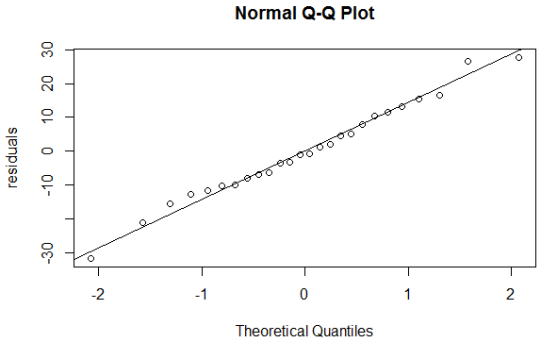

(b) Normal QQplot , the local model

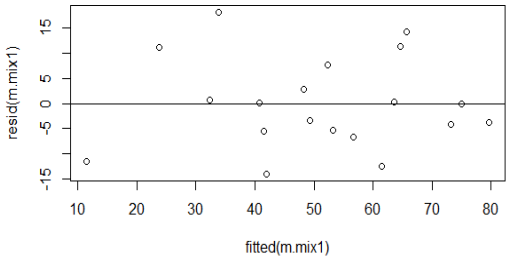

(c) Residual scatterplots, the mixed model

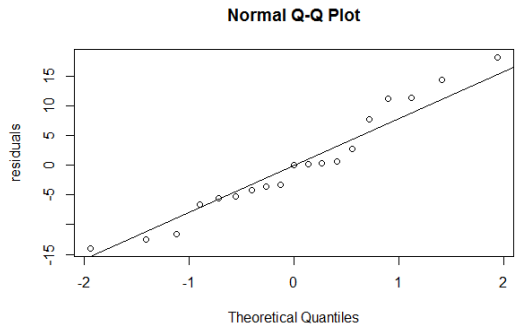

(d) Normal QQplot , the mixed model

Figure 2.24 Residual plots for the PSA thickness models.

From the model performance, I concluded that models based on a combination of significant local and regional terrain attributes would predict PSA thickness better than a model based on local terrain attributes only. The mixed model accounted for a higher proportion of variance and was more accurate than using the local model. Because regional terrain attributes were not developed for all cells across the entire study area, I could not apply this mixed model for the spatial prediction of PSA thickness. However, the mixed model demonstrated the importance of regional terrain attributes to land surface processes. Future development of the automation of regional terrain calculation will be beneficial to soil-landscape modeling. The automation process should help to efficiently generate regional terrain attributes for large areas of interests, and subsequently improve spatial prediction accuracies for soil-landscape modeling.

Spatial distribution and volume of PSA

The spatial distribution of PSA thickness was mapped in Figure 2.25. The resulting predicted PSA thickness ranges from -4.5 cm to 99.5 cm. Of the 61,250 cells, there are 17 cells fitted with negative values for PSA thickness. Because it is impossible to have negative values for soil thickness, I assigned these cells a PSA thickness value of 0. Because almost all erroneous cells are spatially separate from each other, I speculate that these negative values likely result from source data; the ill-predicted cells also have similar landscape characteristics, flat profile curvature, flat plan curvature and a specific catchment area smaller than 1 m^2.

While all cells predicted with PSA present are located on lower hillslopes, Figure 2.25 shows the local variance of PSA thickness among these positions. In general, PSA thickness is moderately high (41-60 cm thick) at footslope positions, and ranges from moderate (21-40 cm) to low (0-20 cm) at toeslope positions. This confirms my conceptual model that the eroded materials are first deposited on upper footslope positions where overland flow loses its momentum due to the topography change from steeper and convex terrain in catena above. Thicker PSA (up to 99.5 cm) is found in the northern part of the study area. PSA accumulation is generally smaller, about 0-40 cm thick, in the northeast of the site where the land is flat and stretches into the permanently saturated pond. The spatial distribution of PSA in the south to southeast is more uniform; its footslope positions are generally comprised of a higher accumulation of PSA compared to the toeslope positions. This spatial distribution map of PSA thickness shows that soil erosion and deposition can have significant variance even in a small depressional landscape, and my terrain modeling allows me to predict this variance.

Based on the two-stage regression analysis results, I estimated the volume of the PSA using the area of PSA presence and the depth of PSA accumulation. For the total area of 61,250 m^2 at the Lake Rebecca site, PSA is estimated to be present in 11,798 m^2. Combining the spatial prediction of PSA thickness at the PSA-present area, I calculated the volume of PSA to be 8082 m^3.

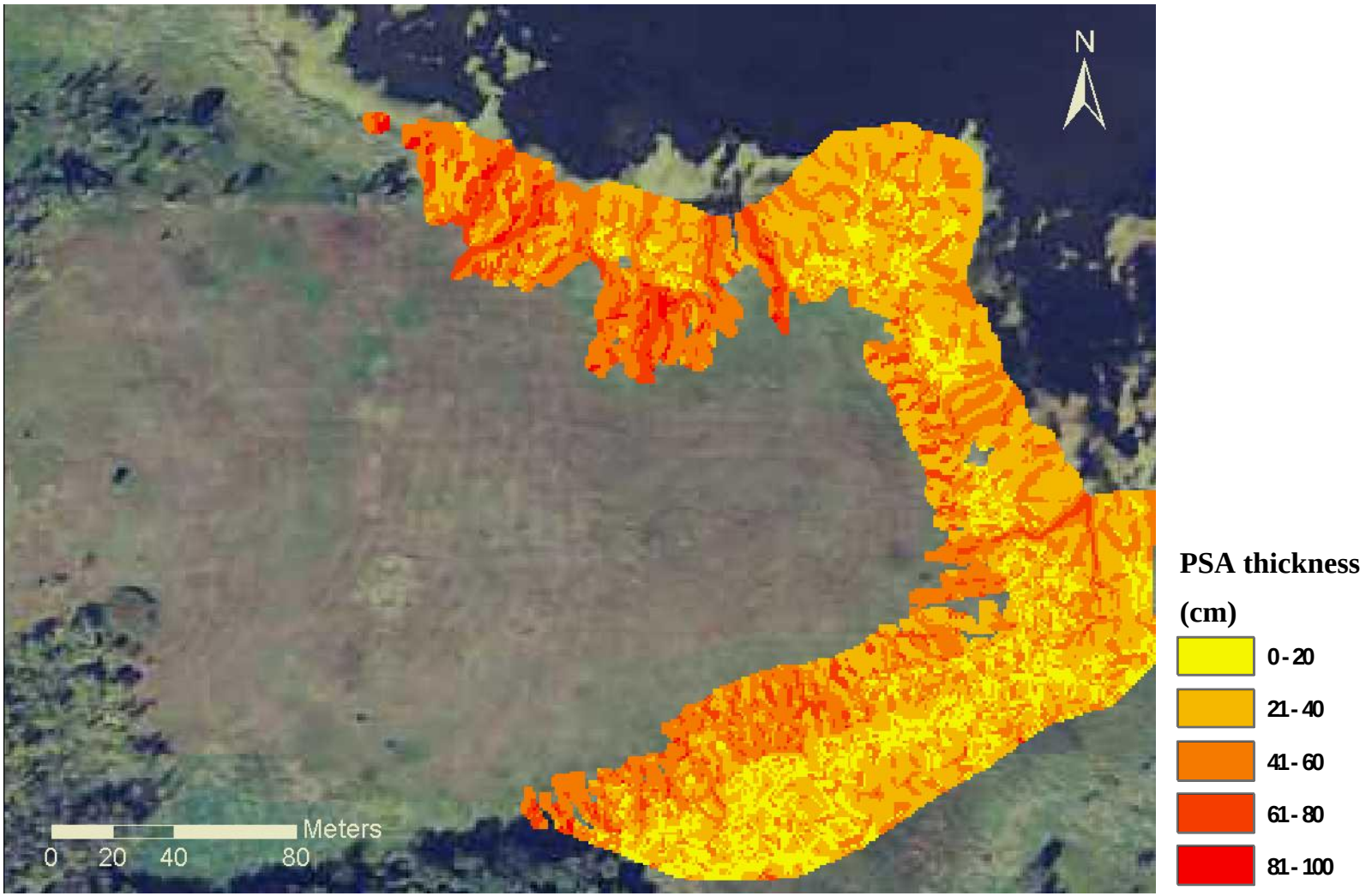

Figure 2.25 The predicted spatial distribution of post-settlement alluvium for the study area.

2.5 Conclusion

The spatial study of PSA at a study area in Lake Rebecca Park Reserve, Minnesota demonstrates the spatial distribution of PSA, its areal extent and depth. My observations at this site confirm that PSA is spatially present on the footslope and toeslope positions in the catena of this landscape. This model can be applied to similar depressional landscapes along the margins of the former Des Moines lobe in south-central Minnesota.

Regional terrain attributes, developed from terrain attributes in upslope areas, prove to be valuable predictors for PSA thickness, and thus are effective terrain controls on the formation of PSA. The performance of the mixed models (the combination of local and regional terrain attributes) shows that both local and regional terrain attributes are significant for erosional and depositional processes in a depressional landscape Specifically, the results from this two-stage regression analysis clearly indicate that local attributes (e.g. relative elevation) are topographic drivers for the presence (or absence) of PSA, and regional terrain attributes are more important in predicting the thickness of PSA in those areas where it is deposited. The development of regional terrain attributes in this study is not only useful for PSA modeling, but it is beneficial for future soil pedology studies in providing a better understanding of the relationships between topography and other landscape soil properties and processes.

Unfortunately, the results of PSA modeling do not allow me to separate the influence of erosion and deposition in determining PSA distribution. A future direction including

upland erosion modeling or simulation will further the understanding of landscape evolution from erosion and deposition.

The spatial prediction of post-settlement alluvium is beneficial for earth scientists to understand the effect of agricultural soil erosion and redistribution since settlement. The PSA models can be coupled with soil carbon data to better predict carbon dynamics, and to evaluate C feedback under the impact of agriculture-induced redistribution in similar landscape settings and land history in this region.

Chapter 3

The spatial prediction of soil organic carbon in Lake Rebecca Park Reserve, Minnesota

3.1 Introduction

Soil is an important carbon (C) reservoir. Globally soil organic carbon (SOC) is estimated to be around 1500-1600 Pg in the uppermost meter of soil, and may be up to 56% more in the top three meters (Amundson, 2001; Jobbagy & Jackson, 2000). As anthropogenic activities continuously increase C emissions and contribute to the unprecedented high carbon dioxide level in the atmosphere, it is essential to protect this large C reservoir and prevent it from being destroyed (Ciais et al., 2013).

To protect C in the soil, it is essential to identify SOC distribution spatially and quantitatively, and its fate under anthropogenic disturbances. Stallard (1998) pointed out that the maximum C sequestration strength induced by human activities occurs in the northern temperate zones in latitudes between 40º N to 50 º N. Within this northern temperate region, freshwater wetlands in closed-depressional landscapes consist of high net primary productivity (NPP) and slow C decomposition due to their long periods of anaerobic conditions, and are expected to store a large quantity of SOC (Bedard-Haughn et al. 2006). The majority of landscape SOC studies, however, have been concentrated only in uplands, and excluded wetlands as a part of the catena. The goal of this study is to predict the spatial distribution of SOC in a depressional landscape. The objectives of this chapter are:

1. To develop spatial predictive models for SOC in depth layers in Lake Rebecca Park Reserve in depressional landscapes of Minnesota;

2. To understand the spatial variability of SOC and the relationship between SOC and terrain attributes; and

3. To estimate the quantity of SOC storage in the top 1 meter of soil at Lake Rebecca site.

I develop a simple yet representative spatial model to capture landscape heterogeneity of SOC in a depressional landscape in Minnesota. I hypothesize that landscape-scale SOC distribution is driven by pedogenic processes and can be predicted by appropriate terrain attributes using a multiple regression method. I expect the terrain attributes that best represent landscape-scale pedogenic processes to include relative elevation, compound terrain index (CTI) and (concave) profile and plan curvatures. Relative elevation captures overall landscape surface process information, such as soil erosion and deposition, on a soil hillslope, whereas CTI and curvatures indicate soil wetness and sediment accumulation capacity (Thompson et al., 2006; Yoo et al., 2006).

3.2 Site description

The study was conducted at Lake Rebecca Park Reserve in Hennepin County, Minnesota (Figure 2.2). The central feature of the study area is a gently rolling hill (93.752W, 45.053N) surrounded by closed depressional wetlands. The landscapes in this area were formed by the Des Moines lobe glacier, the last major glacial advance in North America,

that retreated about 11,700 radiocarbon years before present (ybp). The parent material at the Lake Rebecca site is unsorted Des Moines lobe till.

The soils at the Lake Rebecca site are loamy to fine-loamy and feature a thick, dark A horizon with high organic matter contents. Although deciduous hardwoods like *Aceraceae* and *Fagaceae* dominated the pre-settlement vegetation, the dry Hypsithermal climate in the middle Holocene (~7,000 to 5,000 ybp) has likely provided a prairie environment for the thick, dark Mollic epipedon to form in this forest soil (Anderson et al., 1984; Wright Jr., 1976; Wright Jr., 1992). The upland soils are mainly Lester series (Fine-loamy, mixed, superactive, mesic Molic Hapludalfs), with Hamel series (Fine-loamy, mixed, superactive, mesic Typic Argiaquolls) in the footslope and toeslope positions. The center of the wetland is comprised of organic matter-rich Klossner (Loamy, mixed, euic, mesic Terric Haplosaprists) and Houghton (Euic, mesic Typic Haplosaprists) series (Soil Survey Staff, 2013).

The Lake Rebecca site was settled and farmed in the early 1840s. It was converted from agriculture to grassland in the early 1970s (Marschner, 1974; Larry Gillette, personal communication, 2009) when the land was purchased as a part of the Lake Rebecca Park Reserve for recreational use. The Kasma Marsh, the wetland north of the hill, was plowed and farmed during the drought years of the 1930s, but returned to being seasonally flooded after the 1950s (see the time-series of aerial photos in Figure 2.3). The elevation range on the site is 279m to 300m above mean sea level, and the climate is a typical subhumid, midcontinent condition with annual precipitation of 691mm. Not including the

Kasma Marsh or the wetland in the south, the Lake Rebecca site is around 6 hectares in size.

3.3 Methods

Soil sampling and carbon measurement

I described soil profiles and collected bulk soil samples at a total of 71 locations at the Lake Rebecca site (Figure 3.1). Of the total samples, 36 were taken with a stratified-gradient approach on 6 transects, following hillslope positions – summit, shoulder, backslope, footslope, and toeslope (or wetland) across the entire hillslope during the growing seasons of 2009-2010. The transects were positioned to cover a diverse range of curvatures, slope length and steepness in the landscape. Because my ultimate interest is to understand the influence of post-settlement alluvium (or PSA, the agriculture-induced soil redistribution) to SOC, during 2010-2011 I collected the rest of my soil samples with the same protocol but focused only on lower hillslope positions (i.e. footslope and toeslope positions) to better capture PSA distribution and thickness. Each sample location was georeferenced by a differential Global Positioning System (GPS) device (Magellan® MobileMapper™ 6) and post-processed to sub-meter accuracy as soon as I returned from the field in the Soil and Landscape Analysis Laboratory in the Department of Soil, Water, and Climate at University of Minnesota.

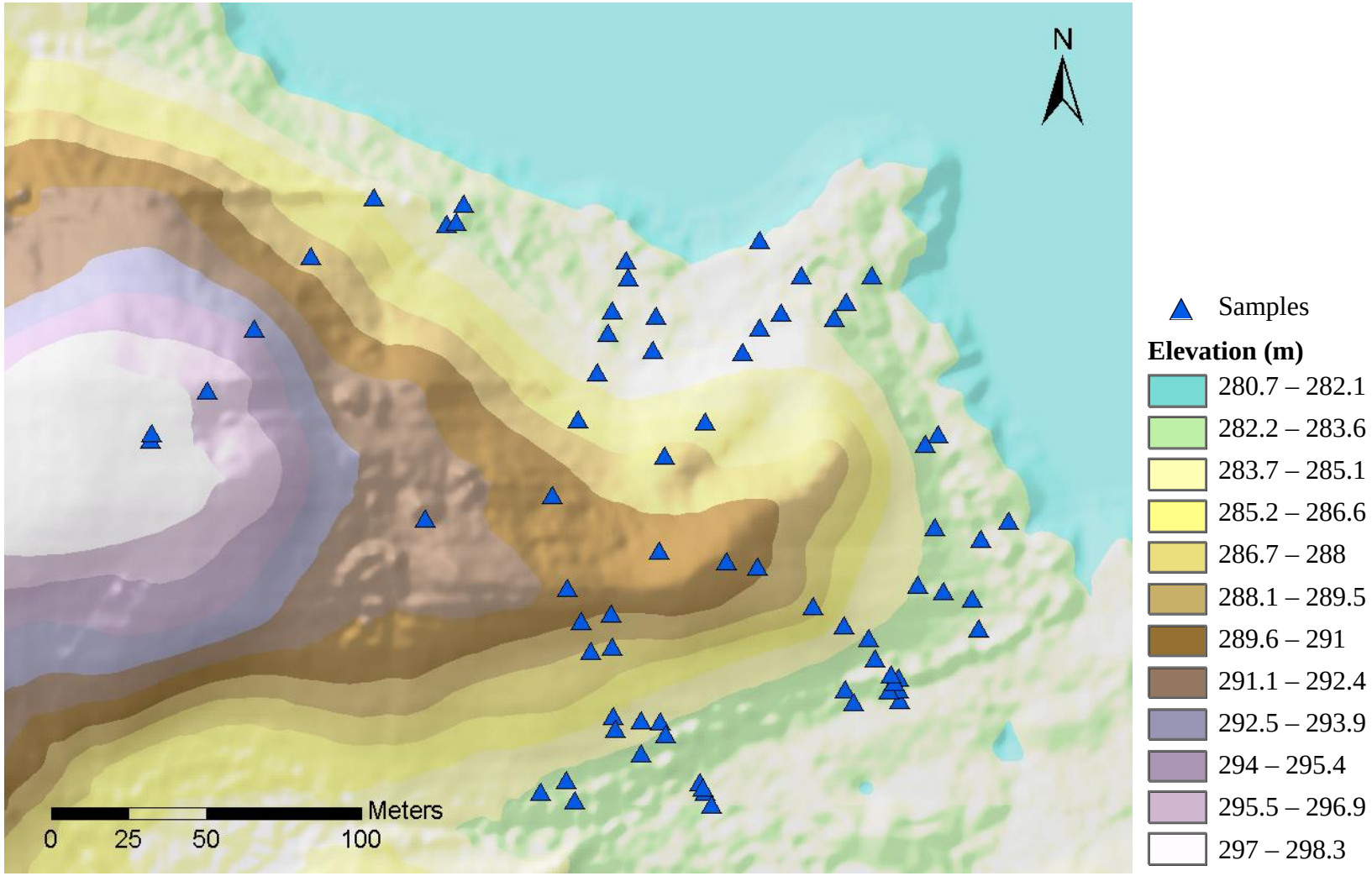

Figure 3.1 Sampling locations for soil carbon modeling at the Lake Rebecca study site.

At each sampling location, a continuous soil profile was excavated by auger boring to the first layer of carbonates. The sampling depth is typically over 1m deep, but could be less when encountering restrictive conditions (e.g. rocks, water table or hard clayey soils). The horizon-based profile description included soil depth, soil color, soil texture, soil structure and consistence, rock fragment content, and a description of redoxmorphic features. In addition to these properties, I also recorded soil morphological features that are important to soil carbon in this landscape when available, including presence of carbonates, depth to water table, and PSA presence and thickness. Carbonate presence was tested by the effervescence field method using 10% hydrochloric acid (HCl), and PSA presence was determined based on the observation of differences between PSA and its underlying darker-colored and better-structured buried horizons (Ab). A more detailed description of PSA identification can be found in *Section 2.3*.

I collected one composite soil sample for each described horizon of all sample locations, and carefully transferred all samples to the laboratory where they were air-dried for 3 days. Soil samples were also collected in surface A and subsurface B horizons in various hillslope positions for dry bulk density (BD) measurement. Mineral soil BD samples were collected in the 5-cm diameter, 5-cm deep soil ring (the ring method). As to organic soil horizons, BD samples were gathered by the 'scoop and fill' method. Unlike the ring method, the 'scoop and fill' method obtained the sample volume by filling in the scooped-out hole (about 200g) with standard fine sand. A graduated cylinder was used to measure the volume of sand required to fill the hole. After sampling, I followed the method in the Soil Survey Laboratory Methods Manual to obtain dry BD values for the

soil samples (Burt, 2004). The calculation of the sample BD was oven-dry sample weight (g) divided by sample volume (cm^3).

The air-dried soil samples were ground, sieved to exclude particle size fractions >2 mm, and treated to remove carbonates in preparation for SOC measurement. The samples with carbonates observed in the field testing were treated by acid fumigation for inorganic carbon removal (Harris et al., 2001). Several samples contained residual carbonates after acid fumigation and were treated with 0.5M HCl in a heated bath to completely remove carbonates before SOC measurement.

Once the samples were free of carbonates, I measured SOC contents for all of the soil samples using an automated dry combustion method with a CN analyzer (Elementar© Vario MAX). The automated dry combustion is the standard, and by far the most reliable and precise approach for soil C measurement (Chatterjee and Lal, 2009). A 10% duplication rate was applied for C measurements. Before the CN analyzer was available in 2010, I estimated my samples' SOC contents from organic matter (OM) contents measured by Loss-On-Ignition (LOI). LOI is an inexpensive method for OM measurement by calculating mass change before and after samples are heated overnight in a muffle furnace at 450°C (Burt, 2004). While most samples' SOC were directly measured again using the CN analyzer, I was unable to recover samples from a total of six horizons at two sample locations. The SOC for these samples were estimated by the LOI method using conversion factors calculated from the samples with both OC and OM measurements. The conversion factor was 0.44 for surficial A horizons, 0.38 for buried A horizons (Ab), and 0.32 for subsurface horizons. These values are lower than the

common conversion factor of 0.58 as well as the newly suggested factor of 0.5 for this region (Pribyl, 2010).

Mass-based (kg/kg) SOC measurements were converted to volumetric (g/cm^3) SOC content (Mäkipää et al.,2012):

$$C_v = \left(\frac{C_m}{100}\right) * \rho_b * 1000 \quad (3.1)$$

where C_v is the volumetric SOC content (kg C $\cdot$ m^{-3}) of a horizon, C_m is the mass-based SOC content (%, or kg C $\cdot$ kg^{-1}), ρ_b is the composite, representative bulk density (or BD, in g $\cdot$ cm^{-3}) at corresponding hillslope positions and horizons (Table 3.1) with a multiplier 1000 to convert to units of kg $\cdot$ m^{-3} (Kempen et al., 2011). Because of distinctive soil characteristics in uplands versus wetlands, I grouped the BD values into these two groups (Figure 3.2). Although it would be ideal to obtain a BD at every single sampling location, my resources were limited. Composite BD for my samples in similar horizons and landscape positions is the approach I could afford, and was verified with the BD values of their matching soil types and depths in Web Soil Survey (Soil Survey Staff, 2013).

Table 3.1 Composite dry bulk density measurements used for carbon unit conversion.

Sampling locations and horizon designation		Average Dry Bulk Density (g/cm^3)	Other Horizons Using the Bulk Density
Hillslope Position(s)	Composite Layer		
Upland	A1	1.086	
Upland	A2, AB	1.364	A3, ABb and AC
Upland	B and below	1.494	Bb, Cb
Upland	Ab	1.24	Ab1, Ab2,...Ab(n)
Wetlands (toeslope/depressions)	Oe, Oi	0.492	Other surface layers with C over 12%
Wetlands	Oa	0.727	
Wetlands	A1	0.944	
Wetlands	A2, AB	1.234	ABb; also AC above 60cm
Wetlands	Buried O horizons	0.559*	
Wetlands	Ab	1.092	
Wetlands	B and below	1.484	Bb, Cb; also AC or ACb below 60cm

*Estimated bulk density (BD) value. Considering post-settlement deposition (PSA) would cause compaction of the underneath (buried) horizons and increase their BD values. I assume that the rate of BD increase between unburied vs. buried organic horizons (OC > 12%) are the same as that between unburied vs buried mineral horizons: (Ab-A1)/Ab = 0.136. The buried O horizon was estimated as: 0.492 * (1+0.136) = 0.559 (g/cm^3).

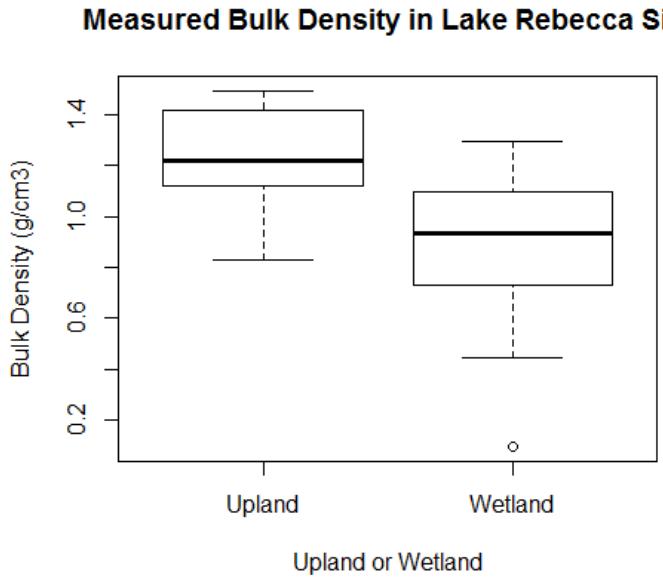

Figure 3.2 Two distinct distributions in measured soil bulk density values at Lake Rebecca site.

In order to model SOC across the entire landscape, I used equal-area quadratic smoothing spline (EAQSS) (Malone et al. 2009, Bishop et al. 1999) to convert my horizon-based bulk SOC measurements into fixed-depth readings in each soil profile. While the horizon-based soil data preserves similar morphological features in a depth profile, my intent to spatially interpolate SOC in various depths requires consistent depth measurements across all sample locations. The EAQSS is a mass-preserving depth function developed by Ponce-Hernandez et al. (1986) and improved by Bishop et al. (1999) to derive continuous soil attributes in a depth profile (Malone et al., 2009). It is assumed that true attribute values represented by a function *f(x)* vary smoothly with depth x, and horizon-based measurements reflect the mean attribute value ($\overline{f_i}$) of the layer i

with the depth interval (x_{i-1}, x_i) and the measurement error e (that has the mean of 0 and a common variance σ^2):

$$y_i = \overline{f_i} + e_i \tag{3.2}$$

Using the spline function, f(x) at any specific depth x can be minimized to

$$\frac{1}{n}\sum_{i=1}^{n}(y_i - \overline{f_i})^2 + \lambda \int_{x_0}^{x_n}[f'(x)]^2\, dx \tag{3.3}$$

The first part of the above spline equation is the fitted value at layer i over the total of n layers in the depth profile, and the second part of the equation is the roughness of the function *f(x)* (Malone et al., 2009). λ is the smoothing parameter that controls trade-offs between the fitted value and the roughness penalty. The EAQSS has accurately represented SOC in depth profiles and has been used in several recent landscape soil property studies (Malone et al., 2009; Adhikari et al., 2012 ; Malone et al 2011, Odgers et al., 2012).

I acquired smoothed SOC profiles using the EAQSS function with λ of 0.1, the value recommended in the literature (Bishop et al., 1999; Malone et al., 2009), and retrieved the EAQSS-estimated SOC to four fixed depths: 0-10 cm, 10-30 cm, 30-60 cm, and 60-100 cm using Spline Tool v2.0. The depth intervals were chosen based on the general vertical distribution of soil morphological features within the study area. Modeling SOC data in four depth layers allows me to identify the types and weights of terrain attributes affecting SOC at each depth, and to accurately predict the 1-m SOC distribution and quantity in the landscape. Spline Tool v2.0, a computer application developed by the

Commonwealth Scientific and Industrial Research Organisation (CSIRO) of Australia, was used to fit the volumetric SOC contents ($kg \cdot m^{-3}$) of my sample data per centimeter for the top 1 meter, and to subsequently obtain the mean SOC for the desired depth layers from the spline-estimated SOC (Australian Soil Resource Information, 2011). Figure 3.3 shows an example of fitting a spline depth function to a horizon-based SOC profile.

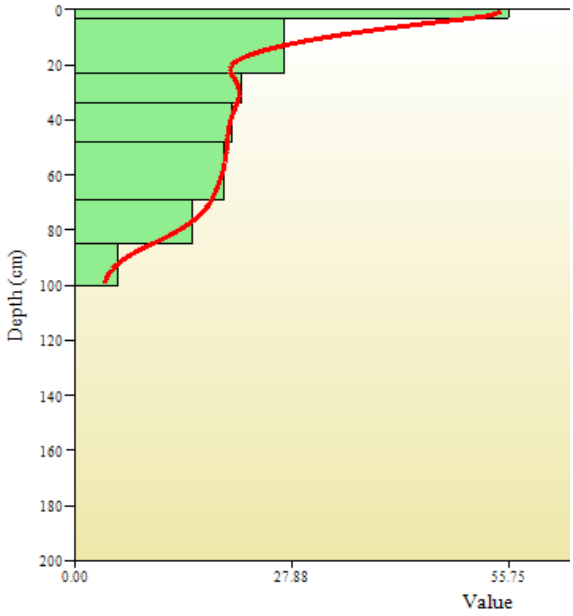

Figure 3.3 The equal-area quadratic smoothing spline function (in a red line) was used to fit a horizon-based soil carbon profile ($kg \cdot m^{-3}$) (in green columns).

The resulting database contained a SOC content value for each fixed-depth layer at each sample location. I applied a 30% missing data allowance rule to every fixed-depth layer data (Table 3.2). This means, that SOC observations should cover at least 70% of depth intervals, or the splined OC contents at that layer would be eliminated prior to spatial

prediction. The EAQSS function generally predicts depth profiles well (most mean squared errors (MSE) were estimated to be far less than 1 $kg \cdot m^{-3}$), but had more uncertainties when the attribute values (i.e. SOC) in soil profiles did not decrease over depths (e.g. profiles with buried Ab layers, in my case). The averaged MSE in my samples is 4.19 ($kg \cdot m^{-3}$).

Table 3.2 Soil carbon data missing criteria for source data use in regression analysis.

Depth Layer (cm)	Interval (cm)	Missing allowance	Missing allowance in depth (cm)	Depth required for analysis (cm)
0 - 10	10	0.3	3	7
10 - 30	20	0.3	6	14
30 – 60	30	0.3	9	21
60 – 100	40	0.3	12	28

After removing disqualified depth layers, the SOC data were ready for spatial modeling. My final dataset consisted of 71 samples for the 0-10 cm layer, 68 samples for the 10-30 cm layer, 59 samples for the 30-60 cm layer, and 38 samples for the 60-100 cm layer.

Terrain modeling for soil organic carbon

Spatial modeling of SOC used multiple linear regressions with local terrain attributes for the four fixed-depth layers:

$$y = \beta_0 + \beta_i x_i + e \ , \ \text{for } i = 1, 2, \dots, n \qquad (3.4)$$

where y is the response (dependent variable) and x_i denotes predictor variables (i.e. terrain attributes in this study) with intercept β_0, regression coefficients β_i, and the residual term e. The predictor variables are local terrain attributes at the Lake Rebecca site developed by the 1-m LiDAR (LIght Detection And Ranging)-derived digital elevation models (DEM) in the GIS programs ArcGIS, Python and SAGA-GIS (See Chapter 2 for the detailed description of terrain attribute development).

I included both primary and secondary terrain attributes for the regression analysis. Primary topographic characteristics consisted of relative elevation, slope, profile curvature (in both numerical and categorical forms), plan curvature (in both numerical and categorical forms), rate change of profile curvature, flow path length, and specific catchment area (SCA). Secondary topographic characteristics are comprised of compound terrain index (CTI) and stream power index (SPI). Just like the DEM source data, all terrain attributes are raster data formats in a 1-m resolution. A multiple flow-direction algorithm (MFD) was used in generating the above-mentioned flow-related primary (i.e. SCA, flow path length) and secondary terrain attributes (i.e. CTI, SPI).

Terrain attribute values were extracted to a spatial sample point database established from the post-processed GPS locations, and joined with volumetric SOC data for the four depth layers at all sample locations in GIS. From this joint database, I conducted exploratory analysis to understand the distribution of SOC in the four fixed-depth layers before regressional modeling.

To find multiple linear regression models for SOC with goodness-of-fit in individual soil depth layers, I applied stepwise regression plus an exhaustive search on model parameter selection for SOC with local terrain attributes in every depth layer. I used both backward and forward approaches in stepwise regression, and applied a function regsubsets ( ) in the library 'leaps' for the search I mentioned above in the R language. The regression models were selected based on the amount of variance (R^2) being captured with significance levels (p-values) of the model and of partial coefficients all greater than 0.10 (90% confidence intervals).

Following model selection, I tested the regression assumptions by evaluating the residual plots and tranformed the regression variables according to the model deficiency needs. The key regression residual assumptions include linearity, independence, homoscedasticity (in other words, having constant error variance), and normality. The residual analysis including scatterplot with LOWESS, normal Q-Q plots, and density plots were used to assess the assumptions. LOWESS is a LOcally WEighted Scatterplot Smoothing line created based on residuals to provide visual information on residual normality and linearity. Normal Q-Q plots is the probability plot comparing for a 'quantile' of one distribution (expected values) to the other 'quantile' distribution (observed values), and therefore it helps to assess the residual normality. Based on residual analysis, transformations for the selected SOC models were performed.

Model transformation is a common remedial measure for model deficiencies in the regression models in meeting regression assumptions (Kutner et al., 2004). Transformation can be on either dependent variable (Y) or independent variables (X), and

can apply different mathematical operations (square, logarithmic, or square root) to the variable according to the model decificiency (Minasny et al., 2012; Kutner et al., 2004).

Significant terrain attributes used for predicting SOC distribution in individual depth layers were compared. The importance of terrain control to SOC in the landscape could be identified from the model variable selection, the partial regression coefficients and coefficient of determination (R^2) of the regression models.

The model performance of the best-fitted SOC models were reported in terms of their adjusted R^2, root mean squared error (RMSE), and mean absolute error (MAE). To validate the SOC models, I used 10-fold cross-validation (CV) to estimate the model accuracy objectively while maintaining the sample size as the training dataset (vs. validation dataset). A detailed description about 10-fold CV can be found in Section 2.3. All statistical analyses in this chapter were conducted using the open source statistical program R.

Mapping the spatial distribution of soil carbon

The spatial distribution of SOC contents ($kg \cdot m^{-3}$) in four depth layers were mapped using the best-fitted SOC regression models. To avoid edge effect, I removed four cells around the entire boundary of the resulting dataset at the Lake Rebecca site using the mosaic database tools in ArcGIS. Terrain controls to SOC and the underlying land surface processes in the depressional landscape were discussed.

The overall SOC storage, also called SOC density, in the top 1m of soils was subsequently mapped. I developed a spatial predictive map of SOC density by summing predictive SOC density in the four depth layers. SOC density was calculated by multiplying the volumetric SOC contents C_v (kg · m^{-3}) with the associated soil depth z_i (in m):

$$C_d = \sum_{i=1}^{n} C_v * z_i \quad (3.5)$$

where C_d is the total SOC density (in kg · m^{-2}) from all depth layers i (n = 1 – 4). The term SOC density represents the storage of SOC per surface area; It has been commonly used in SOC studies (Minasny et al., 2012; Kumar et al., 2012).

To assess the uncertainty of the predicted SOC storage map, I developed 95% confidence interval (C.I.) maps. Because the SOC storage map was created from the four regression models of SOC contents in the four depth layers, the 95% C.I. maps were also calculated based on the 95% C.I. for SOC contents at individual depth layers:

$$y = \hat{y} \pm t_{\frac{\alpha}{2},\mathrm{df}} \cdot se \quad (3.6)$$

where y is the 95% C.I. for the estimated SOC content $\hat{y}$, t is Student's t critical value based on the confidence level α (i.e. α = 0.05) and the degree of freedom (df) in the regression model, and se is the standard error of the estimated SOC (Belia et al., 2005).

The total amount of SOC (kg · m^{-2}) stored in the top 1-m soil at the Lake Rebecca site was calculated by the spatial prediction of SOC.

3.4 Results and discussion

Soil carbon at the Lake Rebecca site

Soil organic carbon contents at sampling locations are listed in Appendix B. In general, SOC decreases with depth in soil profiles. Exceptions occur in some footslope and wetland positions where the SOC contents of some subsurface horizons are higher than horizons above them. These inverted C depth profiles matched our observations for samples with PSA. Figure 3.4 shows some samples' SOC in depth profiles (in green columns). Fitted with the spline depth function (in red lines in Figure 3.4), SOC contents in the four fixed-depth layers (0-10 cm, 10-30 cm, 30-60 cm, and 60-100 cm) were developed (in purple columns in Figure 3.4). Figures 3.4(a) and (b) show the original and splined depth profiles of SOC at the sample 013-FOOT location, a typical soil profile where SOC decreases almost exponentially with depth. Figures 3.4(c) and (d) show SOC in the original and splined depth profiles at 008-TOE, where its SOC content initially decreases but then increases again in the middle of the profiles. The inverted C depth profile suggests that the subsurface horizon with the highest SOC is a buried A horizons (Ab) underlying materials eroded from the upland (i.e. PSA). The resulting SOC contents for the four fixed-depth layers of interest are summarized in Table 3.3.

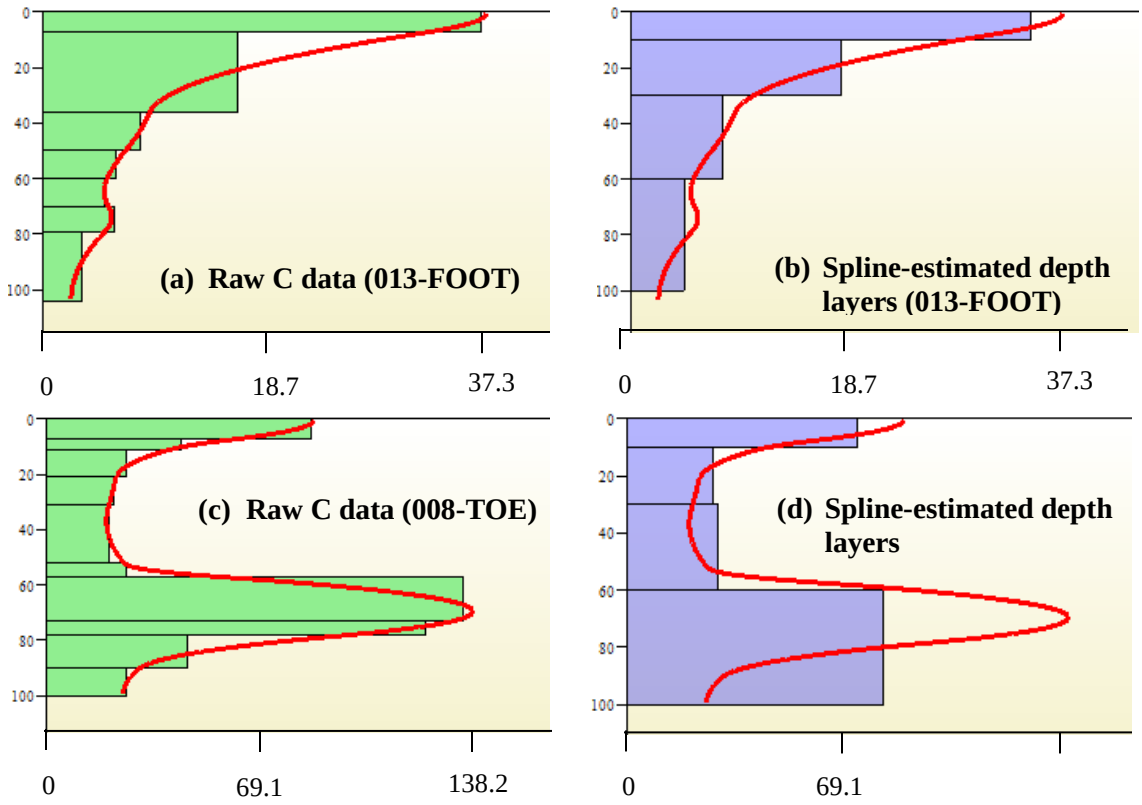

Figure 3.4 Examples of carbon depth profiles for the samples 013-FOOT and 008-TOE ((a) and (c), respectively), their fitted spline depth functions (in red lines), and the spline-derived four depth layer profiles ((b) and (d)).

Table 3.3 Descriptive statistics of soil organic carbon contents (kg · m^{-3}) in the four depth layers of top 1-m soils

Layer Depth	N	Mean	StDev	Median	Min	Max	Range
0-10 cm	71	37.58	21.70	31.46	9.56	112.8	103.24
10-30 cm	68	24.69	14.09	21.16	9.25	74.03	64.78
30-60 cm	59	22.46	17.00	20.09	4.58	81.97	77.38
60-100 cm	38	25.13	27.77	13.07	3.84	107.79	103.95

Both Dlugoβ et al (2010) and Kravchenko and Robertson (2011) reported that soil C variability increases with soil depth, but my data shows that the lowest variability occurred in the middle layers (10-30 cm and 30-60 cm) (Table 3.3). Soil erosion and redistribution (PSA) may have influenced the C variability over depth (Dlugoβ et al., 2010). This suggests that soil C storage and flux studies should consider vertical depths for profile modeling more carefully in landscapes with soil erosion and redistribution influences.

Due to the nature of high spatial variability in SOC (Minasny et al., 2013), some samples had much larger SOC contents than others, producing a right-skewed SOC distribution (Figure 3.5 and Figure 3.6). Extremely large SOC values come from samples collected from wetland locations, where SOC is expected to accumulate due to high biomass inputs and slow rates of decomposition. These large-value SOC samples were kept in the regression analysis even though, from a statistical point of view, they appear to be outliers.

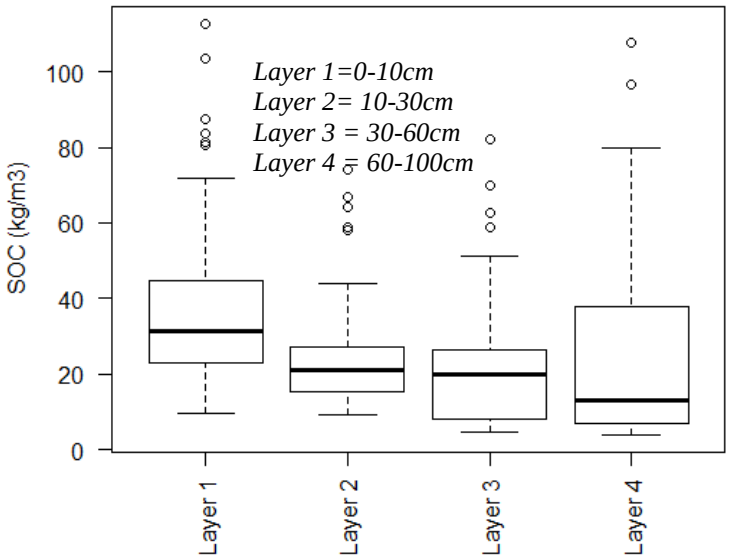

Figure 3.5 Boxplots for sample soil organic carbon data.

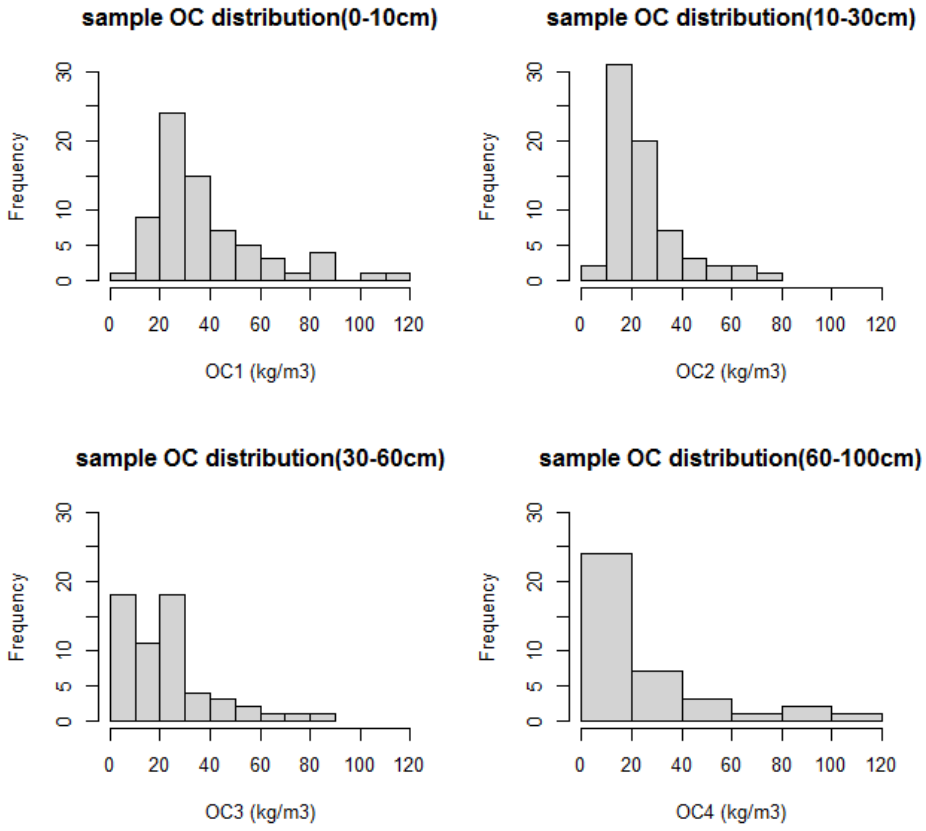

Figure 3.6 The sample distribution of soil organic carbon in four depth layers.

Maps of local terrain attribute databases used for SOC modeling can be found in Section 2.4. Figure 3.7 demonstrates the frequency distributions of terrain attributes at sample locations. Although sample sizes vary in the four depth layers due to data availability, their frequency distribution trends are similar. Among terrain attributes at sample locations, the frequency distributions of relative elevation, slope, rate change of profile curvature, and SCA are skewed to the right. While this behavior is very common for measurements of natural systems, some extra concern had been raised on whether relative elevation and slope skewed due to my intentional over-sampling at the bottom of hillslopes for capturing PSA. The distribution of relative elevation at the entire study site turned out to be skewed as well, but the distribution of slope was normal. This unnatural representation of slope in sample data might reduce the robustness of my models.

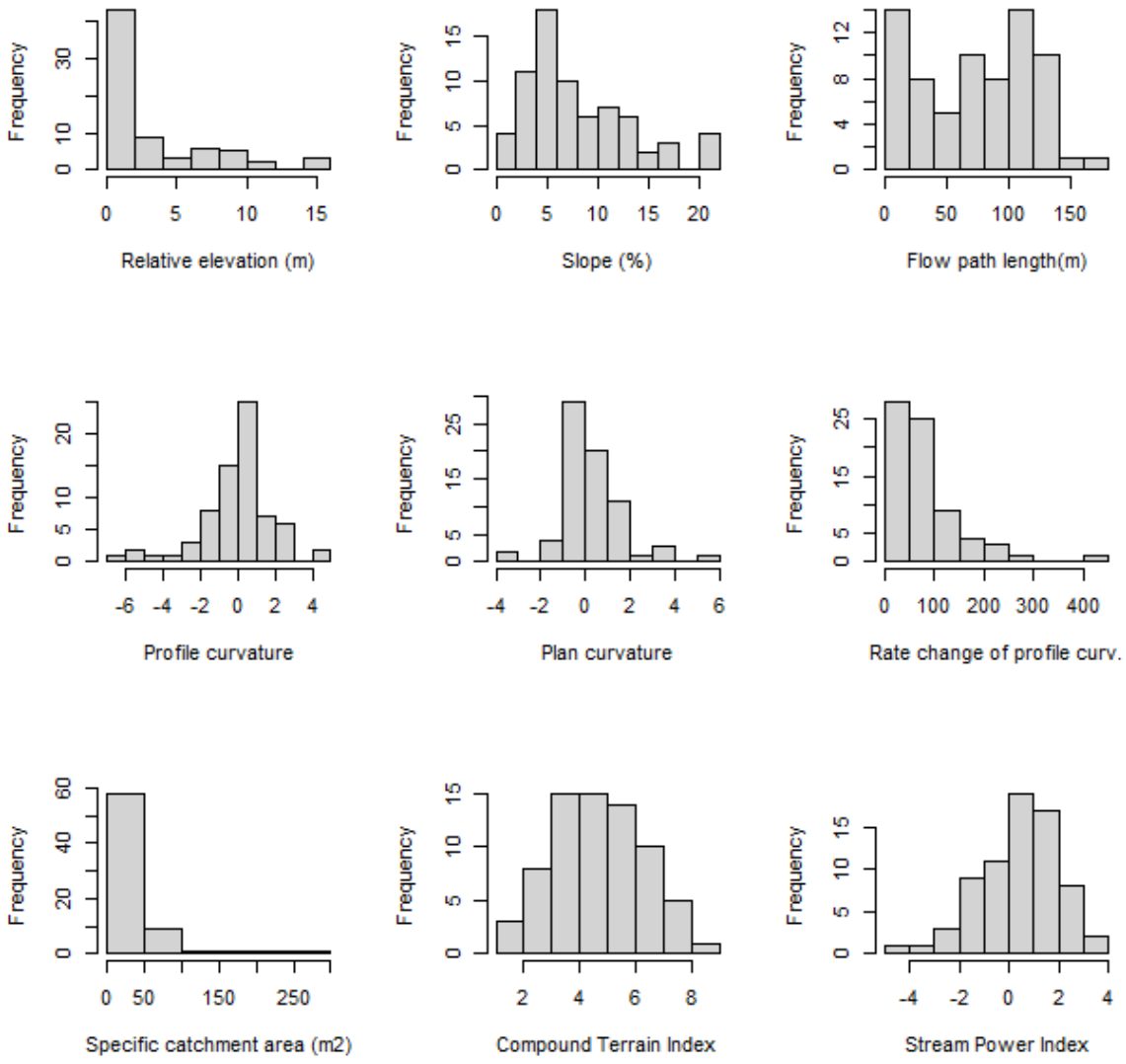

Figure 3.7 The frequency distributions of terrain attribute data at the sample locations (*n*=70).

Log-transformed regression models

During SOC model selection, I carefully tested model assumptions and log-transformed the response variable SOC and one of the predictor variables (relative elevation) in a log base *e* scale. The transformations were remedial measures taken for two model deficiencies –homogeneity of variance (or homoscedasticity, constant error variance) and linearity – in my SOC models. The residual plots in Figure 3.8 show the model-fitting processes for SOC in the 0-10 cm layer. The residual scatterplot in Figure 3.8(a), which was from the regression model built with significant terrain variables, including relative elevation, flow path length, and profile curvature, showed a lack of constant error variance. I took a natural logarithm on the response SOC to fix this homoscedasticity issue; the residuals in the updated model (Figure 3.8(c)) look equally spread out from zero across all levels of predicted values (from left to right). However, the LOWESS line (in red) of the residuals from the model with log-transformed dependent variable SOC (ln(SOC)) still has a strong bend and it falls out of 95% confidence bands (in blue dash lines) in the middle and at the two tails of the line. I transformed the predictor variable 'relative elevation' to improve the curvilinear effect of the variable based on testing the linearity of individual predictors' relations to the response (ln(SOC)). The residuals for the updated model have fairly constant error variance, and the LOWESS line shows acceptable linearity (within the 95% confidence bands) of the model (Figure 3.8(d)).

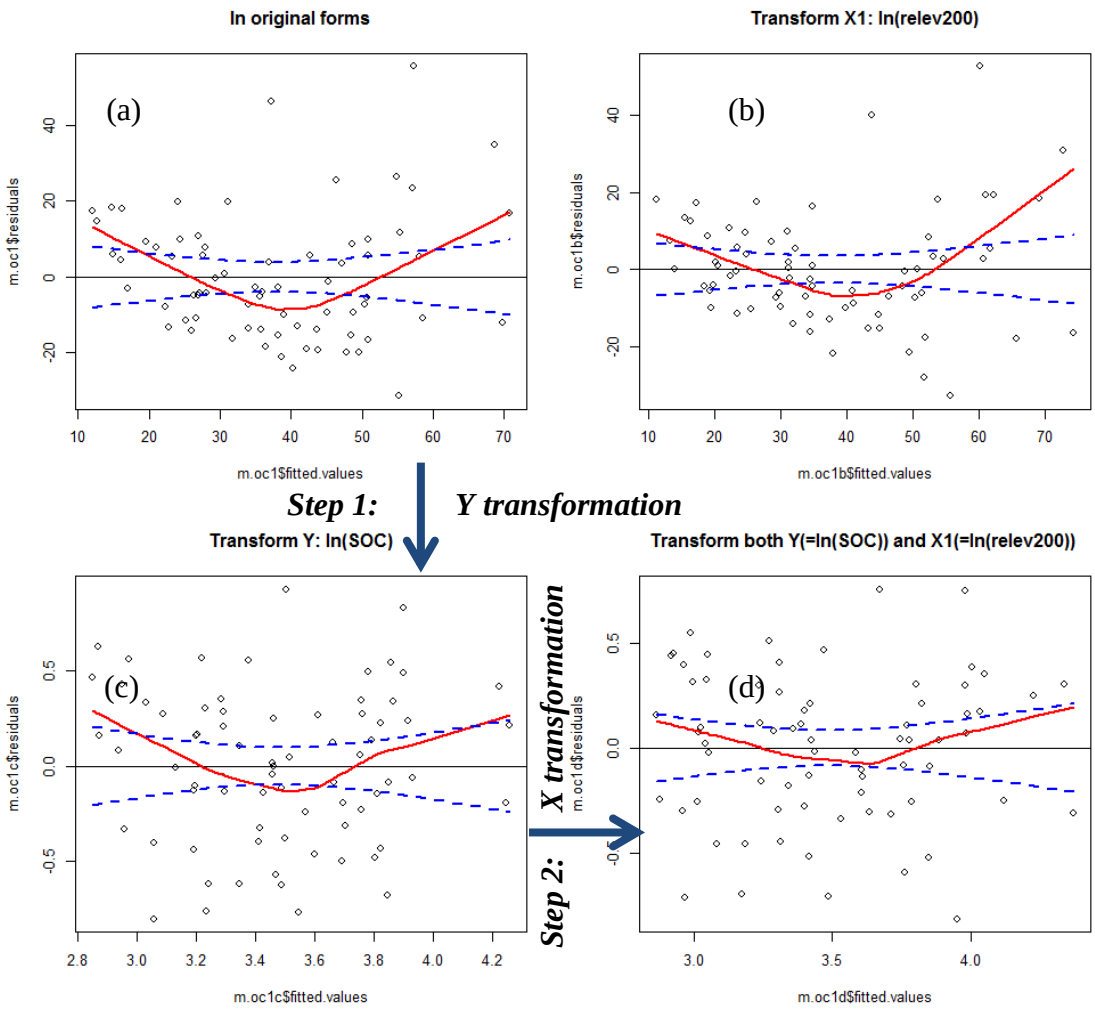

Figure 3.8 Residual plots of the soil organic carbon (SOC) regression model for the 0-10 cm layer with different transformations. Relative elevation (relev200), flow path length, and profile curvature are the predictor variables. When (a) both response and predictor variables are in original scales, the error variance is not constant and the LOWESS line (in red, solid line) falls out of 95% confidence bands (between blue, dash lines); (c) the issue of heterogeneous error variance is fixed when transforming the response in a natural-log scale (ln(SOC)) but the curved effect still exists; (d) the LOWESS line falls within 95% confidence bands when both the response and one of the predictors relev200 are log-transformed. The residual plot from the model with a predictor variable relev200 transformed in a log *e* scale (ln(relev200)) is displays in (b) for a reference purpose.

Soil carbon models for the four depth layers

I list the results of the SOC models with goodness-of-fit measures in Table 3.4. Because of the logarithmic transformation on SOC as the response, the reported R^2 values for the regression models are also associated to SOC in a log *e* scale (ln(SOC)). I will explain the model parameters' relationships with SOC (the original scale) in a later paragraph in this section.

Terrain characteristics explained more than half of the variances of ln(SOC) in the top 1 meter of soil in this landscape. Among the four regression models, the highest variance of ln(SOC) accounted for is the model for the 30 - 60 cm layer. The variance explained (R^2) by the model parameters are 52.25%, 70.17%, 81.3% and 63.12% at the four depths from top to bottom (0 - 10 cm, 10 - 30 cm, 30 - 60 cm, and 60 - 100 cm layers) respectively. The model results confirmed my expectation that terrain attributes would have different predictive capabilities for SOC patterns in different soil depths.

The lowest adjusted R^2 among the four depths is in the surface layer (0 – 10 cm), indicating other environmental covariates driving the amount and distribution of SOC at soil surfaces. The environmental covariates may include climate and biological effects (vegetation and animal disturbances) (Jenny et al., 1949; Yoo et al., 2006). For example, rainfall, litter inputs and various bioturbations (e.g. burrow) add, transform or translocate soil and soil properties at soil surfaces. Compared to the surface layer, biological activities would be much lower at the subsurface layers. The moderately fair prediction for the SOC model in the 60 – 100 cm layer suggests its weaker linkage with land surface

processes due to the soil depth. Because of PSA, human disturbance is likely the most influential factor for SOC in this layer other than terrain attributes.

Table 3.4 The multiple regression models for soil organic carbon (SOC) in current landscapes at the Lake Rebecca site.

Soil Depth (cm)	Response, Y	Model Parameters, X	Coefficients	Adj. R^2
0 - 10	SOC*	(intercept)	4.265	0.5225
		Relative Elevation*	-0.401	
		Flow Path Length	-0.003	
		Profile Curvature - concave	-0.298	
		Profile Curvature - convex	-0.384	
10 - 30	SOC*	(intercept)	3.801	0.7017
		Relative Elevation*	-0.41	
		Flow Path Length	-0.003	
		Profile Curvature - concave	-0.141	
		Profile Curvature – convex	-0.327	
30 - 60	SOC*	(intercept)	3.692	0.813
		Relative Elevation*	-0.706	
		Flow Path Length	-0.004	
60 - 100	SOC*	(intercept)	3.864	0.6312
		Relative elevation*	-0.926	
		Profile Curvature - concave	-0.651	
		Profile Curvature – convex	-0.479	

*variables were transformed into natural logarithmic forms.

The SOC models for the top two layers (0-10 cm and 10-30 cm) had the same predictor variables – relative elevation (in a log *e* scale), flow path length, and profile curvature (in classes). During the model selection process, I noticed that profile curvature was significant in categorical values but not in numerical values. The natural logarithmic term of relative elevation is also significant to the response ln(SOC) at 30-60 cm and 60-100 cm, and the best-fitted models of the two subsurface layers only used one more predictor (either flow path length or profile curvature) besides log-transformed relative elevation. The partial regression coefficients for the predictor variables in all models are statistically significant at a 90% significance level (p-value < 0.1) except for concave profile curvature in the models for the 10-30 cm and 60-100 cm layers. The statistical insignificance of concave profile curvature (p-values > 0.1) indicates that the null hypothesis, which is no difference between the mean coefficient of profile concavity (category '*v*') and that of profile straightness ('*f*', the reference group), cannot be rejected. Because profile curvature (in class) is essentially a single predictor variable with three categories, or a dummy variable, the categories cannot be reported separately and profile concavity remains in my models.

Relative elevation is the main topographic driver for SOC distribution in the landscape. When removing all predictor variables but relative elevation (in a natural-log scale), the regression model accounted for 40.7%, 56.92%, 75.33%, and 58.84% of the variance for the response ln(SOC) in the 0 – 10 cm, 10 – 30 cm, 30 – 60 cm, and 60 - 100 cm layers, respectively. The large influence of relative elevation on SOC suggests that hillslope positions control SOC distribution in the top meter of soils. This is expected, because soil

water and soil drainage are distinct in each hillslope position, and carbon accumulation is affected by soil moisture and water retention (Brady and Weil, 2004).

During model selection, I also found that SPI was a significant predictor for SOC when coupled with relative elevation in predicting SOC, but SPI did not capture SOC variance as well as flow path length did in the studied landscape. Both attributes (SPI and flow path length) suggest the importance of flow accumulation for SOC contents in landscapes. Long (average) flow path lengths means the location accumulates more flow from the top ridge (within a sub-catchment). SPI combines both local slope gradients and flow accumulation and is known to be related to erosive power of overland flows, soil thickness and organic matter contents (Florinsky, 2012; Moore et al., 1993).

I evaluated SOC model performance by MAE and RMSE in Table 3.5. Residuals used in these error-related measures were calculated by back-transforming (anti-log) the predicted response (ln(SOC)) in order to compare with the original observations, SOC. Based on Table 3.5, SOC is best predicted by local terrain attributes at the depth of 30-60cm, with the smallest MAE of 5.17 kg $C \cdot m^{-3}$ and RMSE of 7.52 kg $C \cdot m^{-3}$ compared to the other depth models. The poorest performing SOC models are for the 0-10 cm and 60-100 cm layers, which returned relatively high MAE (10.37 kg $C \cdot m^{-3}$ and 11.36 kg $C \cdot m^{-3}$, respectively) and RMSE (14.32 kg $C \cdot m^{-3}$ and 18.67 kg $C \cdot m^{-3}$, respectively) compared to the two middle soil depth layers. The residual plots (not shown here) of the SOC models also confirmed that regression assumptions (residual randomness, homoscedasticity, normality, and linearity) were met.

Table 3.5 Residual analysis and cross-validation results for soil organic carbon models at Lake Rebecca site.

Layer	MAE*	RMSE^	CVMSE^{+}
0 - 10	10.37	14.32	238.34
10 - 30	5.40	8.12	74.79
30 - 60	5.17	7.52	61.72
60 - 100	11.36	18.67	400.34

*MAE = Mean absolute error, in kg C/m^3;

^RMSE = Root mean square error, in kg C/m^3;

$^{+}$CVMSE = Mean of squared errors in 10-fold cross validation, in kg C/m^3.

I validated the SOC models using 10-fold cross-validation (Table 3.5). The overall MSE in the 10-fold cross-validation data (CVMSE) are relatively small in the 10-30 cm and 30-60 cm layers (74.79 kg $\cdot$ m^{-3} and 61.72 kg $\cdot$ m^{-3}, respectively), and appear to be larger in the 0-10cm and 60-100cm layers (CVMSE = 238.34 kg $\cdot$ m^{-3} and 400.34 kg $\cdot$ m^{-3}, respectively).

The errors of my SOC models come from various sources. First, there were errors associated with measurements from field sampling and laboratory analysis. Second, the spline depth function used to convert horizon-based soil sample data into fixed-depth data also introduced errors (MSE = 4.192 kg C $\cdot$ m^{-3}). Then, when I used regression to model SOC in depth profiles, it also introduced Type I Error ($\alpha = 0.1$). The cross-validation

results suggest more caution should be taken when applying the models to predict the surface and the deep subsurface soils (below 60 cm).

The spatial distribution of soil organic carbon

The spatial distributions of predicted SOC contents in four depth layers are shown in Figure 3.9. Overall, SOC contents increase when elevation decreases. The hill tops (summit positions) were low in SOC, especially below 30 cm in the soil profile. Footslope and toeslope locations, particularly those reaching permanent ponded locations at the bottom of hillslopes, were high in SOC. The mid-slope locations between summits and wetlands have SOC contents between the two extremes. Notice that SOC contents for maps in Figure 3.9 were displayed in the same intervals for a comparison purpose, but the actual ranges of SOC are different in individual depth layer (Table 3.6).

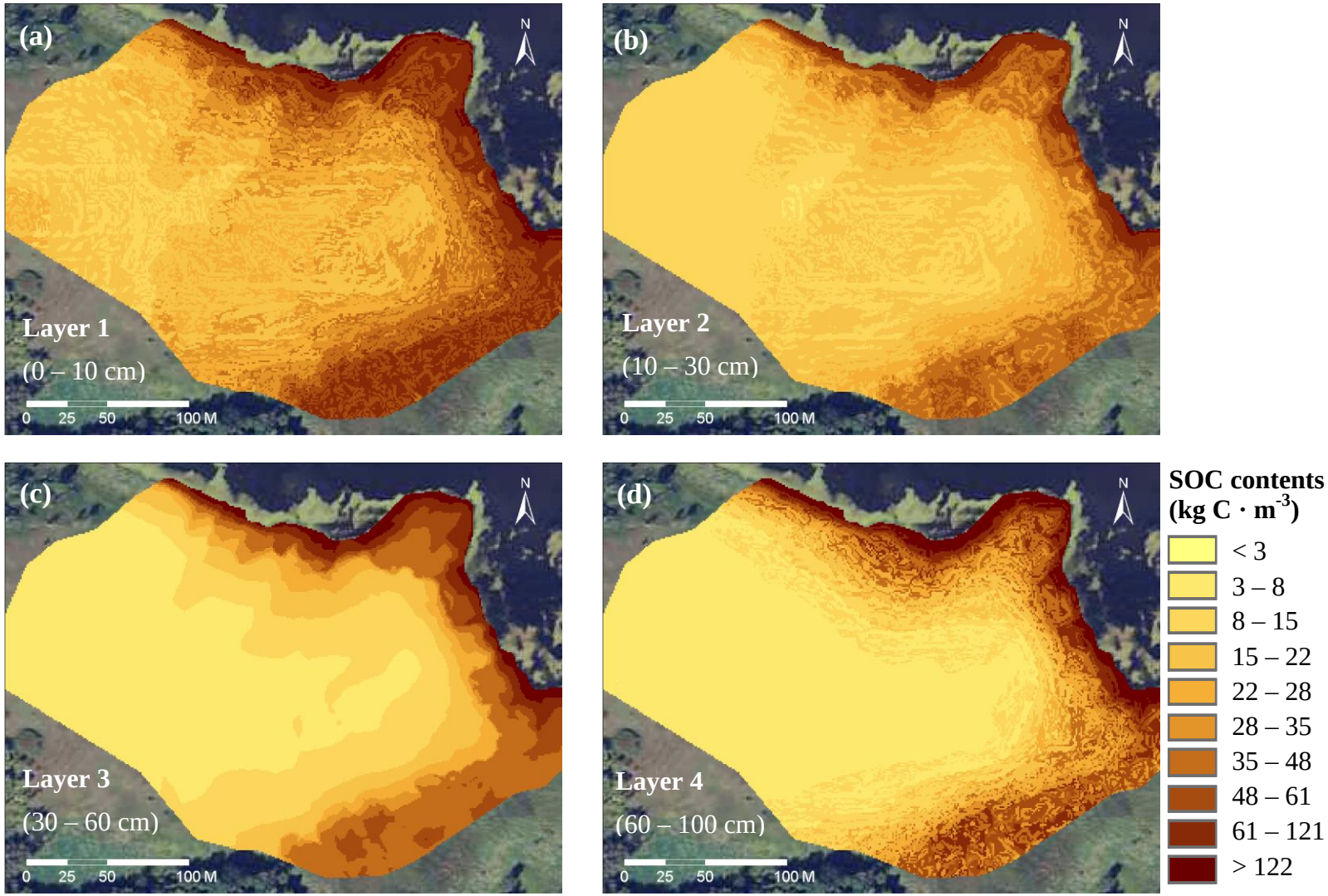

Figure 3.9 Spatial distribution of soil organic carbon contents in the four depth layers.

The spatial pattern and variability of SOC at Lake Rebecca study site vary with soil depth. Table 3.6 shows the summary statistics of predicted SOC in the four depth layers at the entire Lake Rebecca site (a total of 57,582 m^2, after removing the edge buffer)**.** The minimum SOC decreases when soil depth increases, as expected, but the maximum SOC did not follow the decreasing patterns and has very large values in the 30-60 and 60-100 cm layers (535.47 and 1,680.49), respectively. The large predicted SOC contents appear to be very few cells located near the wetlands in the north and northeast. Because I already considered the edge effect and removed edge cells in the prediction maps, these extremely large values suggest that my samples may have not covered enough deep subsurface data in the wetlands and could not accurately predict such environment. The standard deviation in the 60-100 cm layer is also the highest (62.98 $kg \cdot m^3$) among the four, and further confirms that the one should be careful in the use of the deep layer model predictions.

Table 3.6 Summary statistics of soil organic carbon contents at the entire Lake Rebecca study site.

Layer	Depth (cm)	SOC contents ($kg \cdot m^{-3}$)			
		Mean	Min	Max	StDev
1	0 - 10	36.06	12.49	253.66	25.94
2	10 - 30	24.12	8.15	164.48	17.43
3	30 - 60	23.3	4.46	535.47	32.06
4	60 - 100	27.81	1.8	1680.49	62.98

When visually comparing the SOC maps of the four depth layers, carbon contents are highest in the 0-10 cm layer and decrease with depth in the profile (Figure 3.9). Compared to spatial SOC map in 0-10 cm layer, SOC contents in the 10-30 cm layer appear to be much smaller in the entire catena, except at the edge near the permanent ponded area in the north and northeast part of the site. Permanent saturation is likely to retain high organic matter (OM) contents over 30 cm in the depth profiles (and therefore it is not uncommon to have deep, dark A or O horizons in these locations) (USDA-NRCS, 2010). In addition, I suspect that the surface wetland soils consist of relatively undecomposed organic matter (fibric) with very low BD, resulting in lower volumetric SOC contents than the underlying C-rich mineral soil horizon.

As to the spatial patterns of predictive SOC in the 30-60 cm layer, there is less local variance in the map (Figure 3.9 (c)) compared to the other three depth profiles. This is due to the choice of predictor variables. The model predicting SOC in the 30-60 cm layer was comprised of two 'global' predictor variables -- relative elevation and flow path length – that change gradually across the entire landscape, and have far less local variability as the variable profile curvature used in the other depth layer models. For the 60-100 cm layer, as described earlier, unexpectedly high SOC are predicted for some spots in the southern part of the site (Figure 3.9d). It is possibly due to the presence of deep buried A horizons (by PSA) in the field, but can be also caused by the less reliable modeling due to small sample size.

Based on the spatial prediction of SOC contents (Figure 3.9), SOC density in the four depth layers was calculated and summed for the top 1-m soil (Figure 3.10). The predicted

SOC density at the entire Lake Rebecca site ranges from 5.4 kg C · m^{-2} to as high as 824 kg C · m^{-2}.

For uncertainty assessment, I developed the 95% C.I. maps for the top 1-m SOC density (Figure 3.11). The 95% C.I. maps provide an understanding of the uncertainty in my spatial prediction of SOC. Compared to the predicted SOC (Figure 3.10 or Figure 3.11a, ranging from 5.4 - 825 kg C · m^{-2}), the upper 95% C.I. of SOC density ranges from 11.5 to 2,531.4 kg C · m^{-2}, and the lower 95% C.I. ranges from 2.7 to 282.9 kg C · m^{-2}. There are large uncertainties in my SOC prediction toward the bottom of the hillslopes across the entire Lake Rebecca site, especially close to the wetland edge in the north-northeast-east where the predicted SOC density is extremely high (Figure 3.11c).

The total quantity of SOC density in the top 1 m of soil is estimated to be 1,528,308 kg (~1.528 Gg C) at the Lake Rebecca site in a total area of 57, 582 m^2.

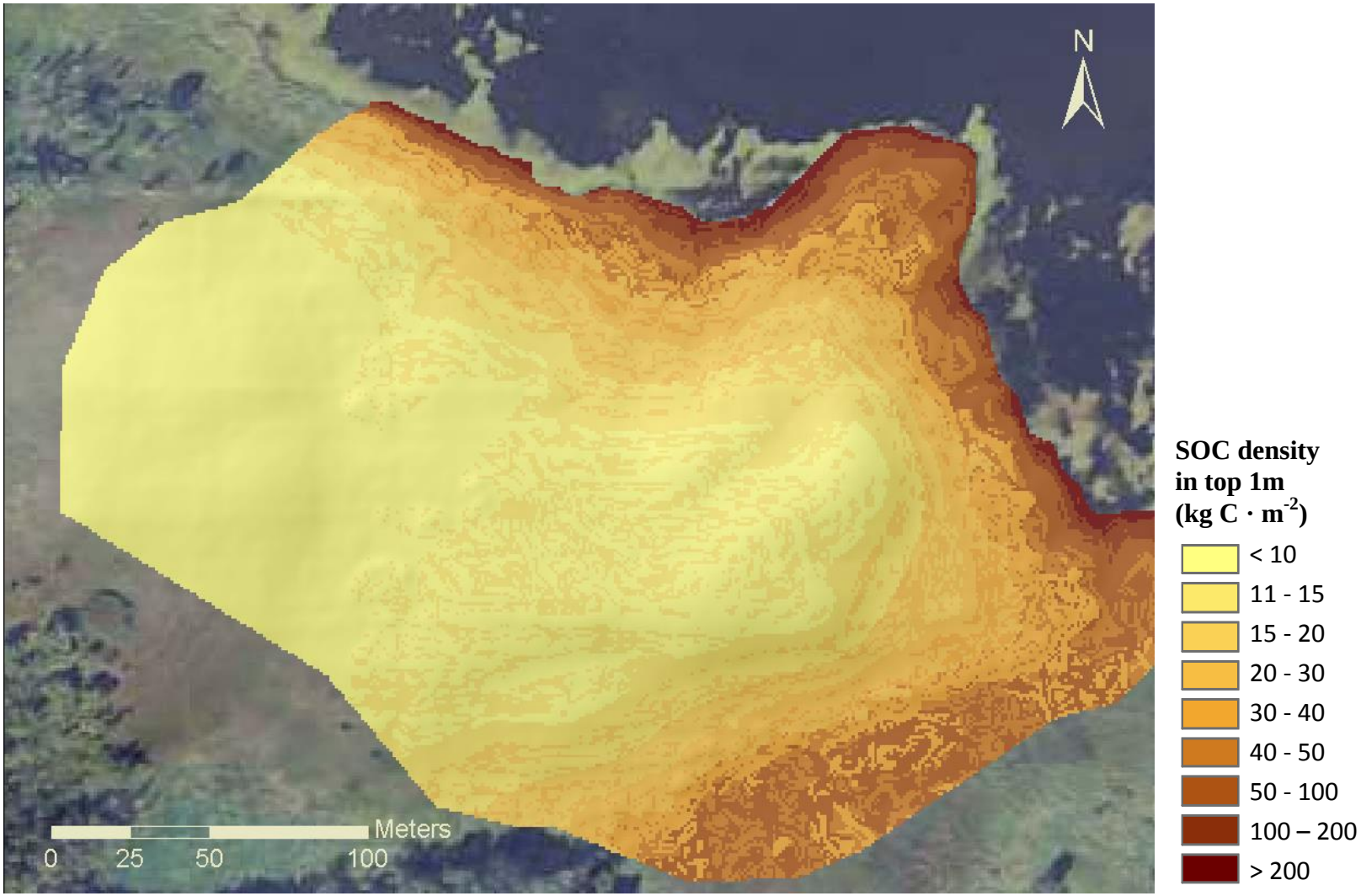

Figure 3.10 Soil organic carbon density in the top 1 meter at Lake Rebecca site.

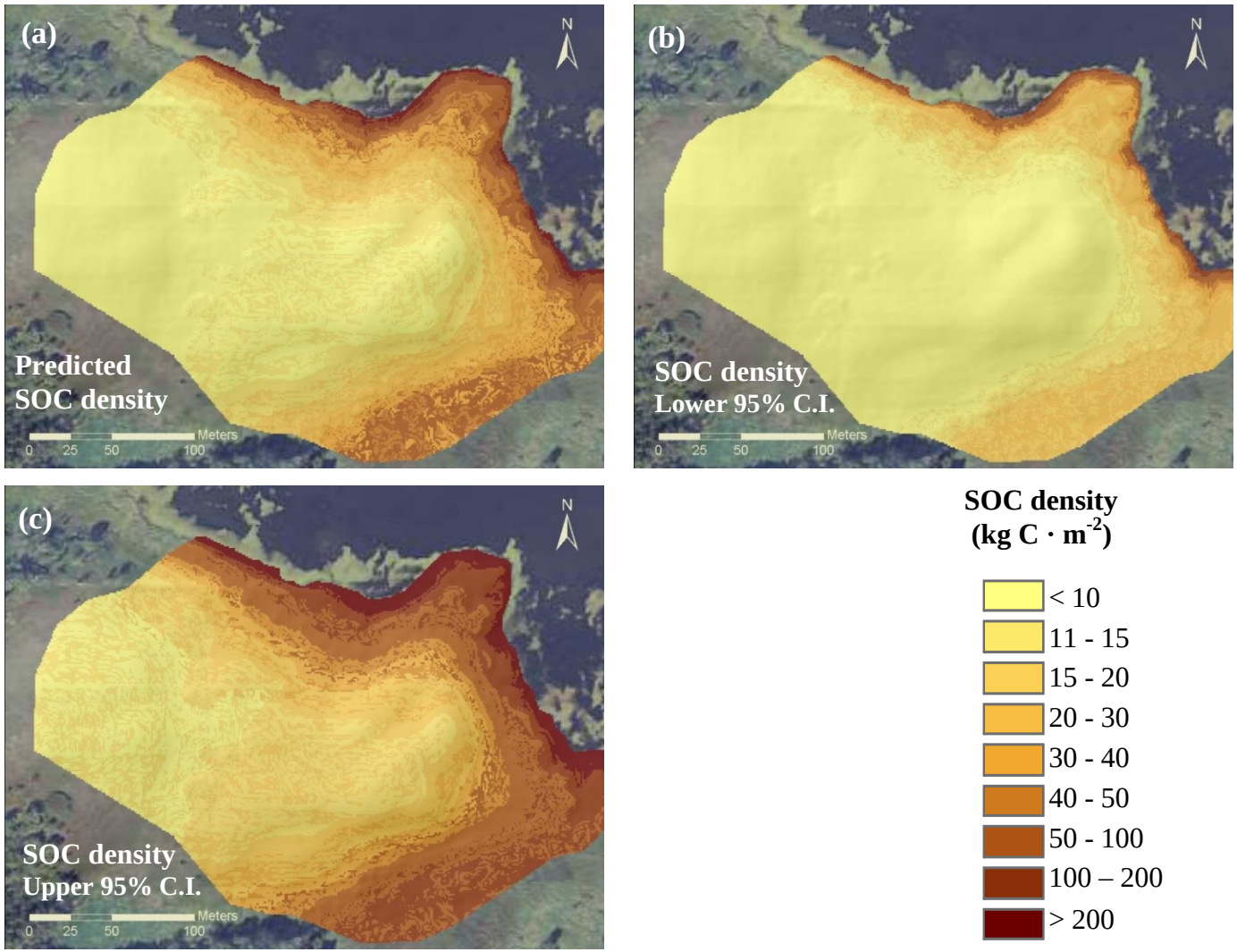

Figure 3.11 The 95% confidence interval maps for soil carbon density in the top 1-meter soil.

3.5 Conclusion

This study demonstrated that the spatial distribution and quantity of SOC in closed-depressional, erosive agricultural landscapes can be predicted by terrain characteristics using a multiple regression analysis.

The distribution of SOC and its relationship with terrain conditions vary vertically in depths. The prediction in different depths according to soil functions and properties is required. In this study, the spatial models of SOC were fit for four depth layers (0 - 10 cm, 10 - 30 cm, 30 - 60 cm, and 60 – 100 cm) and I could capture the differences of SOC variances between layers. The variance of the regression response (log-transformed SOC) captured by terrain attributes ranged from 52.25% (0 - 10 cm) to 80.1% (30 - 60 cm). My results confirmed the need for predicting whole-profile SOC in various depths as stated in Syswerda et al. (2011) and Kravchenko and Robertson (2011).

However, instead of decreasing predictive accuracy with depth as suggested by Syswerda et al. (2011) and Dlugoβ et al. (2010), terrain attributes predicted the SOC distribution most accurately at the depths of 10-30 and 30-60cm in this study. This indicates that PSA has changed the vertical SOC distribution in the landscape. Breaking the soil profile into depth intervals for spatial prediction of SOC should be considered in each specific landscape according to agricultural erosion condition and soil wetness. Terrain attributes were able to explain more variability in SOC density in the 10-30 and 30-60 cm layers than in the 0-10 and 60-100 cm layers which indicates that variables other than topography affect SOC density. Future modeling efforts should consider including other

environmental covariates especially agricultural activities and erosion-induced deposition (PSA) to improve our understanding of SOC storage and sequestration potentials in the modern environment.

Chapter 4

Spatial and temporal changes in soil carbon under the influence of agricultural erosion

4.1 Introduction

Agricultural tillage promotes soil erosion and degrades soil quality (Gregorich et al., 1998; Tilman et al., 2002; Mamo and Hain, 2005). Soil organic carbon (SOC) has been a main component for studying the impact of agricultural erosion on soil quality. Previous studies have shown that agricultural erosion altered SOC dynamics at a landscape scale (Gregorich et al., 1998; Six et al., 2002; McCarty and Ritchie, 2002), and the erosion-induced soil redistribution affects SOC storage (Stallard, 1998; Berhe et al., 2007). However, the actual change in SOC storage since European settlement varies in basins (Berhe et al., 2007).

In the past decade, studies have shown that agricultural erosion can be a net C increase or loss (Lal, 2003; van Oost et al., 2005; Moorman et al., 2004). Depending on the fate of eroded soils, SOC can be lost to the atmosphere as CO_2, transported to rivers or lakes as sediment, and/or re-deposited within the landscape (Figure 4.1) (van Oost et al., 2012; Berhe et al., 2007; Harden et al., 1999). Soil that is redistributed and re-deposited within the landscape, particularly in wetter parts of the landscape, is likely to produce an increase in landscape SOC storage, due to slower decomposition in these landscape positions (see the concept model in Figure 2.1). A depressional landscape, such as that on the Des Moines lobe till plain in South-Central Minnesota, can keep eroded soils re-

deposited in depressional wetlands, and therefore has the potential to increase net SOC. However, a net change in whole-landscape SOC storage for these landscapes due to agricultural erosion is not clearly known.

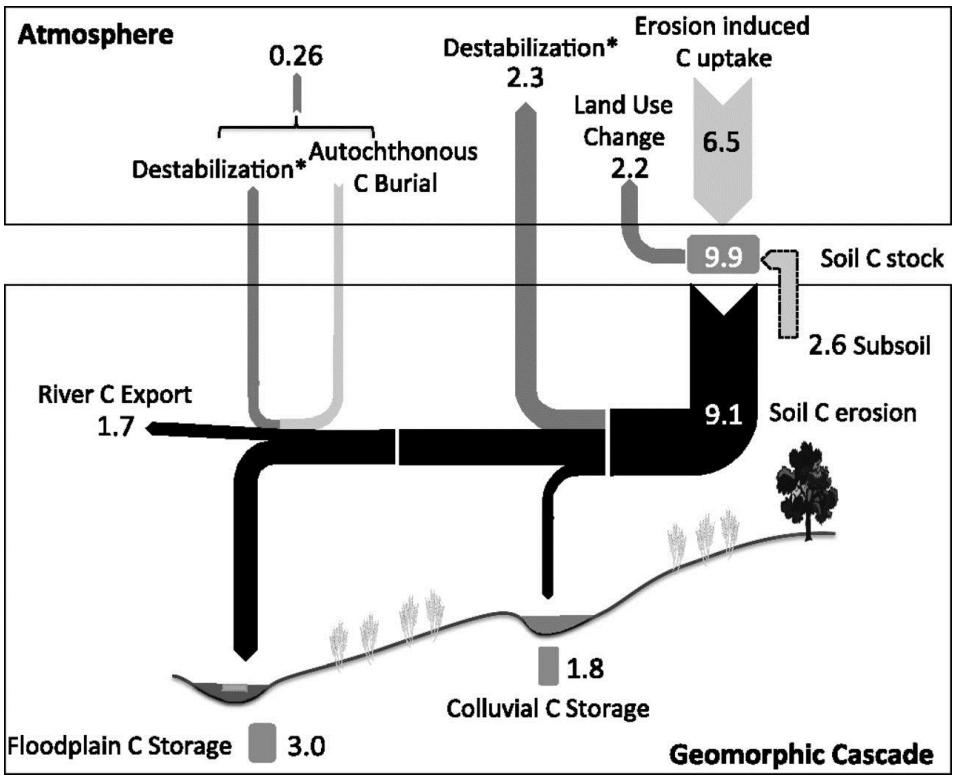

Figure 4.1 Previously estimated carbon flux and storage (in Tg C, 1Tg = 10^{12} kg) between soil and the atmosphere from 4000 B.C. to A.D. 2000 in the Dijle watershed, the Netherlands. *(*Adapted from *Figure 3* in *Van Oost et al., 2012)*

The goal of this project is to estimate the whole-landscape change in SOC in a depressional landscape in Minnesota since European settlement. Here I integrate results from the previous chapters to understand the spatial change in SOC since European

settlement and to determine whether PSA sediments represent a carbon sink. The spatial distribution of PSA at the Lake Rebecca Park Reserve in South-Central Minnesota was predicted in Chapter 2, and its current SOC distribution and inventory were estimated in Chapter 3. In this chapter, the three objectives are to:

1. Develop a baseline SOC model representative of pre-settlement conditions at the Lake Rebecca study site;

2. Estimate pre-settlement SOC density in the uppermost 1 meter of soil at the Lake Rebecca site; and

3. Assess spatial and quantitative SOC changes since European settlement by comparing current landscape SOC density to the pre-settlement baseline SOC density.

Soil organic carbon content and SOC density are the two measurement types of SOC mentioned in this chapter. SOC content is the concentration of SOC in volume basis (in $kg \cdot m^{-3}$) converted from the mass-based SOC (%, or $kg \cdot kg^{-1}$) measured in the laboratory. On the other hand, SOC density (also known as SOC inventory or storage) is the amount of SOC per surface area in the soil (in $kg \cdot m^{-2}$). SOC density is the product of volumetric SOC content and its associated soil depth (m). Of the two types, SOC density is used to report and compare the amount of SOC in different spatial extent and temporal scales (Minasny et al., 2013).

I estimate the pre-settlement SOC density in the top 1m of soil at the Lake Rebecca site from predictive baseline models, and then calculate the differences in quantity and spatial

distribution between current SOC density (described in Chapter 4) and the pre-settlement SOC density. The baseline model in the erosional uplands is developed by a SOC model from a reference grassland. The baseline model for the depositional areas is developed from soil data of the PSA-buried original soil profile at the Lake Rebecca site.

I hypothesize that erosional uplands have lost SOC due to surface soil translocation and decomposition, even with dynamic C replacement following erosion. I expect a SOC increase at depositional sites with the addition of PSA eroded from upland surfaces. Even with the continuous C increase after soil redistribution, I expect the overall SOC density to show a net loss since settlement because of the large quantities of SOC lost during cultivation.

4.2 Site description

The study site is a hillslope in a young glaciated landscape located in the southwestern part of Lake Rebecca Park Reserve in Hennepin County, Minnesota. The Lake Rebecca site was converted to agriculture following European settlement (traced back to as early as 1842). Agricultural cultivation of this site ceased in the early 1970s when the site was transformed to prairie as a part of Lake Rebecca Park Reserve. A more detailed description of the Lake Rebecca site can be found in Sections 2.3 and 3.3.

A relatively undisturbed site was needed to serve as a reference for pre-settlement SOC distribution in Lake Rebecca. I selected a grassland that has been used for hay production since the early 1920s in Morristown, Minnesota. According to the landowner, the

Morristown grassland has no known history of plowing, and also no such evidence is visible in historical aerial photos of the site. While not adjacent to Lake Rebecca, this reference site is the best grassland site I could identify for building the baseline model for Lake Rebecca. The Morristown grassland site (44.213336, -93.429981) is also located in the Des Moines lobe till region of Minnesota about 96 km south of the Lake Rebecca site (Figure 4.2).

The two study areas have similar parent materials, climate, pre-settlement vegetation, and soil types (Hobbs and Goebel 1982; Marschner, 1974; Dunevitz and Epp, 1995; Soil Survey Staff, 2013). . Both sites are in depressional landscapes due to the geological settings. More specifically, the Lake Rebecca site is located on the Pine City end moraine of Des Moines Lobe. The Morristown site, on the other hand, sits on the Bemis ground moraine and has less relief. Compared to the Lester-Hamel-Klossner or Houghton soil series in catena of Lake Rebecca, the Morristown site has Lester-Storden complex (Mollic Hapludalfs and Typic Eutrudepts) at summits, Hamel series (Typic Argiaquolls) in midslope to footslope positions, and Klossner muck (Terric Haplosaprists) in at toeslope positions (Soil Survey Staff, USDA-NRCS, 2013). The comparable natural properties indicate the reference site was a good control location to model pre-settlement baseline SOC.

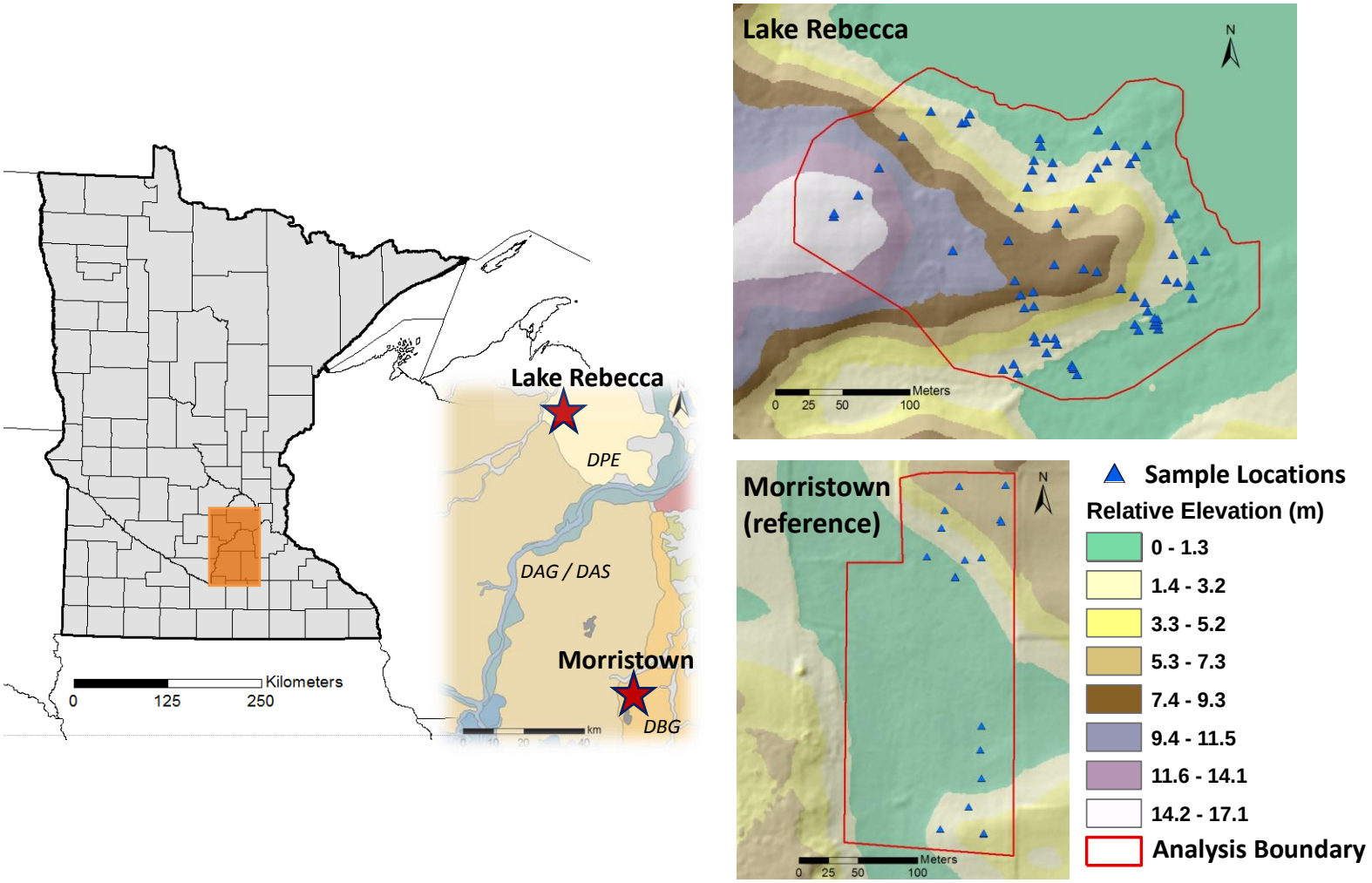

Figure 4.2 The reference map for the Lake Rebecca study site and the Morristown reference site. Both sites are located on Des Moines lobe till, with Rebecca on Pine City Moraine (DPE) and Morristown on Bemis Ground Moraine (DBG).

4.3 Methods

Soil sampling for the reference site

Soil sample profiles at the Lake Rebecca site described in Section 4.3 were used for the baseline SOC modeling (see *Section 4.3* for more detailed description). Soil samples at the reference grassland in Morristown, Minnesota were collected during the growing season of 2012 for a soil research project in Southern Minnesota. Bulk soil samples at the Morristown site were collected in a stratified-gradient following hillslope positions from summit to footslope. Soil pits (approximately 60 - 75 cm deep) were dug in a total of 18 sample sites within three hillslope transects, and bulk soil samples were collected at 12 depths (0-5 cm, 5-10 cm, 10-15 cm, 15-20 cm, 20-25 cm, 25-30 cm, 30-40 cm, 40-50 cm, 50-75 cm, 75-100 cm, 100-125 cm and 125-150 cm) at each soil pit. At each sampling depth between 0 and 50 cm, soil was also carefully collected with minimal compaction in a brass cylinder (about 3.5-cm-diameter and 7-cm height) for bulk density analysis. Soils in the 50-150 cm depth were collected with a 5-cm diameter hammer-driven corer with plastic sleeves (AMS, Inc., American Falls, ID) to hold the soil core. Bulk density was determined as the dry mass of soil contained in each core divided by its volume.

Geographic positions (latitude/longitude) at all sample locations were also collected using a handheld Global Positioning System (GPS) device. After returning from field sample collection, bulk soil samples were dried, ground, and sieved. Subsamples were taken for organic carbon measurement and were subjected to an acid fumigation pretreatment (Harris et al., 2001) before measurement. I measured soil organic carbon based on the

standard dry combustion method using an Elementar Vario Max CN Analyzer. Soil dry bulk density was measured from soil core samples following the Soil Survey Laboratory Methods Manual (Burt, 2004).

Presettlement baseline soil carbon estimation

The pre-settlement baseline SOC at the Lake Rebecca site was estimated by two modeling approaches. The baseline model for the erosional uplands was developed by a SOC model from the reference grassland, and the model for the depositional sites was developed from original soil profiles buried under the depth of PSA at the Lake Rebecca site.

The reference-site SOC model was only applied to erosional uplands for two reasons: First, I was not able to test model transferability since no pre-settlement C data was available for the Lake Rebecca site. Even with similar geological settings and climatic conditions, transferring models have been found to lower prediction accuracy (Thompson et al., 2006). Second, sampling at the reference site did not adequately cover toeslope positions (where PSA is deposited) and would be inappropriate for estimating toeslope SOC at the Lake Rebecca site. The preliminary analysis showed that the reference model predicted negative SOC values at toeslope positions in the Morristown site. Because of these concerns, I developed a separate reference SOC model for the bottom of the hillslopes at the Lake Rebecca site, using sample profiles at the Lake Rebecca site with the observed PSA depths removed (see Section 3.3 for the sample collection protocol).

Spatial carbon modeling for the reference site

I first prepared spatial terrain databases as potential predictor variables for reference SOC modeling using the Geographic Information Systems (GIS) programs SAGA-GIS and ESRI ArcGIS 10.0. Local terrain attributes were derived from a 1-m LiDAR (Light detecting and ranging)-derived digital elevation model (DEM) (Minnesota Geospatial Information Office, 2014). The terrain attribute datasets included relative elevation, slope, profile and plan curvatures (in both numerical and categorical forms), flow path length, specific catchment area (SCA), compound terrain index (CTI), and stream power index (SPI). To remove possible artifacts from the DEM source data, the DEM was smoothed twice using the low-pass filter method before terrain attribute development. The terrain attribute information was then extracted by sample GPS position data so I have the terrain properties of sample locations at the reference grassland for SOC regression modeling.

The modeling method used for mapping SOC at the Lake Rebecca site was first adopted for the reference SOC modeling. Volumetric soil carbon content ($kg \cdot m^{-3}$) sample data were converted into four fixed depths (0-10 cm, 10-30 cm, 30-60 cm, and 60-100 cm) using an equal-area spline depth function, and then joined with sample locations' terrain attribute information (see Chapter 3). However, preliminary statistical analysis for this dataset revealed the inability of capturing SOC variance using terrain attributes in the reference site. This issue could be a result of the small sample size (n=18), but was also a signal for the lack of relationships between local terrain attributes and soil carbon in undisturbed landscapes.

I updated the approach for reference SOC modeling based on the above concerns. In order to increase the sample size, carbon data from all sample depths were pooled together. Table 3.1 describes the summary statistics of SOC contents in this big pool of dataset (n=190). The SOC dataset has a mean of 29.44 $kg \cdot m^{-3}$ with a standard deviation of 17.56 $kg \cdot m^{-3}$. In addition to terrain attributes, I added the mean sample depth as a new potential predictor variable. Soil depth was previously found to be highly correlated to SOC in grassland landscapes in Southeastern Minnesota (Brent Dalzell, personal communication, 2014). Because all sample depths were collected from 18 sample locations, the actual degrees of freedom (df) remained small, even though the sample size increased more than 10 times.

Table 4.1 Descriptive statistics of sample soil carbon contents ($kg \cdot m^{-3}$) at the reference site in Morristown, Minnesota.

N	mean	stdev	median	min
190	29.44	17.56	27.63	2.12
Max	range	skew	kurtosis	se
73.96	71.84	0.41	-0.63	1.27

A multiple linear regression analysis was then applied to find the best reference SOC model. The variable selection utilized stepwise regression and the best-fit model was chosen with a 90% significance level followed by model evaluation. Residual scatterplots and normality plots were used to assess whether regression assumptions were met, and if

variable transformation were required. I assessed model accuracy using coefficient of determination (R^2), mean absolute errors (*MAE*) and root mean square error (*RMSE*).

Spatial carbon modeling for PSA-buried profiles

In depositional areas (where PSA is present), a second, different baseline SOC model was developed from the buried soil profile data at the Rebecca site. Figure 4.3 demonstrates the concept framework for modeling pre-settlement baseline SOC in depositional areas using all sample profile data below the PSA layers. I assumed that original soil surface was buried by PSA and buried soil carbon was essentially inert with low decomposition rates. I reconstructed baseline soil profiles by removing sample profile data above the observed buried surface horizons (Ab1) and re-setting the soil surface (0 cm) to the top of the buried horizon. Because the spatial distribution of erosion source in upland was unknown, I was not able to reconstruct the pre-erosion soil profiles for the upland. But the profile C data in erosional uplands were still included with the reconstructed baseline depressional site profiles for modeling SOC. The erosional upland samples were used for better capturing overall topographic trends of SOC in the landscape.

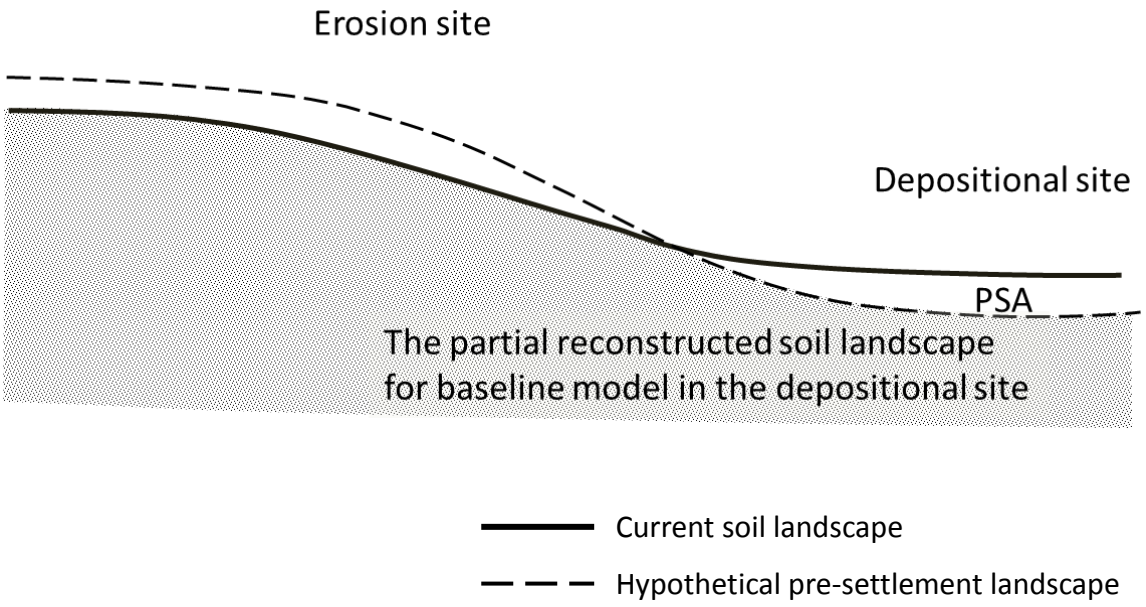

Figure 4.3 A cross-sectional hillslope view for the concept of modeling baseline SOC in buried soil profiles in the depositional site.

In the depositional areas, I developed pre-settlement baseline SOC models in four fixed depth layers (0-10 cm, 10-30cm, 30-60cm, 60-100cm) using multiple linear regression. This is the same approach used for current Lake Rebecca SOC contents in Chapter 3. Table 4.2 summarizes the statistics for sample profile SOC contents used for this baseline modeling.

I converted horizon-based sample SOC content data into four depth layers using a spline depth function and developed predictive SOC content model for individual layers using terrain attributes. Mapping SOC in four depth layers at the PSA-present zone was not only beneficial in predicting more accurate pre-settlement baseline SOC, but would be

applicable for the estimation of potential C sequestration in PSA later (Objective 3). The variability of SOC contents was found in previous literature to decrease with depths. The soil spatial prediction of SOC was suggested to break into various depths (Kravchenko and Robertson, 2011; Dlugoβ et al., 2010).

Table 4.2 The summary statistics of sample profile soil carbon ($kg \cdot m^{-3}$) for pre-settlement baseline carbon modeling in depositional areas.

Layer	N	Mean	StDev	Median	Min	Max	Range
0-10 cm	66	36.92	27.54	27.85	9.56	135.50	125.94
10-30 cm	60	28.02	21.31	19.64	9.25	99.08	89.83
30-60 cm	42	14.95	13.98	10.83	5.46	87.33	81.87
60-100 cm	18	6.88	2.60	6.44	3.84	11.71	7.87

Estimating pre-settlement soil carbon density

The spatial distribution of pre-settlement (baseline) SOC density ($kg \cdot m^{-2}$) in the top 1 meter was mapped by the reference SOC model for the erosional upland and by the buried profile SOC model for the depositional areas. The spatial boundary between the two mutually exclusive zones (erosional vs. depositional) was defined by the PSA presence (or absence) mapped in Chapter 3 (Figure 4.4).

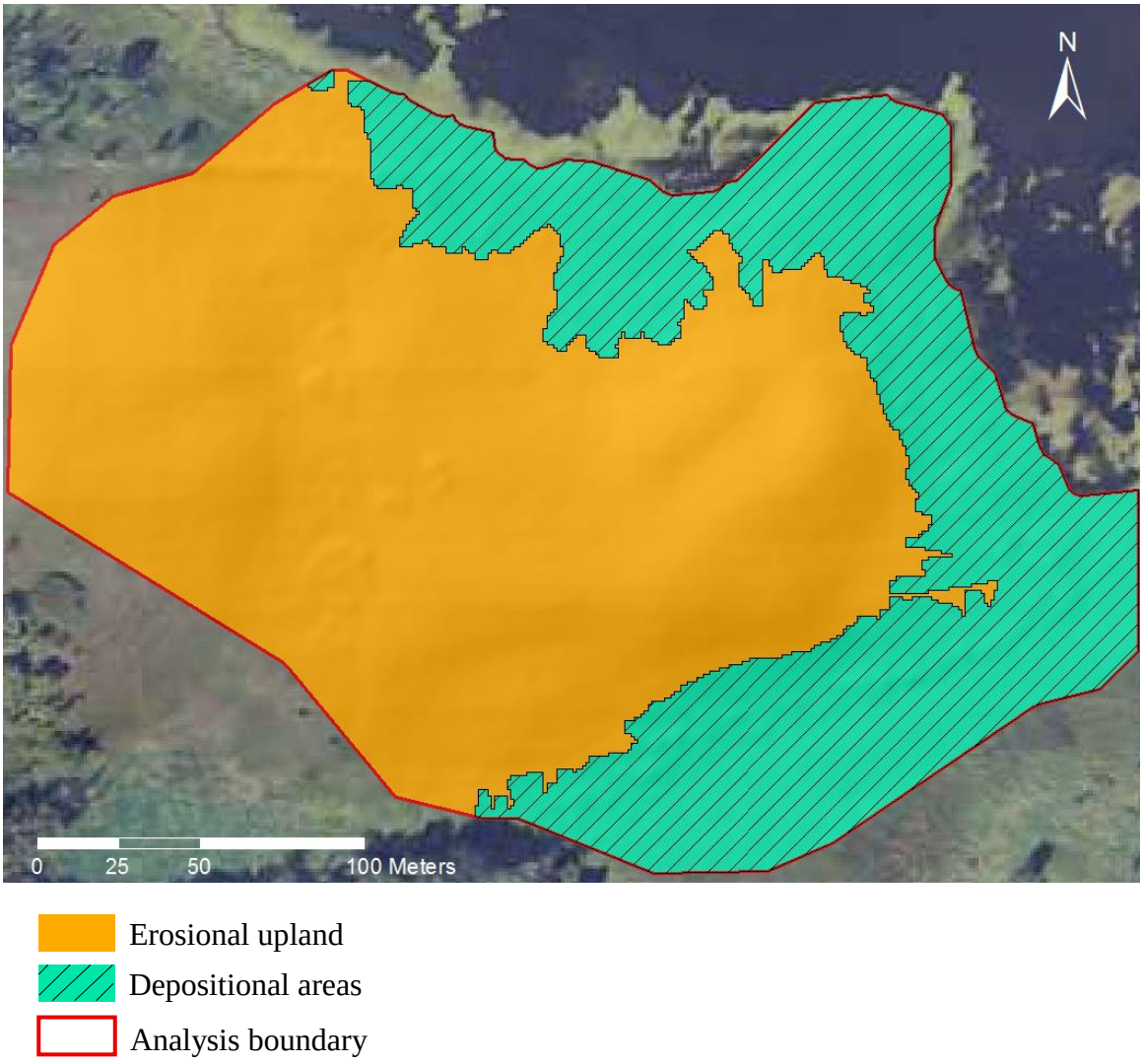

Figure 4.4 The spatial boundary for modeling baseline soil carbon at the Lake Rebecca site. The boundary was defined by the PSA absence (erosional upland, in orange) and presence (depositional area, in green with stripes).

Spatial SOC density maps were first created for the entire Lake Rebecca site with the two pre-settlement baseline regression models, and subsequently clipped to their corresponding boundaries (Figure 4.4). In the depositional area, the spatial distribution of baseline SOC density was developed by summing the products of predicted SOC contents

and the matching soil depths (Minasny et al., 2013), similar as SOC density calculated in Eq. (3.5). The composite SOC storage map was then clipped to the spatial extent of PSA presence.

The clipped SOC storage maps of both the erosional upland and the depositional area were merged into a single 1-m spatial raster map, and the total SOC density at the Lake Rebecca site was estimated. Because the merged map was a floating-point raster (the gridded dataset that carries values in decimal places), the raster did not have an attribute table for cell values (SOC) calculation. I converted the raster into integer format, and generated an attribute table using the scripting language Python. The total baseline SOC content of the entire landscape was calculated by combining SOC density values from all cells in the converted raster attribute table.

The change in SOC density following settlement was determined by subtracting the baseline SOC density map from the current SOC density map (developed in Chapter 3) at every grid cell:

$$C_{diff} = C_{current} - C_{baseline} \tag{4.1}$$

The resulting difference of SOC density C_{diff} between the current and baseline SOC density ($C_{current}$ and $C_{baseline}$, respectively) showed the estimated spatial changes in SOC storage since settlement.

4.4 Results and discussion

Relationship between soil carbon and soil depth in the grassland

The baseline SOC model at the reference grassland site was based on mean soil depth and CTI:

$$\ln(C_v) = 2.898 - 0.017 * \bar{Z} + 0.13 * w \quad (4.2)$$

where $\ln(C_v)$ is volumetric SOC content in a log e scale, $\bar{Z}$ is average soil depth, and w is compound terrain index, or CTI. I log-transformed SOC for residual linearity required for linear regression models. Eq. (4.2) returns an R^2 of 58.6%. When back-transformed (anti-log) the predicted values for sample SOC, I received the MAE of 8.55 and the RMSE of 11.52.

Mean soil depth captured 40% of the SOC variance, which confirmed its significant relationship with SOC in undisturbed landscapes (Brent Dalzell, personal communication, 2014). Unlike soil depth, terrain attributes were less correlated to SOC at the reference site. Together with average soil depth, adding CTI increased the R^2 to 58.6% . During model selection, I found that the combination of slope and SPI in additional soil depth resulted in a slightly higher R^2 (60.7%), but predicted negative SOC contents in steep mid-slope positions at the Lake Rebecca site, most likely due to lack of relief and slope steepness at the reference site. The overall low correlation of terrain attributes with SOC density supports my hypothesis, suggesting that soil materials in uncultivated grasslands without agricultural disturbances remain stable on hillslopes.

Using the reference model, the spatial pattern of SOC density at the erosion upland of the Lake Rebecca site showed a clear spatial pattern of CTI (Figure 4.5). In fact, because the average soil depth applied for the spatial estimation of SOC density in top 1 meter of soil is constant (=0.5 m), the baseline SOC density calculated from the model is merely a scale shift of CTI. Even so, the overall variability of SOC density is fairly small (ranges from 11.1 kg C m^{-2} to 39.2 kg C m^{-2}), and the prediction accuracy should not be a concern due to this spatial pattern. Compared to current SOC density at the Lake Rebecca, low variability in the baseline SOC in erosional upland revealed landscape stability prior to settlement.

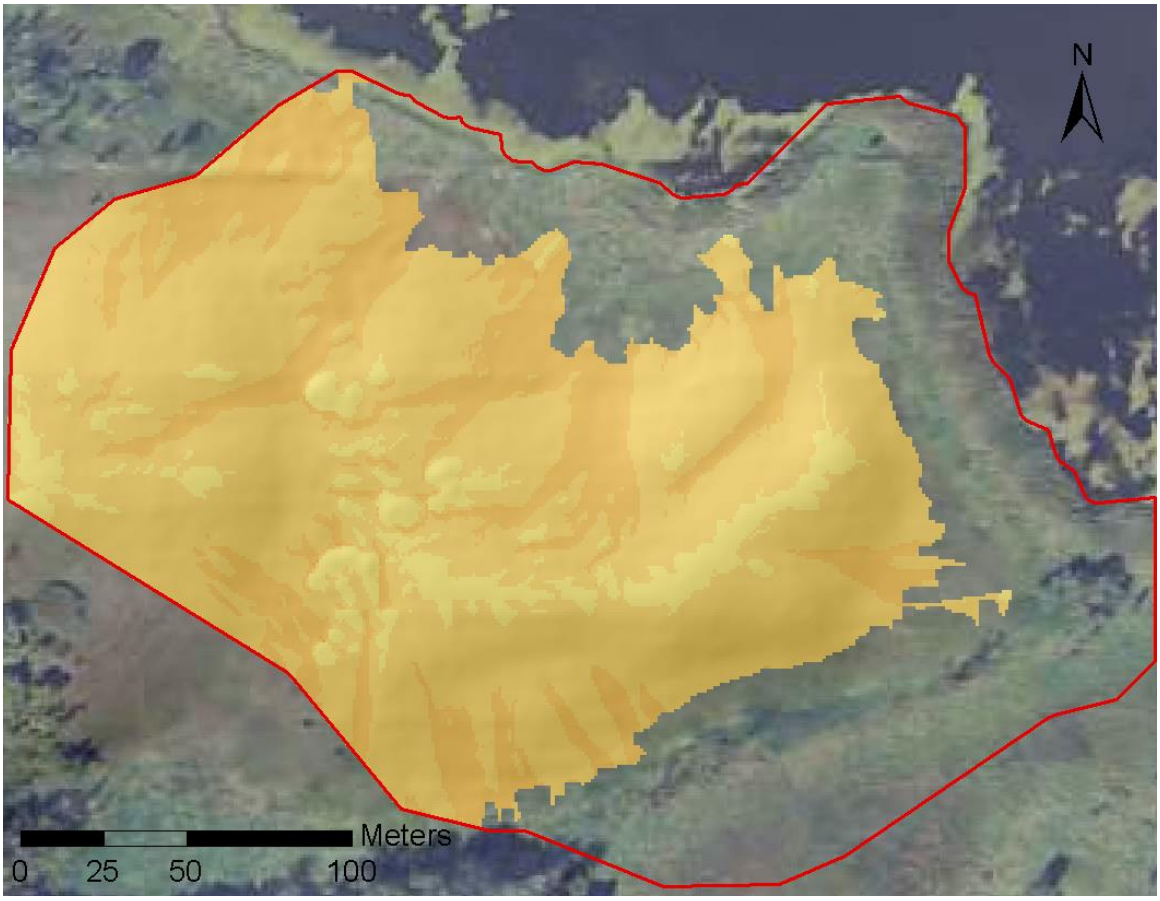

Figure 4.5 The spatial distribution of baseline soil carbon storage in upland locations of the Lake Rebecca study area.

Terrain controls of baseline soil carbon in the depressional area

As to baseline SOC models in the depressional area, the regression models for SOC contents in four depth layers employed relative elevation, slope, and either plan curvature or profile curvature as predictor variables (Table 4.3). The response variable in these baseline models also transformed SOC contents in a log e scale in order to correct heterogeneity issue in error variance.

Table 4.3 Regression results for baseline soil carbon contents in depressional sites.

Depth (cm)	Response, *Y*	Model Parameters, *X*	Regression Coefficient	Adj. R^2
0 - 10	SOC^+	(intercept)	4.153	27.65%
		Relative Elevation	-0.037	
		Slope	-0.049	
		Plan Curvature – concave	-0.311*	
		Plan Curvature – convex	-0.374	
10 - 30	SOC^+	(intercept)	4.014	53.62%
		Relative Elevation	-0.062	
		Slope	-0.058	
		Plan Curvature – concave	-0.242*	
		Plan Curvature – convex	-0.342	
30 - 60	SOC^+	(intercept)	3.434	47.94%
		Relative Elevation	-0.089	
		Slope	-0.044	
		Profile Curvature – concave	-0.325*	
		Profile Curvature – convex	-0.248^	
60 - 100	SOC^+	(intercept)	2.813	35.56%
		Relative Elevation	-0.063	
		Slope	-0.028*	
		Profile Curvature – concave	-0.621	
		Profile Curvature – convex	-0.334^	

+denotes the soil organic carbon in natural logarithmic forms.
*denotes the regression coefficient significant at a 90% level (p-value < 0.10) but not at a 95% level (p-value < 0.05).

^ denotes coefficients insignificant at 90% level (p-value < 0.10).

Relative elevation and slope were two dominant predictor variables in the depressional baseline SOC models for all depths. While curvatures (in three categories: 'straight', 'concave', and 'convex') were found significant to SOC, the models for the top 30 cm of soil (0-10 cm and 10-30 cm) utilized plan curvature and those for the deeper layers (30-60cm and 60-100cm) used profile curvature in addition to relative elevation and slope. The baseline SOC models for the depressional area returned relatively low R^2 values (Table 4.3). Nonetheless, a vertical trend in the SOC variance predicted by terrain attributes was found in both current (in Chapter 3) and baseline (buried) soil. That is, the R^2 values for SOC models at the middle 10 -30 and 30 -60 cm depths (53.62% and 47.94%, respectively) were higher than those for the 0 - 10 and 60-100 cm depths (27.65% and 35.56%, respectively). This trend illustrates that the variance of SOC density captured by terrain attributes changes over depths, and confirmed the need to separate soil profile data into multiple depths for SOC prediction (Kravchenko and Robertson, 2011).

Among the four baseline SOC models, the smallest R^2 (27.65%) occurred in the model at the depth of 0-10 cm, which was assumed to be the original surface layer (Ab1) prior to PSA burial. Surface soil is rich in organic matter but also is biologically active, and it can be influenced by various environmental factors (or soil-forming factors) such as organism (litter quality, root respiration, bioturbation) and climatic conditions (temperature and rainfall) (Jenny, 1941, Davidson and Janssen, 2006; Kramer and Gleixner, 2007). In addition, there are measurement errors in the field. As to deep soil (60-100 cm), the

relatively low R^2 in the depressional baseline SOC model (35.56%) was expected, as deep subsoils are likely to less associate with surface soil processes in the landscape.

The depositional baseline SOC models also display negative relationships between terrain attributes and baseline SOC. That is, any increase of the predictor terrain attributes (relative elevation, slope, and profile and plan curvatures) decreases SOC values. The negative effects of relative elevation and slope to SOC are expected, because soil materials, water, and thus soil carbon is likely to accumulate where elevation is lower (toward the hillslope bottoms) and slope is smaller (in flat areas). As to the relationship between curvatures and SOC, significant regression coefficients suggest a negative effect of convex plan curvature to SOC in the top 30 cm of soil, and a negative effect of concave profile curvature to SOC in the lower depths (30 - 60 and 60 - 100 cm).

The spatial distribution of baseline SOC density ($kg \cdot m^{-2}$) predicted by the four depth models using buried soil profile data are displayed in Figure 4.6. Overall, SOC increases over topographic positions (from summit – midslope – footslope – toeslope) within individual depth layers. SOC also decreases when soil depth increases (from 0 to 100 cm). Footslope and toeslope positions (where these baseline SOC models were developed) in the 0 – 10 cm and 10 – 30 cm layers showed higher soil carbon densities (up to 62.66 $kg \cdot m^{-2}$ and 54.29 $kg \cdot m^{-2}$, respectively) and more variability than the upper hillslope positions (Figures 4.6(a) and (b)). The estimated baseline SOC in the 30 – 60 cm layer ranges from 2.68 $kg \cdot m^{-2}$ to 30.48 $kg \cdot m^{-2}$ (Figure 4.6 (c)), and the estimated SOC in the 60 – 100 cm layer ranges from 2.20 $kg \cdot m^{-2}$ to 16.47 $kg \cdot m^{-2}$ (Figure 4.6 (d)).

Based on the baseline SOC contents estimated in the four depth layers (Figure 4.6), the spatial distribution of SOC density in the top 1m of soil in the depressional area was predicted (Figure 4.7). The SOC density ranges from 6.4 $kg \cdot m^{-2}$ to 32.9 $kg \cdot m^{-2}$ with the mean of 21.2 $kg \cdot m^{-2}$ and standard deviation of 4.9 $kg \cdot m^{-2}$. Variability between cells in Figure 4.7 suggests the 1-m DEM might be too sensitive with respect to tiny elevation changes in local neighborhoods. Possible solutions to avoid such unrealistic local variability include resampling, or applying a 3-m DEM as source data.

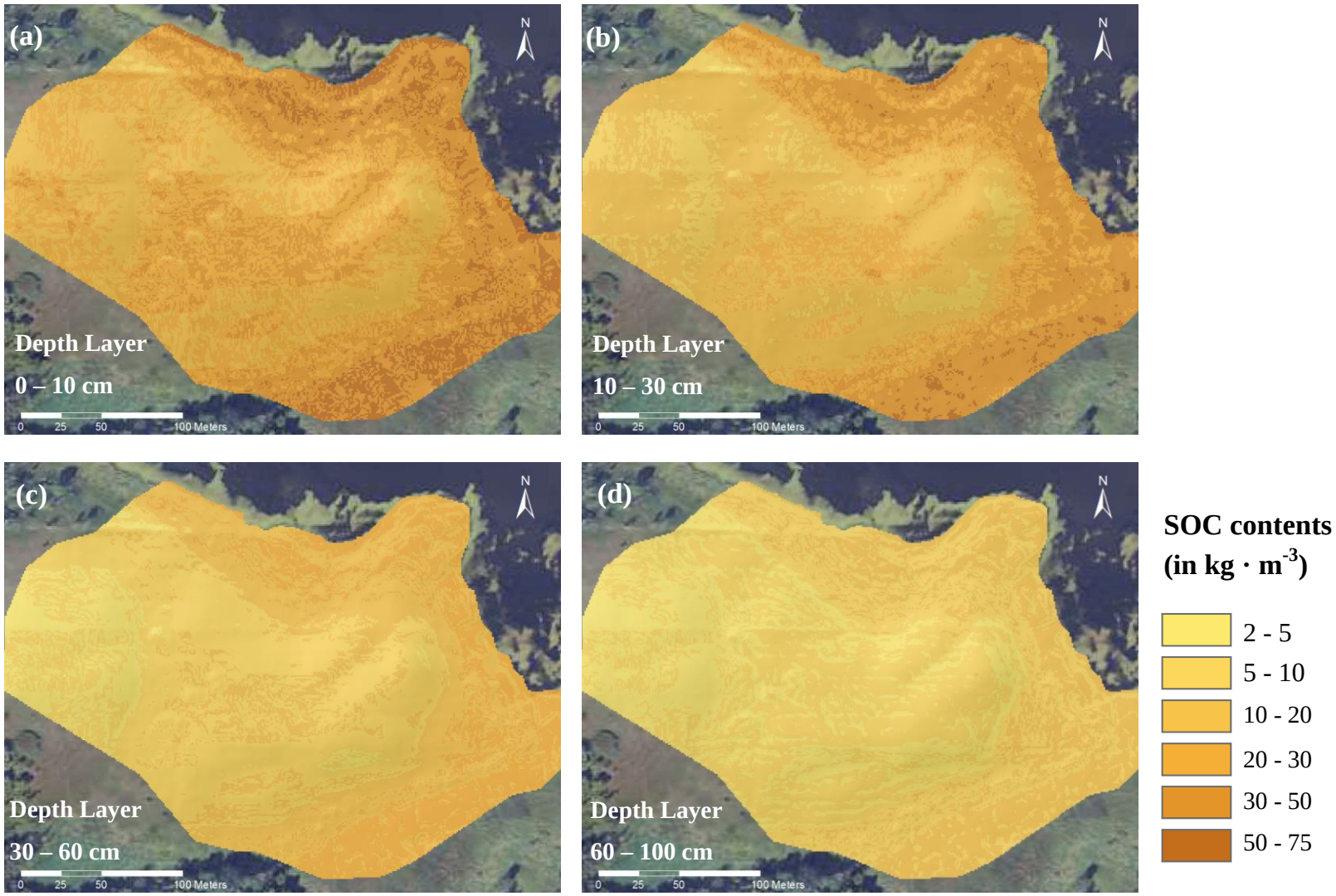

Figure 4.6 The spatial distribution of buried soil profile carbon contents in four depth layers.

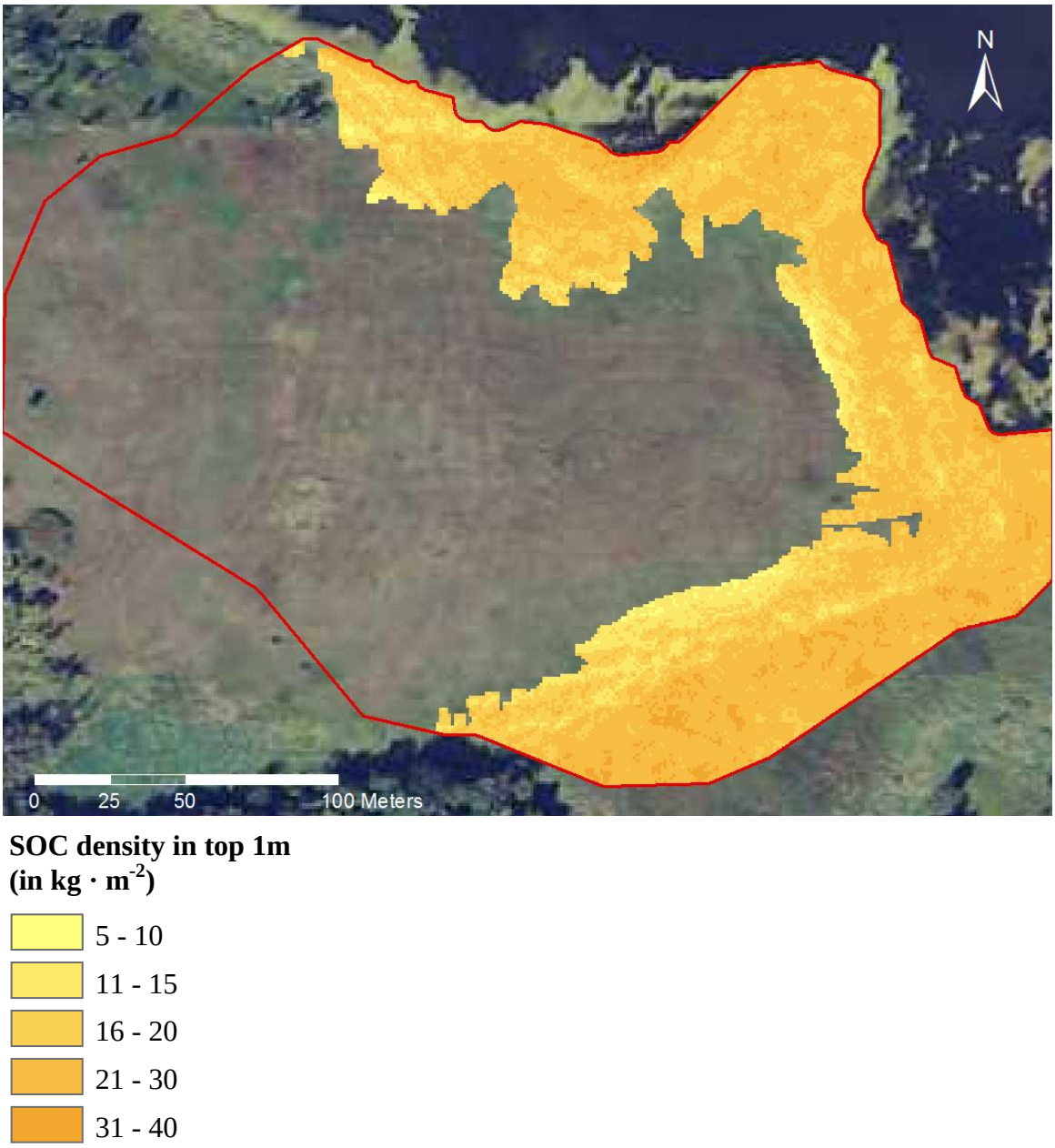

Figure 4.7 The spatial estimation of baseline soil carbon density in depositional sites of the Lake Rebecca site.

By combining Figure 4.5 and Figure 4.7, the overall baseline SOC density in the top 1 meter for the Lake Rebecca site is displayed in Figure 4.8. SOC density at the entire spatial extent ranges from 6.4 $kg \cdot m^{-2}$ to 39.2 $kg \cdot m^{-2}$. Because baseline SOC density was predicted by two approaches and with different sets of terrain attributes, Figure 4.8 shows the mismatched spatial trends between erosional upland and depressional areas. A future direction would be to improve the spatial prediction of the baseline SOC using a more holistic approach applicable to the entire study area. The reference site in Morristown, Minnesota was a suitable analogue for the Lake Rebecca site for its geological settings and climatic conditions, but the lower relief at Morristown limited the model's ability to predict SOC density on higher relief portions of the landscape . Alternatively, using a process-based model (such as SPERO-C) to simulate the environmental conditions (e.g. erosion) and SOC at the Lake Rebecca site in different timeframes may provide a better estimation for the baseline SOC and subsequently for understanding the soil carbon evolution over time (van Oost et al., 2005).

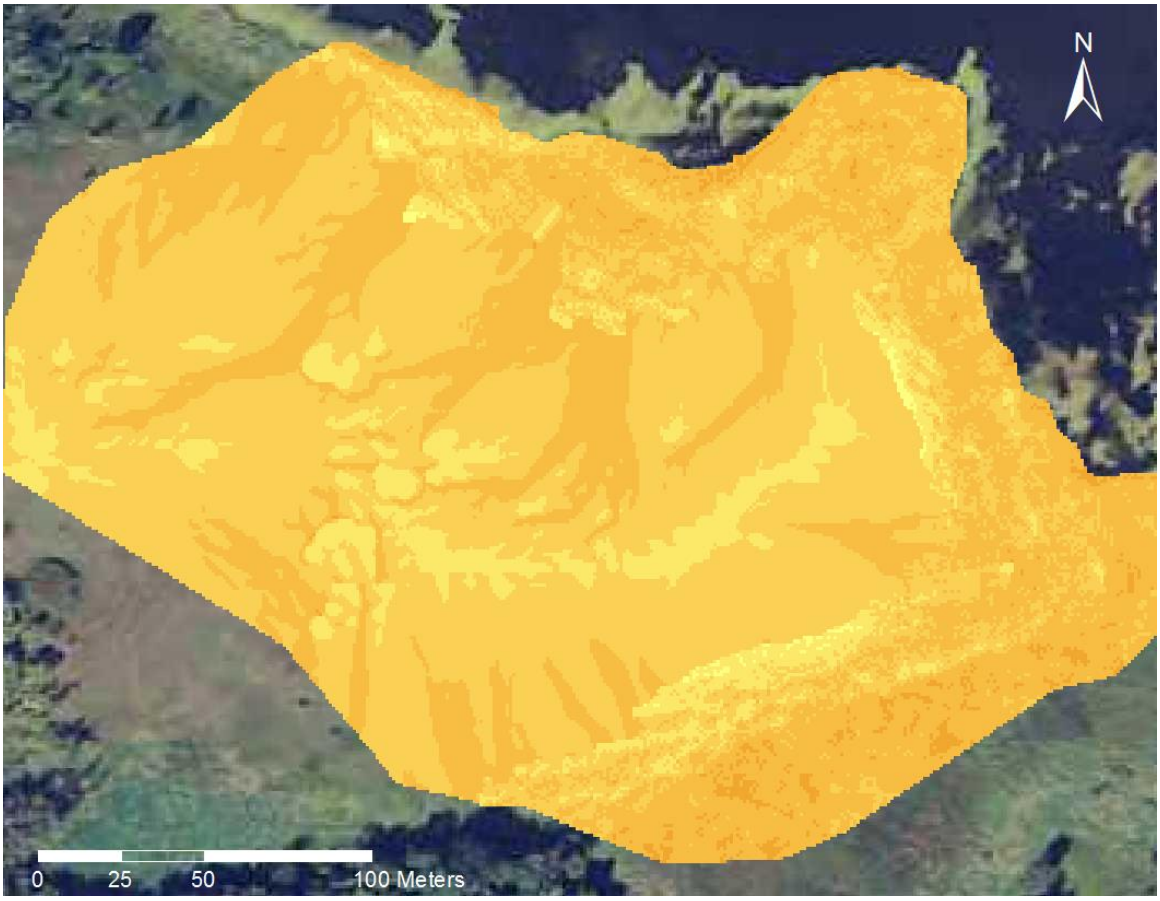

Figure 4.8 The spatial distribution of reference soil carbon storage at the Lake Rebecca site.

By comparing the current SOC density (Figure 3.10) for the Lake Rebecca site with the pre-settlement baseline SOC density (Figure 4.8), the spatial change in SOC density can be mapped (Figure 4.9). This map shows that SOC density has decreased in upland areas following European settlement. The greatest declines in SOC density (in red in Fig. 4.9) have occurred largely on steep hillslopes in the western portion of the site and in a concave profile in the north-central portion of the site, where slopes are steep and CTI is high. Moderately small SOC density losses (5 to 10 kg ·m-2, in orange-red color) occur in the central to eastern side and small SOC density losses (0 to 5 kg · m-2, in orange) occur along the very narrow ridge top in the same area.

The greatest change in SOC density occurs in the depositional area, which shows a large increase (Figure 4.9). The SOC density increase in footslope positions is moderately small (0 – 10 kg · m^{-2}, yellow to very light green), and gradually increases to moderate (10 – 50 kg · m^{-2}, in light green) in the toeslope positions around (north – northeast – east - southeast). In toeslope positions adjacent to permanent marsh in the north and northeast, however, the estimated SOC density increased from 50 to several hundred kg C per m^2.

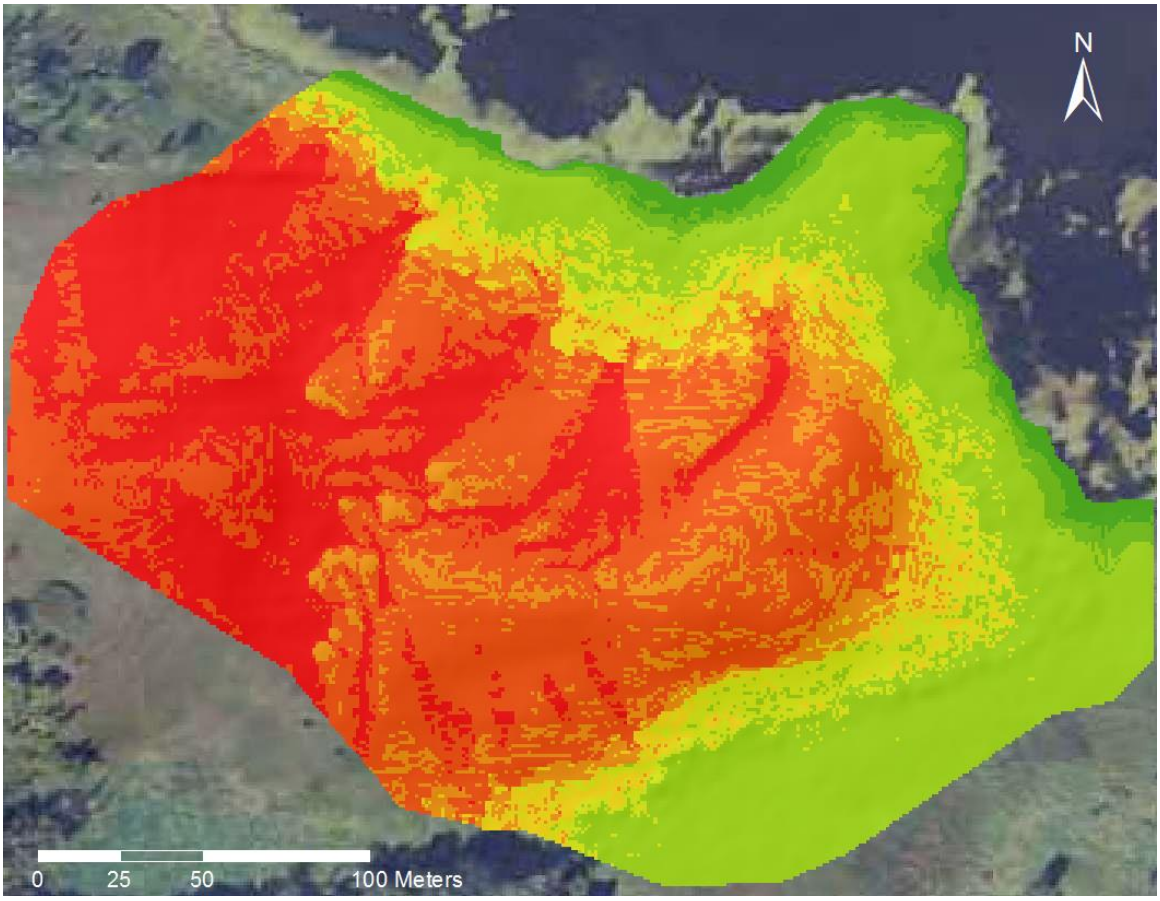

Figure 4.9 The change of soil carbon storage (in the top 1m) since European settlement at the Lake Rebecca site.

Table 4.4 shows the summary statistics for the SOC density change at the Lake Rebecca site. Changes in SOC density ranges from a loss of 30.06 kg C (-30.06 kg · m^{-2}) to a gain of 793.6 kg C per m^2 (793.6 kg · m^{-2}). The total mean change of SOC density for the entire Lake Rebecca site is +7.12 kg C · m^{-2} with the standard deviation of 37.97 kg C · m^{-2}. I suspect that the extremely large increases in SOC density in the wetland locations are inaccurate due to extrapolation issue (no samples were taken in the north and northeast wetlands).

Table 4.4 The summary statistics of changes in soil organic carbon density (kg C · m^{-2}) since European settlement.

Mean	StDev	Min*	Max*	Range
7.12	37.97	-30.06	793.62	824.1

***** Positive number (+) indicates carbon increase and negative number (-) indicates carbon loss.

Although some wetland locations showed very large increases in SOC density since settlement, the area associated with these large increases is relatively small. The estimated whole landscape change in SOC density to 1m deep at the Lake Rebecca site was an increase of 0.409 Gg (1 Gg = 10^6 kg) since settlement. The C increase was estimated between the total quantity of baseline SOC storage (1.119 Gg) and the current SOC storage (1.528 Gg). This result did not support my hypothesis that agricultural erosion and deposition resulted in a net C loss since settlement. An increase in total SOC density of 36.7% since European settlement is not realistic, even if one considers SOC recovery after cultivation ceased in the 1970s.

There are a number of reasons why an increase in whole-landscape SOC density might be observed at the Lake Rebecca site. First, SOC recovery is amplified when surface SOC is eroded, known as 'dynamic replacement' (Harden et al., 1999; Liu and Bliss, 2003). Subsoils in erosional uplands that were exposed to the surface by agricultural erosion and tillage mixing have triggered dynamic replacement. The SOC increase due to dynamic replacement may or may not show in the change map (Figure 4.9), but probably reduces the magnitude of the losses from the upland. Second, conversion of the Lake Rebecca site from agriculture to prairie in the 1970s also has contributed to an increase in SOC at the site (Conant et al., 2001). Third, SOC storage changes in time series with a fixed depth (0 – 100 cm) in erosive landscapes account for different soil bodies within the estimated 1-meter depth window (see Fig. 1.2). Similarly, large SOC increases found in depressional areas have been also influenced by the result of the top 1-meter window comparison. Although PSA contains a lower SOC than its underlying Ab horizons, PSA is likely to still consist of higher SOC density than subsoil horizons that were accounted for within 1-m deep prior to settlement. As a result, sampling of these different depths would underestimate losses from erosional sites as well as underestimate gains in the depositional sites.

Last but not least, the current SOC density values in the lowest part of the depositional sites were overestimated by the model. My spatial models predicted some extremely large values of SOC density (i.e. up to 825 kg $C \cdot m^{-2}$) in the lowest landscape positions. These large predicted values occurred beyond the sampling sites on the hillslopes, and the extrapolation of the spatial models did not accurately predict SOC for the cells close to

permanent wetlands (Figure 4.10). From the perspective of erosion process, PSA would have re-deposited when the overland flow lost kinetic energy (e.g. sudden decrease in slope steepness passing the inflection point on a hillslope) and its deposition would have ended somewhere in the landscape when the flow no longer had sufficient energy to carry eroded materials. The spatial models of SOC at the Lake Rebecca site, however, do not include a mechanism to reduce PSA thickness in lower landscape positions and therefore predict increasing thickness of PSA all the way up to the wetland boundary where the DEM was clipped (Section 3.4). For these reasons, the change in SOC density since European settlement in this portion of the model is highly overestimated. Therefore, the whole landscape estimation of SOC density change is also overestimated and should be further investigated.

Because PSA has lower SOC contents than buried original surface horizons in the depositional area, I expect future SOC density in PSA to increase because of high net primary productivity and low decomposition rates in the depositional areas of depressional landscapes in humid climates. SOC in PSA at depositional surface is unlikely to restore up to 100% of pre-settlement SOC. The new C equilibrium in PSA depends on soil type, properties, and hydrology.

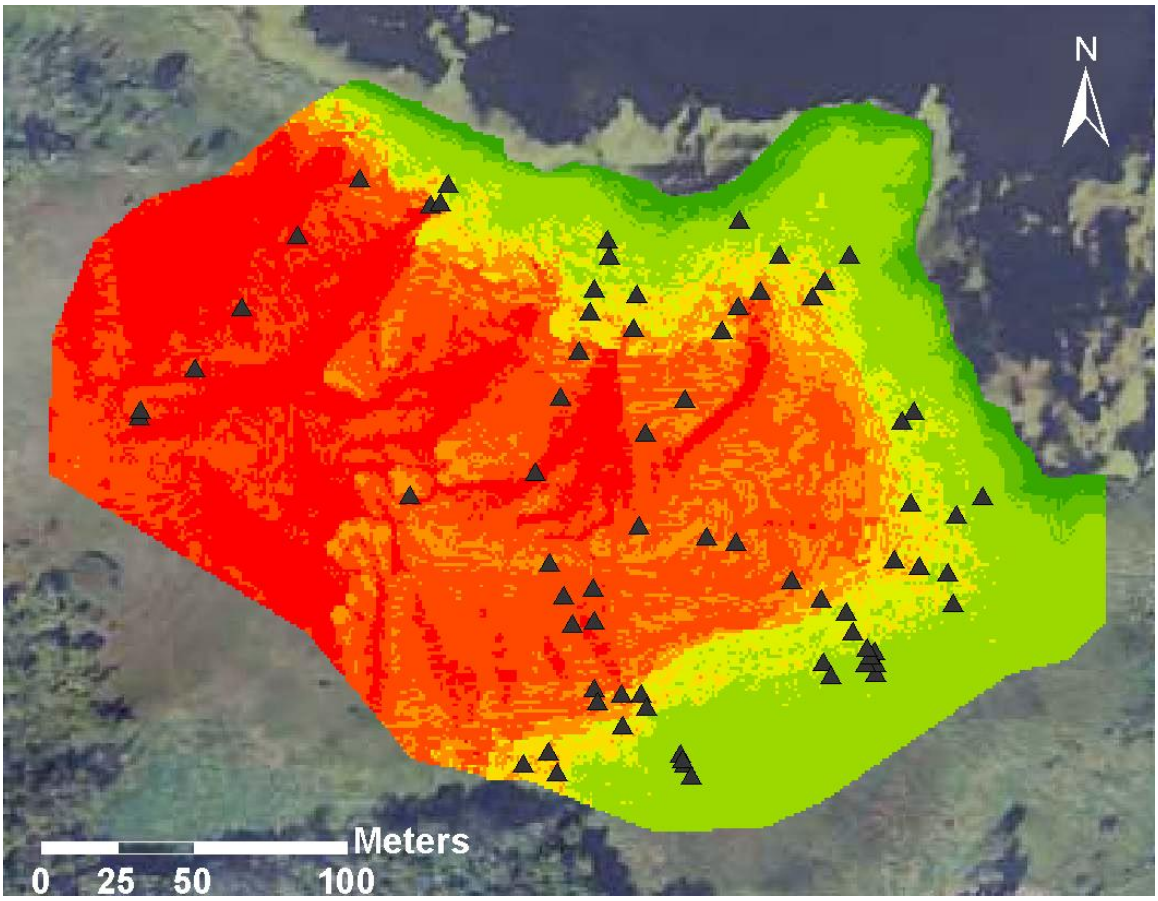

Sample locations

Change in SOC density (kg · m^{-2})

- > 100
- 50 - 100
- 10 - 50
- 5 - 10
- 0 - 5
- -5 - 0
- -10 - -5
- -30.1 - -10

Figure 4.10 The extremely large estimates of change in SOC density are situated beyond sample locations in the lowest landscape positions.

4.5 Conclusion

The reference baseline (pre-settlement) SOC density model developed from data collected from an uncultivated grassland site in Morristown, Minnesota, used mean soil depth and compound terrain index to predict SOC density. Baseline SOC lacked robust relationships with terrain attributes but was highly correlated to soil depth in uncultivated landscapes, as noted by Dalzell (2014).

The baseline SOC density map combined two approaches: (1) estimation of SOC density for the erosional upland from the Morristown site reference model and (2) estimation of SOC density for the depositional areas from depth layer C models using SOC data from buried soil profiles at the Lake Rebecca site. Caution should be taken for data interpretation as no actual pre-settlement measurement is available for verifying the predicted accuracy of the baseline model.

The spatial distribution of change between the pre-settlement and current SOC density confirmed that agriculture-induced redistribution had occurred at the Lake Rebecca site. The soil redistribution has contributed to decreases in SOC density in upland locations and increases in SOC density in depositional areas. On a whole-landscape basis, the model predicted that total SOC density in the 0-1 m soil depth has increased by 0.409 Gg, (36.7%) over the total area (57,527 m^2) of the Lake Rebecca site since European settlement. The increase predicted is surely an overestimation of the change in SOC density. The increase in SOC density can arise from several causes, but is most likely due to poor model performance in areas where SOC density was extrapolated beyond my

sampling locations in the very lowest parts of hillslopes at the study site. This predicted increase in SOC density stands in stark contrast to common assertions that croplands have lost 30-50% of their SOC since settlement.

While this result did not agree with my hypothesis that agricultural erosion results in a net C loss in this depressional landscape, it is difficult to say whether agricultural erosion has increased SOC density due to the uncertainties surrounding these estimates. Based on these considerations, further investigation, more intense sampling, and model improvement will be required in order to better estimate the change in SOC density since agricultural settlement.

Chapter 5
Summary and conclusion

This study investigated the spatial distribution of post-settlement alluvium (PSA) and soil organic carbon (SOC) in a depressional landscape in Minnesota, and the net SOC storage change due to erosion-induced redistribution since agricultural settlement. Chapter 2 investigated the spatial presence and thickness of PSA at Lake Rebecca Park Reserve, Minnesota, and Chapter 3 examined the spatial distribution and quantity of SOC at the same study site. In Chapter 4, I evaluated whole-landscape SOC storage change by synthesizing the results of previous chapters with the estimated pre-settlement SOC.

The significant findings and contribution in Chapter 2 include: First, the newly developed regional terrain attributes showed the importance of upslope topography in soil-landscape modeling. A spatial predictive model with a combination of selected local and regional terrain attribute predictors explained PSA thickness much better than models built with only local terrain attributes. Together with specific catchment area (SCA), upslope area with moderately high slope steepness (8-12%), the percentage of upslope area (%UA) with straight profile curvature, and %UA with straight plan curvature explained 73.8% of the variance in PSA thickness.

Second, local terrain attributes predicted the spatial distribution of PSA presence very well (pseudo-R^2= 85.8%) and predicted PSA thickness moderately well (R^2=41.3%). The results show that PSA was only present in lower hillslope positions (footslope and toeslope/wetland). The PSA presence model used relative elevation, flow path length and

stream power index (SPI) as predictors. Relative elevation is especially important in determining PSA presence, indicating that hillslope position is the most important control on PSA presence in the landscape. On the other hand, SCA and plan curvature were the best predictors used for PSA thickness. The variance explained (R^2) greatly increased if using a mix of local and regional terrain attributes as predictors, but spatial prediction was still limited to local terrain attributes. Due to the large demand on computational time, it was not feasible to calculate regional terrain variables across the entire study area for PSA prediction.

Third, the spatial distribution of PSA thickness had high variability, but locations (1-m cells) with the largest deposition (61-99.5 cm thick) were found in the north-central footslope and the northwest toeslope positions. Moderate PSA deposition (41-80 cm thick) was found in southern footslope positions. Finally, PSA occupied about 1/5 of the study area (61,250 m^2), with a total estimated volume of 8082.6 m^3.

There are two key conclusions in Chapter 3: First, SOC in agriculture-influenced, closed-depressional landscapes can be accurately predicted by terrain attributes. Terrain attributes explained 52.25% to 81.3% of SOC variability, depending on soil depth intervals, in the top 1 m of soil.

Second, it is necessary to analyze SOC in multiple profile depths. SOC distribution patterns were strongly related to terrain attributes at depths of 10-30 cm (R^2 = 70.17%) and 30-60 cm (R^2 = 81.3%). This strong response of SOC to topography in subsoil layers is different from previous studies that showed decreasing trends of topographic

influences with increasing depth, and suggests that the original surface layers have been buried by PSA due to agricultural erosion. This model estimated that the uppermost meter of soil in the 6-ha study site contained 1.528 Gg SOC.

Chapter 4 has three important findings: First, SOC in uncultivated grassland had no significant correlations with terrain attributes. Topographic control of SOC distribution in agricultural landscapes (e.g. the Lake Rebecca site) is likely attributed to erosion-induced soil redistribution. Without observable erosion and deposition, grassland SOC is not correlated to topography but only to depth within the soil.

Second, the spatial distribution of SOC density at the Lake Rebecca site has changed due to erosion and deposition since European settlement. There has been an increase in SOC density (kg m^{-2}) in the uppermost meter in the footslope and toeslope positions due to the deposition of PSA. Compared to the current SOC density distribution (5.4 - 825 kg C $\cdot$ m^{-2}), the estimated pre-settlement SOC density had a much smaller range (6.4 - 39.2 kg C $\cdot$ m^{-2}). The smaller variability in the pre-settlement SOC density revealed landscape stability before agriculture started. Note that the SOC density in the upper 30 cm of PSA is still less than that of the original soil surface. As such, the total SOC in the upper 30 cm across the site is less than that of the pre-settlement surface.

Third, the net change in whole-landscape SOC storage in this depressional landscape since European settlement is positive, but an improvement of model performance is required. The overall increase in SOC storage (0.409 Gg, or 36.7%) is surely an overestimation, most likely due to poor model performance in the very lowest part of the

hillslope beyond sample locations. The lack of mechanism in the spatial models to reduce PSA thickness beyond the end of the zone of deposition, as a natural sediment pattern, results in unreasonably large values of SOC density predicted in the wetlands at the edge of the analysis boundary. Nonetheless, the prediction of increase in SOC density still challenges the unlikely but common assertions of large SOC loss (30-50%) for the depressional landscapes similar to the Lake Rebecca site.

Limitations and Future Research

One of the challenges faced in estimating net SOC storage change since settlement in this and other studies is the paucity of reference data. While the spatial variability of SOC was well predicted by terrain attributes, I could not find proper controls on temporal changes. I used a combination of two models – one from a reference grassland and the other from buried original soil profiles – to estimate pre-settlement SOC distribution. These estimates are not ideal because the reference site may or may not produce an accurate portrayal of pre-settlement conditions at the Lake Rebecca site. One of the possibilities for filling the temporal gap is to couple with process-based tillage erosion models (e.g. SPERO-C) to estimate the past erosion rates and associated SOC movement in the landscape. Another approach is to use radionuclide tracers (i.e. ^{210}Pb, ^{137}Cs) to accurately quantify erosion and redistribution and to improve the prediction of landscape sediment distribution. Time-series data can also be generated for the future scenarios and used for better predicting carbon sequestration potential in the future.

While regional terrain attributes suggest significant promise in predicting the spatial distribution of PSA thickness, the actual spatial prediction of PSA thickness could only be predicted with local terrain attributes. Building regional terrain attributes for every single cell of the entire spatial extent is prohibitively time consuming. Automation for building upslope contributing areas (UCAs) and the subsequent spatial extraction of terrain attributes in the UCAs will accelerate the process in developing regional terrain attributes and improves the spatial prediction of PSA. The automation process may be beneficial in using the SAGA's module library or API in scripting language such as Python.

Another improvement in the future is also in the line of regional terrain attributes. This will be to develop an algorithm to spatially quantify the trend of slope and curvatures over the entire upslope area (of any given location). I suspect that the significance of the 'straight' upslope plan and profile curvatures in response to PSA thickness was a signal for erroneously bundling upslope cells with curvatures developed per local (3x3 cells) window basis for upslope curvature. Identifying true regional curvature through more advanced techniques of digital terrain analysis will help to accurately quantify upslope landforms and improve the spatial prediction of soil properties.

In summary, upscaling spatial models of SOC and PSA to a regional scale is a priority for future direction of this research. When thinking about usability of scientific research, it is essential to obtain results applicable at a regional or even a global scale, so they can be of greater benefit to society. Because of similar landforms and climatic conditions, depressional landscapes in Southern Minnesota (where the Des Moines lobe till plain is

located) are likely to produce spatial patterns of PSA and SOC similar to the results obtained in this study at the Lake Rebecca site. The actual model transferability and upscaling effects, however, require further evaluation and validation. More environmental covariates including land cover, land use history, vegetation, and soil properties (e.g. texture classes, soil moisture) might be required in order to obtain suitable regional models for PSA and SOC.

Regional landscape models for SOC and agriculture-induced redistribution will provide stakeholders, including land managers, policy makers, and farmers, with the tools to determine the best practices and suitable regulations in preserving land resources and soil carbon for a sustainable future. Additionally, for the purpose of future carbon credits or taxes, the determination of possible SOC sequestration will rely on the accurate determination of PSA distribution as well as the understanding of additional SOC sequestration potential in PSA.

References

Adhikari, K., Kheir, R. B., Greve, M., Bøcher, P. K., Malone, B., Minasny, B., McBratney, A., & Greve, M. 2012. Progress towards GlobalSoilMap. net soil database of denmark. *Digital Soil Assessment and Beyond.* CRC Press, Boca Raton, FL, 445-451.

Amundson, R. 2001. The carbon budget in soils. *Annual Review of Earth and Planetary Sciences, 29*(1), 535-562.

Anderson, J. L., Grigal, D., & Cooper, T. 1984. *Soils and landscapes of minnesota* Minnesota Extension Service, University of Minnesota.

Arrouays, D., Balesdent, J., Mariotti, A., & Girardin, C. 1995. Modelling organic carbon turnover in cleared temperate forest soils converted to maize cropping by using 13C natural abundance measurements. *Plant and Soil,173*(2), 191-196.

Australian Soil Resource Information System. 2011. ASRIS - Australian Soil Resource Information System. Retrieved from: http://www.asris.csiro.au.

Baker, J. M., Ochsner, T. E., Venterea, R. T., & Griffis, T. J. 2007. Tillage and soil carbon sequestration—What do we really know? *Agriculture, Ecosystems & Environment, 118*(1), 1-5.

Balco, G., Stone, J. O., & Jennings, C. 2005. Dating Plio-Pleistocene glacial sediments using the cosmic-ray-produced radionuclides 10Be and 26Al. *American Journal of Science*, 305(1), 1-41.

Balesdent, J., Wagner, G. H., & Mariotti, A. 1988. Soil organic matter turnover in long-term field experiments as revealed by carbon-13 natural abundance. *Soil Science Society of America Journal, 52*(1), 118-124.

Beach, T. 1994. The fate of eroded soil: Sediment sinks and sediment budgets of agrarian landscapes in southern minnesota, 1851-1988. *Annals of the Association of American Geographers, 84*(1), 5-28.

Bedard-Haughn, A., Jongbloed, F., Akkerman, J., Uijl, A., De Jong, E., Yates, T., & Pennock, D. 2006. The effects of erosional and management history on soil organic carbon stores in ephemeral wetlands of hummocky agricultural landscapes. *Geoderma, 135*, 296-306.

Belia, S., Fidler, F., Williams, J., & Cumming, G. 2005. Researchers misunderstand confidence intervals and standard error bars. *Psychological Methods, 10*(4), 389.

Berhe, A. A., Harden, J. W., Torn, M. S., Kleber, M., Burton, S. D., & Harte, J. 2012. Persistence of soil organic matter in eroding versus depositional landform positions. *Journal of Geophysical Research: Biogeosciences (2005–2012), 117*(G2)

Berhe, A. A., Harte, J., Harden, J. W., & Torn, M. S. 2007. The significance of the erosion-induced terrestrial carbon sink. *Bioscience, 57*(4), 337-346.

Bishop, T. F. A., McBratney, A. B., & Laslett, G. M. 1999. Modelling soil attribute depth functions with equal-area quadratic smoothing splines. *Geoderma, 91*(1–2), 27-45.

Bishop, T.F.A. and Minasny, B. 2006. Digital soil-terrain modeling: the predictive potential and uncertainty. In Grunwald, S. (Eds.), *Environmental soil-landscape modeling: Geographic information technologies and pedometrics*, 185-214. Boca Raton, FL, USA: CRC Press.

Borra, S., & Di Ciaccio, A. 2010. Measuring the prediction error. A comparison of cross-validation, bootstrap and covariance penalty methods. *Computational Statistics & Data Analysis, 54*(12), 2976-2989.

Brabyn, L. 1996. Landscape classification using GIS and national digital databases. *Landscape Research, 21*(3), 277-300.

Bradford, J. B., Lauenroth, W. K., & Burke, I. C. 2005. The impact of cropping on primary production in the US great plains. *Ecology, 86*(7), 1863-1872.

Brady, N. C., & Weil, R. R. 2004. *Elements of the nature and properties of soils.* Upper Saddle River, NJ: Pearson Educational International.

Brown, D. 2006. A historical perspective on soil-landscape modeling. In Grunwald, S. (Eds.), *Environmental soil-landscape modeling: Geographic information technologies and pedometrics*, 61-103. Boca Raton, FL, USA: CRC Press.

Bui, E., Henderson, B., & Viergever, K. 2009. Using knowledge discovery with data mining from the Australian Soil Resource Information System database to inform soil carbon mapping in Australia. *Global biogeochemical cycles, 23*(4).

Burt, R. 2004. *Soil survey laboratory methods manual:* Soil survey investigations report no. 42 version 4.0. Nebraska: Natural Resources Conservation Service, United states department of agriculture.

Bushnell, T. M. 1943. Some aspects of the soil catena concept. *Soil Science Society of America Journal, 7*(C), 466-476.

Chatterjee, A., Lal, R., Wielopolski, L., Martin, M. Z., & Ebinger, M. H. 2009. Evaluation of different soil carbon determination methods. *Critical Reviews in Plant Sciences, 28*(3), 164-178.

Ciais, P., C. Sabine, G. Bala, L. Bopp, V. Brovkin, J. Canadell, A. Chhabra, R. DeFries, J. Galloway, M. Heimann, C. Jones, C. Le Quéré, R.B. Myneni, S. Piao and P. Thornton. 2013. Carbon and Other Biogeochemical Cycles. In: *Climate Change 2013: The Physical Science Basis. Contribution of Working Group I to the Fifth Assessment Report of the Intergovernmental Panel on Climate Change* [Stocker, T.F.,

D. Qin, G.-K. Plattner, M. Tignor, S.K. Allen, J. Boschung, A. Nauels, Y. Xia, V. Bex and P.M. Midgley (eds.)]. Cambridge, United Kingdom and New York, NY, USA: Cambridge University Press.

Cimmery, V. 2010. SAGA-GIS Manual. User Guide for SAGA (version 2.0.5) Volume 1. Retrieved from: http://sourceforge.net/projects/saga-gis/files/SAGA%20-%20Documentation/SAGA%202%20User%20Guide/

Conant, R. T., Paustian, K., & Elliott, E. T. 2001. Grassland management and conversion into grassland: Effects on soil carbon. *Ecological Applications, 11*(2), 343-355.

Cowardin, L. M., Carter, V., Golet, F. C., & LaRoe, E. T. 1979. *Classification of wetlands and deepwater habitats of the united states.* Fish and Wildlife Service, US Department of the Interior Washington, DC.

Dahl, P.M. 1898. *Plat book of Hennepin County, Minnesota* (Compiled and drawn from official records and actual surveys). The Northwestern Map Publishing Co.

Dalzell, B. 2014. Personal communication.

De Alba, S., Lindstrom, M., Schumacher, T. E., & Malo, D. D. 2004. Soil landscape evolution due to soil redistribution by tillage: A new conceptual model of soil catena evolution in agricultural landscapes. *Catena, 58*(1), 77-100.

Dlugoß, V., Fiener, P., Van Oost, K., & Schneider, K. 2012. Model based analysis of lateral and vertical soil carbon fluxes induced by soil redistribution processes in a small agricultural catchment. *Earth Surface Processes and Landforms, 37*(2), 193-208.

Dunevitz, H. and Epp, A. 1995. Natural communities and rare species of Rice County, Minnesota. *Minnesota County Biological Survey Map Series* No. 8. Department of Natural Resources.

Eddins, S. 2009. File Exchange -- Upslope area functions. Matlab® Central. Retrieved from: http://www.mathworks.com/matlabcentral/fileexchange/15818-upslope-area-functions.

ESRI. 2013. ArcGIS Help 10.2 – Curvature (Spatial Analyst). Retrieved from: http://resources.arcgis.com/en/help/main/10.2/index.html#//009z000000tw000000.

Euliss Jr, N. H., Gleason, R., Olness, A., McDougal, R., Murkin, H., Robarts, R., Bourbonniere, R., & Warner, B. 2006. North American prairie wetlands are important nonforested land-based carbon storage sites. *Science of the Total Environment, 361*(1), 179-188.

Fissore, C., Giardina, C. P., Kolka, R. K., Trettin, C. C., King, G. M., Jurgensen, M. F., Barton, C. D., & McDowell, S. D. 2008. Temperature and vegetation effects on soil

organic carbon quality along a forested mean annual temperature gradient in North America. *Global Change Biology*, 14(1), 193-205.

Florinsky, I.V. 2012. *Digital Terrain Analysis In Soil Science And Geology*. Elsevier/Academic Press, Amsterdam, 379 p. ISBN 978-0-12-385036-2.

Foley, J. A., DeFries, R., Asner, G. P., Barford, C., Bonan, G., Carpenter, S. R., Chapin, F. S., Coe, M. T., Daily, G. C., Gibbs, H. K., Helkowski, J. H., Holloway, T., Howard, E. A., Kucharik, C. J., Monfreda, C., Patz, J. A., Prentice, I. C., Ramankutty, N., & Snyder, P. K. 2005. Global consequences of land use. *Science, 309*(5734), 570-574.

Follain, S., Minasny, B., McBratney, A. B., & Walter, C. 2006. Simulation of soil thickness evolution in a complex agricultural landscape at fine spatial and temporal scales. *Geoderma, 133*(1), 71-86.

Freeman, T. G. 1991. Calculating catchment area with divergent flow based on a regular grid. *Computers & Geosciences, 17*(3), 413-422.

Fugro Horizons, Inc. & Minnesota Department of Natural Resources (MN-DNR). 2011. LiDAR Elevation. Twin Cities Metro Region, Minnesota. (Metadata of LiDAR DEM) Retrieved from: http://www.mngeo.state.mn.us/chouse/metadata/lidar_metro2011.html#Data_Quality_Information.

Fuller, L. G., & Anderson, D. W. 1993. Changes in soil properties following forest invasion of black soils of the Aspen Parkland. *Canadian journal of soil science, 73*(4), 613-627.

Gallant, J. C. and Wilson, J. P. 2000.Primary topographic attributes. In: Wilson, J. P. & Gallant, J. C. (Eds.). *Terrain analysis: Principles and applications*, 1-28. New York, NY, USA: John Wiley & Sons, Inc.

Gaspar, L., Navas, A., Walling, D., Machín, J., & Gómez Arozamena, J. 2013. Using ^{137}Cs and $^{210}Pb_{ex}$ to assess soil redistribution on slopes at different temporal scales. *Catena, 102*, 46-54.

Gessler, P., Chadwick, O., Chamran, F., Althouse, L., & Holmes, K. 2000. Modeling soil–landscape and ecosystem properties using terrain attributes. *Soil Science Society of America Journal, 64*(6), 2046-2056.

Gessler, P., Moore, I., McKenzie, N., & Ryan, P. 1995. Soil-landscape modelling and spatial prediction of soil attributes. *International Journal of Geographical Information Systems, 9*(4), 421-432.

Govers, G., Vandaele, K., Desmet, P., Poesen, J., & Bunte, K. 1994. The role of tillage in soil redistribution on hillslopes. *European Journal of Soil Science, 45*(4), 469-478.

Grandy, A. S., & Neff, J. C. 2008. Molecular C dynamics downstream: The biochemical decomposition sequence and its impact on soil organic matter structure and function. *Science of the Total Environment, 404*(2), 297-307.

Gregorich, E., Greer, K., Anderson, D., & Liang, B. 1998. Carbon distribution and losses: Erosion and deposition effects. *Soil and Tillage Research, 47*(3), 291-302.

Grimm, R., Behrens, T., Märker, M., & Elsenbeer, H. 2008. Soil organic carbon concentrations and stocks on Barro Colorado Island—digital soil mapping using Random Forests analysis. *Geoderma, 146*(1), 102-113.

Grunwald, S. 2005. *Environmental soil-landscape modeling:* Geographic information technologies and pedometrics. CRC Press.

Grunwald, S. 2009. Multi-criteria characterization of recent digital soil mapping and modeling approaches. *Geoderma, 152*(3), 195-207.

Grunwald, S., Thompson, J., & Boettinger, J. 2011. Digital soil mapping and modeling at continental scales: Finding solutions for global issues. *Soil Science Society of America Journal, 75*(4), 1201-1213.

Harden, J., Sharpe, J., Parton, W., Ojima, D., Fries, T., Huntington, T., & Dabney, S. 1999. Dynamic replacement and loss of soil carbon on eroding cropland. *Global Biogeochemical Cycles, 13*(4), 885-901.

Harris, D., Horwath, W., & van Kessel, C. 2001. Acid fumigation of soils to remove carbonates prior to total organic carbon or carbon-13 isotopic analysis. *Soil Science Society of America Journal, 65*(6), 1853-1856.

Hennepin County, 1873. Collection of Minnesota County Atlases. 175, Roll 3, Microfilm, Minnesota History Society.

Hobbs, H.C. and Goebel, J.E. 1982. Geologic map of Minnesota, Quaternary geology. Minnesota Geological Survey.

Houghton, R. A., Hackler, J. L., & Lawrence, K. T. 1999. The US carbon budget: Contributions from land-use change. *Science, 285*(5427), 574-578.

Jacinthe, P., & Lal, R. 2001. A mass balance approach to assess carbon dioxide evolution during erosional events. *Land Degradation & Development, 12*(4), 329-339.

Jenkinson, D., & Coleman, K. 2008. The turnover of organic carbon in subsoils. part 2. modelling carbon turnover. *European Journal of Soil Science, 59*(2), 400-413.

Jenny, H. 1941. Factors of Soil Formation. *A System of Quantitative Pedology* 1st edn. New York: McGraw-Hill Book Co.

Jenny, H. 1946. Arrangement of soil series and types according to functions of soil-forming factors. *Soil Science, 61*(5), 375-392.

Jenny, H. 1949. Comparative study of dcomposition rates of organic matter in temperate and tropical regions. *Soil Science, 68*(6), 419-432.

Jobbagy, E. G., & Jackson, R. B. 2000. The vertical distribution of soil organic carbon and its relation to climate and vegetation. *Ecological Applications, 10*(2), 423-436.

Kempen, B., Brus, D. J., & Stoorvogel, J. J. 2011. Three-dimensional mapping of soil organic matter content using soil type–specific depth functions. *Geoderma, 162*(1–2), 107-123.

Kramer, C., & Gleixner, G. 2008. Soil organic matter in soil depth profiles: Distinct carbon preferences of microbial groups during carbon transformation. *Soil Biology and Biochemistry, 40*(2), 425-433.

Kravchenko, A. N., & Robertson, G. P. 2011. Whole-profile soil carbon stocks: The danger of assuming too much from analyses of too little. *Soil Science Society of America Journal, 75*(1), 235-240.

Kumar, S., Lal, R., & Liu, D. 2012. A geographically weighted regression kriging approach for mapping soil organic carbon stock. *Geoderma, 189–190*(0), 627-634.

Kutner, M. H., Nachtsheim, C., & Neter, J. 2004. *Applied linear regression models* McGraw-Hill/Irwin.

Lal, R. 2003. Soil erosion and the global carbon budget. *Environment International, 29*(4), 437-450.

Lennon, M. J. 2009. *Carbon sequestration in prairie pothole wetlands.* Thesis (M.S.) -- University of Minnesota, 2009.

Lobb, D., Kachanoski, R., & Miller, M. 1995. Tillage translocation and tillage erosion on shoulder slope landscape positions measured using 137Cs as a tracer. *Canadian Journal of Soil Science, 75*(2), 211-218.

Magellan Professional. 2006. MobileMapper™ Office User Manual. Magellan®. Retrieved from: https://www.msu.edu/~ashton/classes/428/labs/lab02/MM6_users_manual.pdf

Mäkipää, R., Liski, J., Guendehou, S., Malimbwi, R., & Kaaya, A. 2012. *Soil carbon monitoring using surveys and modelling: General description and application in the united republic of tanzania* Food and Agriculture Organization of The United Nations.

Malone, B. P., McBratney, A. B., Minasny, B., & Laslett, G. M. 2009. Mapping continuous depth functions of soil carbon storage and available water capacity. *Geoderma, 154*(1–2), 138-152.

Mamo, M. and Hain, P. 2005. *Erosion Control Measures: ECM for Cropped Environments - Tillage Management*. University of Nebraska, Lincoln. Plant & Soil Sciences eLibraryPRO. Retrieved from: http://passel.unl.edu/pages/informationmodule.php?idinformationmodule=1088801071&topicorder=10&maxto=16.

Mann, L. K. 1986. Changes in soil carbon storage after cultivation. *Soil Science*, 142(5), 279-288.

Marchetti, A., Piccini, R., Francaviglia, R., Santucci, S., & Chiuchiarelli, I. 2010. Estimating soil organic matter content by regression kriging. In: J.L. Boettinger, D.W. Howell, A.C. Moore, A.E. Hartemink, S. Kienast-Brown (Eds.), *Digital Soil Mapping: Bridging Research, Environmental Application, and Operation*, 241 – 254. Progress in Soil Science, Springer, Heidelberg.

Marschner, F. 1974. The original vegetation of minnesota, a map compiled in 1930 by FJ marschner under the direction of ML Heinselman of the U.S. Forest Service. St. Paul, MN: Cartography Laboratory of the Department of Geography, University of Minnesota. map (1:500,000).

Martinez, C., Hancock, G. R., & Kalma, J. D. 2010. Relationships between 137Cs and soil organic carbon (SOC) in cultivated and never-cultivated soils: An Australian example. *Geoderma, 158*(3), 137-147.

Mendonça-Santos, M. L., M.L. Mendonça-Santos, A.B. McBratney, & B. Minasny. 2006. Soil prediction with spatially decomposed environmental factors. In: P. Lagacherie, A.B. McBratney, M. Voltz (Eds.), *Developments in Soil Science*, pp. 269 – 278. Elsevier.

McBratney, A. B., Mendonça Santos, M. L., & Minasny, B. 2003. On digital soil mapping. *Geoderma, 117*(1–2), 3-52.

McBratney, A., Minasny, B., MacMillan, R., & Carré, F. 2011. Digital soil mapping. *Handbook of Soil Science, Volume 1: Properties and Processes* (2nd Eds.) pp. 1-44. CRC Press.

McCarty, G., & Ritchie, J. 2002. Impact of soil movement on carbon sequestration in agricultural ecosystems. *Environmental Pollution, 116*(3), 423-430.

McKenzie, N.J., Gessler, P.E., and Ryan, P.J. 2000. The role of terrain analysis in soil mapping. In: Wilson, J. P., & Gallant, J. C. (Eds.). *Terrain analysis: Principles and applications*, 245-266. New York, NY, USA: John Wiley & Sons, Inc.

McKenzie, N.J. & Ryan, P.J. 1999. Spatial prediction of soil properties using environmental correlation. *Geoderma, 89*, 67 – 94.

McLauchlan, K. 2006. The nature and longevity of agricultural impacts on soil carbon and nutrients: A review. *Ecosystems, 9*(8), 1364-1382.

Miklos, M., Short, M.G., McBratney, A.B. & Minasny, B. 2010. Mapping and comparing the distribution of soil carbon under cropping and grazing management practices in Narrabri, north-west New South Wales. *Australian Journal of Soil Research 48*, 248 – 257.

Milne, G. 1935. Some suggested units of classification and mapping for East African soils. *Soil Research*, 4:183–198.

Minasny, B., McBratney, A. B., Malone, B. P., & Wheeler, I. 2013. Digital mapping of soil carbon. *Advances in Agronomy*, 118, 1-47.

Minasny, B., McBratney, A.B., Mendonça-Santos, M.L., Odeh, I.O.A. & Guyon, B. 2006. Prediction and digital mapping of soil carbon storage in the Lower Namoi Valley. *Australian Journal of Soil Research 44*, 233 – 244

Minnesota Geospatial Information Office. 2012. LiDAR Elevation Data for Minnesota. Retrieved from: http://www.mngeo.state.mn.us/chouse/elevation/lidar.html).

Mishra, U., Lal, R., Liu, D., & Van Meirvenne, M. 2010. Predicting the spatial variation of the soil organic carbon pool at a regional scale. *Soil Science Society of America Journal, 74*(3), 906-914.

Moore, I. D., Gessler, P., Nielsen, G. A. e., & Peterson, G. 1993. Soil attribute prediction using terrain analysis. *Soil Science Society of America Journal, 57*(2), 443-452.

Moorman, T. B., Cambardella, C. A., James, D. E., Karlen, D. L., & Kramer, L. A. 2004. Quantification of tillage and landscape effects on soil carbon in small iowa watersheds. *Soil & Tillage Research, 78*(2), 225-236.

Mueller, T. G., & Pierce, F. J. 2003. Soil Carbon Maps. *Soil Science Society of America Journal, 67*(1), 258-267.

Muñoz, J. D., & Kravchenko, A. 2011. Soil carbon mapping using on-the-go near infrared spectroscopy, topography and aerial photographs. *Geoderma,166*(1), 102-110.

Norton, L. D. 1986. Erosion-sedimentation in a closed drainage basin in northwest indiana. *Soil Science Society of America Journal, 50*(1), 209-213.

Odgers, N. P., Libohova, Z., & Thompson, J. A. 2012. Equal-area spline functions applied to a legacy soil database to create weighted-means maps of soil organic carbon at a continental scale. *Geoderma, 189–190*(0), 153-163.

Olaya, V. 2009. Basic Land-Surface Parameters. In Hengl T., Reuter H. I. and ScienceDirect (Online service) (Eds.), *Geomorphometry : Concepts, software, applications*. Amsterdam ; Oxford : Elsevier.

Olaya, V., & Conrad, O. 2009. Geomorphometry in SAGA. Chapter 12 in geomorphometry concepts, software, applications. *Developments on Soil Science, 33*, 293-308.

Paul, E., Harris, D., Collins, H., Schulthess, U., & Robertson, G. 1999. Evolution of CO_2 and soil carbon dynamics in biologically managed, row-crop agroecosystems. *Applied Soil Ecology, 11*(1), 53-65.

Pennock, D. & Frick, A. 2001. The role of field studies in landscape-scale applications of process models: An example of soil redistribution and soil organic carbon modeling using CENTURY. *Soil and Tillage Research, 58*(3), 183-191.

Ponce-Hernandez, R., Marriott, F. H. C., & Beckett, P. H. T. 1986. An improved method for reconstructing a soil profile from analyses of a small number of samples. *Journal of Soil Science, 37*(3), 455-467.

Post, W. M., Emanuel, W. R., Zinke, P. J., & Stangenberger, A. G. 1982. Soil carbon pools and world life zones. *Nature, 298*, 156 - 159

Post, W. M., & Kwon, K. C. 2000. Soil carbon sequestration and land-use change: Processes and potential. *Global Change Biology, 6*(3), 317-327.

Pribyl, D. W. 2010. A critical review of the conventional SOC to SOM conversion factor. *Geoderma, 156*(3), 75-83.

Razakamanarivo, R. H., Grinand, C., Razafindrakoto, M. A., Bernoux, M., & Albrecht, A. 2011. Mapping organic carbon stocks in eucalyptus plantations of the central highlands of Madagascar: a multiple regression approach. *Geoderma, 162*(3), 335-346.

Reuter, R. J., & Bell, J. C. 2003. Hillslope hydrology and soil morphology for a wetland basin in south-central minnesota. *Soil Science Society of America Journal, 67*(1), 365-372.

Richardson, J., Arndt, J. L., & Freeland, J. 1994. Wetland soils of the prairie potholes. *Advances in Agronomy, 52*, 121-172.

Ritchie, J. C., & McHenry, J. R. 1990. Application of radioactive fallout cesium-137 for measuring soil erosion and sediment accumulation rates and patterns: A review. *Journal of Environmental Quality, 19*(2), 215-233.

Ritchie, J. C., McCarty, G. W., Venteris, E. R., & Kaspar, T. 2007. Soil and soil organic carbon redistribution on the landscape. *Geomorphology, 89*(1), 163-171.

Rosenbloom, N. A., Harden, J. W., Neff, J. C., & Schimel, D. S. 2006. Geomorphic control of landscape carbon accumulation. *Journal of Geophysical Research-Biogeosciences, 111*(G1), G01004.

Russell, A. E., Cambardella, C. A., Laird, D. A., Jaynes, D. B., & Meek, D. W. 2009. Nitrogen fertilizer effects on soil carbon balances in midwestern US agricultural systems. *Ecological Applications, 19*(5), 1102-1113.

Schaetzl, R. J. & Anderson, S. 2005. *Soils : Genesis and geomorphology*. Cambridge, UK ; New York; New York: Cambridge University Press.

Schlesinger, W. H. 1995. An overview of the carbon cycle. *Soils and Global Change, 25*

Schulp, C. J. E., & Verburg, P. H. 2009. Effect of land use history and site factors on spatial variation of soil organic carbon across a physiographic region. *Agriculture, Ecosystems & Environment, 133*(1), 86-97.

Schwanghart, W., & Jarmer, T. 2011. Linking spatial patterns of soil organic carbon to topography—a case study from south-eastern Spain. *Geomorphology,126*(1), 252-263.

Simbahan, G. C., & Dobermann, A. 2006. Sampling optimization based on secondary information and its utilization in soil carbon mapping. *Geoderma,133*(3), 345-362.

Six, J., & Jastrow, J. D. 2002. Organic matter turnover. *Encyclopedia of soil science,* 936-942.

Six, J., Conant, R., Paul, E., & Paustian, K. 2002. Stabilization mechanisms of soil organic matter: Implications for C-saturation of soils. *Plant and Soil, 241*(2), 155-176.

Smith, S. V., Renwick, W. H., Buddemeier, R. W., & Crossland, C. J. 2001. Budgets of soil erosion and deposition for sediments and sedimentary organic carbon across the conterminous united states. *Global Biogeochemical Cycles, 15*(3), 697-707.

Soil Survey Staff. 2013. Web Soil Survey. Natural Resources Conservation Service, United States Department of Agriculture (USDA-NRCS). Retrieved from: http://websoilsurvey.nrcs.usda.gov.

Stallard, R. F. 1998. Terrestrial sedimentation and the carbon cycle: Coupling weathering and erosion to carbon burial. *Global Biogeochemical Cycles, 12*(2), 231-257.

Stewart, C. E., Paustian, K., Conant, R. T., Plante, A. F., & Six, J. 2007. Soil carbon saturation: Concept, evidence and evaluation. *Biogeochemistry, 86*(1), 19-31.

Syswerda, S., Corbin, A., Mokma, D., Kravchenko, A., & Robertson, G. 2011. Agricultural management and soil carbon storage in surface vs. deep layers. *Soil Science Society of America Journal, 75*(1), 92-101.

Thompson, J. A., & Kolka, R. K. 2005. Soil carbon storage estimation in a forested watershed using quantitative soil-landscape modeling. *Soil Science Society of America Journal, 69*(4), 1086-1093.

Thompson, J. A., Pena-Yewtukhiw, E. M., & Grove, J. H. 2006. Soil-landscape modeling across a physiographic region: Topographic patterns and model transportability. *Geoderma, 133*(1-2), 57-70.

Tilman, D., Cassman, K. G., Matson, P. A., Naylor, R., & Polasky, S. 2002. Agricultural sustainability and intensive production practices. *Nature, 418*(6898), 671-677.

Tivet, F., de Moraes Sa, Joao Carlos, Lal, R., Briedis, C., Borszowskei, P. R., dos Santos, J. B., Farias, A., Eurich, G., Hartman, D. d. C., & Nadolny Junior, M. 2013. Aggregate C depletion by plowing and its restoration by diverse biomass-C inputs under no-till in sub-tropical and tropical regions of brazil. *Soil and Tillage Research,* 126, 203-218.Tiner, R. W. 2003. Geographically isolated wetlands of the united states. Wetlands, 23(3), 494-516.

Torn, M. S., Trumbore, S. E., Chadwick, O. A., Vitousek, P. M., & Hendricks, D. M. 1997. Mineral control of soil organic carbon storage and turnover. *Nature, 389*(6647), 170-173.

Toy, T. J., Foster, G. R., & Renard, K. G. 2002. *Soil erosion: Processes, prediction, measurement, and control.* John Wiley & Sons.

Trumbore, S. 2009. Radiocarbon and soil carbon dynamics. *Annual Review of Earth and Planetary Sciences, 37*, 47-66.

United States General Land Office. n.d. Original Entry Tract Books. *State Archives Microfilm 46*. Minnesota History Society.

USDA- NRCS. 2010. *Field Indicators of Hydric Soils in the United States: A guide for identifying and delineating hydric soils, Version 7.0.* L.M. Vasilas, G.W. Hurt, and C.V. Noble (eds.). USDA-NRCS in cooperation with the National Technical Committee for Hydric Soils, Fort Worth, TX.

van Hemelryck, H., Govers, G., van Oost, K., & Merckx, R. 2010. Evaluating the impact of soil redistribution on the in situ mineralization of soil organic carbon. *Earth Surface Processes and Landforms,* , n/a-n/a.

van Oost, K., Govers, G., & Desmet, P. 2000. Evaluating the effects of changes in landscape structure on soil erosion by water and tillage. *Landscape Ecology, 15*(6), 577-589.

van Oost, K., Govers, G., Quine, T. A., Heckrath, G., Olesen, J. E., de Gryze, S., & Merckx, R. 2005. Landscape-scale modeling of carbon cycling under the impact of soil redistribution: The role of tillage erosion. *Global Biogeochemical Cycles, 19*(4), GB4014.

van Oost, K., Quine, T. A., Govers, G., De Gryze, S., Six, J., Harden, J. W., Ritchie, J. C., McCarty, G. W., Heckrath, G., Kosmas, C., Giraldez, J. V., da Silva, J. R., & Merckx, R. 2007. The impact of agricultural soil erosion on the global carbon cycle. *Science, 318*(5850), 626-629.

van Oost, K., Verstraeten, G., Doetterl, S., Notebaert, B., Wiaux, F., Broothaerts, N., & Six, J. 2012. Legacy of human-induced C erosion and burial on soil-atmosphere C exchange. *Proceedings of the National Academy of Sciences of the United States of America, 109*(47), 19492-19497.

Vasques, G. M., Grunwald, S., Comerford, N. B., & Sickman, J. O. 2010. Regional modelling of soil carbon at multiple depths within a subtropical watershed. *Geoderma, 156*(3), 326-336.

Viaud, V., Angers, D. A., Parnaudeau, V., Morvan, T., & Aubry, S. M. 2011. Response of organic matter to reduced tillage and animal manure in a temperate loamy soil. *Soil use and management, 27*(1), 84-93.

Vitousek, P. M. 1994. Beyond global warming - ecology and global change. Ecology, 75(7), 1861-1876.

von Lützow, M., Kögel-Knabner, I., Ekschmitt, K., Flessa, H., Guggenberger, G., Matzner, E., & Marschner, B. 2007. SOM fractionation methods: relevance to functional pools and to stabilization mechanisms. *Soil Biology and Biochemistry, 39*(9), 2183-2207.

von Lützow, M. V., Kögel-Knabner, I., Ekschmitt, K., Matzner, E., Guggenberger, G., Marschner, B., & Flessa, H. 2006. Stabilization of organic matter in temperate soils: mechanisms and their relevance under different soil conditions–a review. *European Journal of Soil Science, 57*(4), 426-445.

Walling, D., He, Q., & Blake, W. 1999. Use of 7Be and 137Cs measurements to document short-and medium-term rates of water-induced soil erosion on agricultural land. *Water Resources Research, 35*(12), 3865-3874.

Walling, D., He, Q., & Quine, T. 1995. Use of caesium-137 and lead-210 as tracers in soil erosion investigations. *IAHS Publications-Series of Proceedings and Reports-Intern Assoc Hydrological Sciences, 229*, 163-172.

Wilson, J. P. and Gallant, J. C. 2000. Digital terrain analysis. In: Wilson, J. P. & Gallant, J. C. (Eds.). *Terrain analysis: Principles and applications*, 1-28. New York, NY, USA: John Wiley & Sons, Inc.

Wright Jr, H. 1976. The dynamic nature of holocene vegetation: A problem in paleoclimatology, biogeography, and stratigraphic nomenclature. *Quaternary Research, 6*(4), 581-596.

Wright Jr., H. E. 1992. Patterns of holocene climatic change in the midwestern united states. *Quaternary Research, 38*(1), 129-134.

Yadav, V., & Malanson, G. 2008. Spatially explicit historical land use land cover and soil organic carbon transformations in Southern Illinois. *Agriculture, ecosystems & environment, 123*(4), 280-292.

Yadav, V., & Malanson, G. P. 2009. Modeling impacts of erosion and deposition on soil organic carbon in the big creek basin of southern illinois. *Geomorphology, 106*(3-4), 304-314.

Yoo, K., Amundson, R., Heimsath, A. M., & Dietrich, W. E. 2005. Erosion of upland hillslope soil organic carbon: Coupling field measurements with a sediment transport model. *Global Biogeochemical Cycles, 19*(3), GB3003.

Yoo, K., Amundson, R., Heimsath, A. M., & Dietrich, W. E. 2006. Spatial patterns of soil organic carbon on hillslopes: Integrating geomorphic processes and the biological C cycle. *Geoderma, 130*(1-2), 47-65.

Zhao, Y,-C., Shi, X.-Z., 2010. Spatial prediction and uncertainty assessmenet of soil organic carbon in Hebei province, China. In: Boettinger, J.L., Howell, D.W., Moore, A.C., Hartemink, A.E., Kienast-Brown, S (Eds.), *Digital Soil Mapping: Bridging Research Environmental Application, and Operation,* 227-239. Progress in Soil Science, Springer, Netherlands.

Appendix A. Sample locations and the observed thickness of post-settlement alluvium.

SAMPLE ID	X_UTM	Y_UTM	PSA Thickness (cm)
001-TOE	440866.5	4989022.241	60
002-FOOT	440870.2839	4989152.362	46
003-TOE	440871.1432	4989163.432	80
004-TOE	440862.3801	4989175.849	76
005-FOOT	440928.7035	4989162.756	0
006-TOE	440932.5668	4989167.821	36
007-TOE	440842.137	4989013.758	47
008-DEP	440861.4872	4989181.266	50
009-DEP	440940.7629	4989176.426	29
010-FOOT	440958.0774	4989121.899	49
011-TOE	440962.1411	4989125.273	64
012-TOE	440845.0991	4989007.11	69
013-FOOT	440803.6087	4989192.931	0
014-TOE	440809.4374	4989199.49	51
015-TOE	440806.7925	4989193.566	42
016-FOOT	440960.8409	4989095.054	33
017-TOE	440975.7849	4989091.311	41
018-DEP	440984.5765	4989097.357	52
019-FOOT	440955.6304	4989076.568	35
020-TOE	440974.9414	4989062.427	0
021-TOE	440973.1157	4989072.262	0
022-FOOT	440963.7571	4989074.498	53
023-FOOT	440855.7898	4989157.751	76
025-FOOT	440852.2874	4989145.015	35
026-BACK	440846.072	4989129.89	0
027-SUM	440837.9167	4989105.373	0
028-DEP	440904.6364	4989187.745	48
029-SUM	440872.0678	4989087.729	0
031-BD1	440857.1161	4989165.126	75
1A	440893.9503	4989084.271	0

SAMPLE ID	X_UTM	Y_UTM	PSA Thickness (cm)
1B	440903.911	4989082.448	0
1C	440921.9454	4989069.672	0
1D	440939.8224	4989059.448	28
1E	440946.2806	4989042.633	26
2A	440708.7799	4989125.638	0
2AB	440708.4159	4989123.306	0
2B	440726.5514	4989139.264	0
2C	440741.8823	4989159.316	0
2D	440759.9967	4989182.681	0
2E	440780.3458	4989201.396	0
3A	440842.7046	4989075.699	0
3B	440847.105	4989064.809	0
3C	440850.061	4989055.412	0
3D	440858.2918	4989030.051	0
3DB	440857.2778	4989034.305	0
4C	440931.6257	4989063.646	0
4D1	440941.8649	4989052.936	33
4E1	440946.7798	4989047.732	27
4E3	440947.8578	4989045.289	31
5B	440856.8805	4989067.342	0
5C	440857.1899	4989056.505	0
5D1	440872.6552	4989032.625	33
5D2	440866.3048	4989032.786	0
5E2	440874.3504	4989028.389	36
6S1	440796.9516	4989097.863	0
7B	440874.0699	4989118.175	0
7C	440886.9006	4989129.142	0
7D1	440899.1778	4989151.709	0
7E1	440904.5538	4989159.558	18
7E2	440911.5011	4989164.466	20
7E3	440917.9121	4989176.28	34

Appendix B.

Soil organic carbon contents at sampling locations.

Sample ID	Upper Depth (cm)	Lower Depth (cm)	Raw C ($kg \cdot m^{-3}$)
1A	0	10	9.555
1A	10	55	8.595
1A	55	95	4.37
1A	95	132	4.244
1A	132	144	4.491
1A	144	170	10.588
1B	0	16	13.777
1B	16	33	7.095
1B	33	67	5.771
1B	67	80	4.635
1B	80	98	4.273
1B	98	120	3.522
1B	120	136	3.282
1B	136	146	3.045
1B	146	163	3.263
1C	0	8	23.212
1C	8	20	10.433
1C	20	40	9.04
1C	40	50	7.58
1C	50	60	7.583
1C	60	64	
1C	64	75	5.528
1C	75	80	4.461
1D	0	28	17.46
1D	28	62	23.575
1D	62	71	13.407
1D	71	90	9.197
1D	90	98	6.393
1D	98	105	8.484
1D	105	125	9.738
1D	125	140	8.616
1D	140	150	8.14
1D	150	160	37.488
1E	0	4	115.677
1E	4	10	62.559
1E	10	30	40.568
1E	30	43	66.365
1E	43	50	
1E	50	60	17.003
2A	0	3	40.445
2A	3	26	17.108
2A	26	40	9.382
2A	40	55	8.135
2A	55	66	7.25
2A	66	85	7.606
2A	85	100	5.192
2AB	0	22	20.118
2AB	22	35	14.843
2AB	35	55	8.491
2AB	55	72	6.361
2AB	72	85	6.938
2AB	85	108	5.087
2AB	108	120	
2AB	120	135	3.473
2AB	135	142	5.924
2AB	142	153	2.569
2AB	153	164	2.693
2AB	164	180	7.302
2B	1	10	27.623
2B	10	18	21.911

Sample ID	Upper Depth (cm)	Lower Depth (cm)	Raw C ($kg \cdot m^{-3}$)
2B	18	32	7.126
2B	32	48	6.017
2B	48	55	4.849
2C	0	15	32.412
2C	15	30	12.744
2C	30	38	0.867
2C	38	53	6.64
2D	0	30	12.597
2D	30	54	6.652
2D	54	90	5.85
2D	90	99	9.606
2D	99	120	5.107
2E	0	10	29.682
2E	10	43	13.176
2E	43	68	11.002
2E	68	80	7.074
2E	80	91	7.325
2E	91	95	
2E	95	118	3.152
3A	0	15	20.884
3A	15	26	12.693
3A	26	50	
3A	50	64	
3A	64	80	
3A	73	90	3.921
3B	0	10	13.809
3B	10	21	16.317
3B	21	40	9.382
3B	40	72	6.122
3C	0	7	23.032
3C	7	26	13.821
3D	0	30	13.775
3D	30	57	20.614

Sample ID	Upper Depth (cm)	Lower Depth (cm)	Raw C ($kg \cdot m^{-3}$)
3D	57	62	
3D	62	90	11.639
3DB	0	8	15.542
3DB	8	20	13.375
3DB	35	69	
3DB	69	80	
3DB	80	103	
3DB	103	150	6.616
4C	0	29	15.726
4C	29	59	6.483
4D1	0	33	27.756
4D1	33	60	23.539
4D1	60	86	7.725
4D1	86	150	5.68
4E1	0	27	32.474
4E1	27	70	19.105
4E1	70	90	12.115
4E1	90	97	13.147
4E1	97	130	9.621
4E1	130	145	6.727
4E1	145	152	15.603
4E3	0	3	70.175
4E3	3	24	40.875
4E3	24	34	29.863
4E3	34	60	43.68
4E3	60	75	15.616
5B	0	20	18.564
5B	20	45	6.348
5B	45	59	
5B	59	74	8.905
5C	0	20	15.014
5C	20	45	9.097
5C	45	78	5.5

Sample ID	Upper Depth (cm)	Lower Depth (cm)	Raw C ($kg \cdot m^{-3}$)
5C	78	100	4.393
5C	100	130	4.931
5D1	0	20	22.088
5D1	20	33	18.207
5D1	33	52	18.096
5D1	52	80	16.41
5D1	80	90	11.743
5D1	90	115	8.023
5D2	0	14	20.254
5D2	14	30	17.436
5D2	30	70	6.107
5D2	70	80	4.496
5D2	80	95	5.092
5D2	95	128	4.849
5E2	0	30	17.893
5E2	30	40	17.082
5E2	40	98	18.194
5E2	98	110	17.122
6S1	0	24	20.224
6S1	24	50	7.075
7B	0	7	30.827
7B	7	30	12.07
7B	30	54	7.281
7C	0	7	31.938
7C	7	21	14.755
7C	21	28	8.569
7C	28	44	5.639
7C	44	54	6.031
7C	54	60	6.723
7C	60	75	4.206
7C	75	100	3.422
7D	0	44	21.651
7D	44	69	11.027

Sample ID	Upper Depth (cm)	Lower Depth (cm)	Raw C ($kg \cdot m^{-3}$)
7D	69	85	7.871
7D	85	97	6.891
7D	97	110	7.526
7E	0	18	28.662
7E	18	40	19.137
7E	40	58	11.988
7E2	0	5	33.195
7E2	5	20	16.412
7E2	20	33	13.197
7E3	0	3	55.754
7E3	3	23	26.863
7E3	23	34	21.416
7E3	34	48	20.128
7E3	48	69	19.192
7E3	69	85	15.09
7E3	85	100	5.483
001-TOE	0	21	26.001
001-TOE	21	43	21.184
001-TOE	43	60	20.962
001-TOE	60	78	13.986
001-TOE	78	100	14.418
001-TOE	100	116	13.571
001-TOE	116	141	12.796
002-FOOT	0	10	37.1
002-FOOT	10	32	15.585
002-FOOT	32	46	18.167
002-FOOT	46	59	24.936
002-FOOT	59	68	26.652
002-FOOT	68	90	18.817
002-FOOT	90	104	18.584
002-FOOT	104	121	15.521
002-FOOT	121	130	5.599
002-FOOT	130	150	12.886

Sample ID	Upper Depth (cm)	Lower Depth (cm)	Raw C ($kg \cdot m^{-3}$)
003-TOE	0	3	42.965
003-TOE	3	39	22.58
003-TOE	39	50	22.807
003-TOE	50	60	34.927
003-TOE	60	80	37.413
003-TOE	80	90	42.721
003-TOE	90	110	31.868
003-TOE	110	143	23.941
003-TOE	143	155	19.572
004-TOE	0	4	74.986
004-TOE	4	9	46.982
004-TOE	9	12	26.614
004-TOE	12	30	18.315
004-TOE	30	50	
004-TOE	50	73	
004-TOE	73	80	67.939
004-TOE	80	88	144.411
004-TOE	88	100	53.032
004-TOE	100	124	19.427
005-FOOT	0	10	44.61
005-FOOT	10	29	21.039
005-FOOT	29	41	10.986
005-FOOT	41	56	10.251
005-FOOT	56	73	5.255
005-FOOT	73	84	3.404
006-TOE	0	6	55.349
006-TOE	6	26	31.705
006-TOE	26	36	22.739
006-TOE	36	45	20.485
006-TOE	45	58	14.363
006-TOE	58	68	10.963
007-TOE	0	18	29.72
007-TOE	18	47	24.561
007-TOE	47	74	25.228
007-TOE	74	90	14.896
008-DEP	0	7	85.529
008-DEP	7	11	43.398
008-DEP	11	21	25.723
008-DEP	21	31	21.894
008-DEP	31	52	20.401
008-DEP	52	57	25.562
008-DEP	57	73	134.278
008-DEP	73	78	122.257
008-DEP	78	90	45.68
008-DEP	90	100	25.849
009-DEP	0	5	105.05
009-DEP	5	13	123.139
009-DEP	13	29	52.32
009-DEP	29	49	51.175
009-DEP	49	56	43.968
009-DEP	56	67	34.08
010-FOOT	0	9	44.642
010-FOOT	9	23	22.153
010-FOOT	23	49	17.329
010-FOOT	49	59	15.477
010-FOOT	59	69	14.625
011-TOE	0	3	96.67
011-TOE	3	12	74.276
011-TOE	12	24	39.562
011-TOE	24	38	36.391
011-TOE	38	44	37.414
011-TOE	44	50	32.772
011-TOE	50	67	25.854
011-TOE	67	74	40.994
011-TOE	74	80	69.883
011-TOE	80	90	63.606

Sample ID	Upper Depth (cm)	Lower Depth (cm)	Raw C ($kg \cdot m^{-3}$)
011-TOE	90	100	20.067
012-TOE	0	1	
012-TOE	1	7	35.367
012-TOE	7	27	19.762
012-TOE	27	53	17.667
012-TOE	53	69	41.889
012-TOE	69	104	52.479
012-TOE	104	120	29.289
012-TOE	120	156	43.126
013-FOOT	0	7	36.612
013-FOOT	7	36	16.24
013-FOOT	36	50	8.199
013-FOOT	50	60	6.086
013-FOOT	60	70	5.208
013-FOOT	70	79	6.007
013-FOOT	79	104	3.266
014-TOE	0	2	
014-TOE	2	49	22.245
014-TOE	49	53	16.848
014-TOE	53	63	20.616
014-TOE	63	75	29.557
014-TOE	75	88	23.495
014-TOE	88	103	16.095
014-TOE	103	110	18.506
015-TOE	0	1	
015-TOE	1	7	35.4
015-TOE	7	43	16.004
015-TOE	43	77	31.357
015-TOE	77	92	13.791
015-TOE	92	110	10.672
016-FOOT	0	33	25.625
016-FOOT	33	47	30.839
016-FOOT	47	55	22.056
016-FOOT	55	70	12.254
016-FOOT	70	90	8.84
017-TOE	0	2	
017-TOE	2	11	32.234
017-TOE	11	33	22.574
017-TOE	33	41	25.042
017-TOE	41	70	28.648
017-TOE	70	80	
017-TOE	80	90	
017-TOE	90	105	17.55
018-DEP	0	4	102.581
018-DEP	4	8	72.231
018-DEP	8	28	19.927
018-DEP	28	40	25.737
018-DEP	40	56	31.918
018-DEP	56	68	106.541
018-DEP	68	78	104.515
018-DEP	78	82	
018-DEP	82	93	81.515
019-FOOT	0	8	31.632
019-FOOT	8	25	17.535
019-FOOT	25	35	21.48
019-FOOT	35	48	31.626
019-FOOT	48	70	27.055
019-FOOT	70	90	17.982
019-FOOT	90	100	12.104
019-FOOT	100	128	
019-FOOT	128	154	12.177
020-TOE	0	1	69.68
020-TOE	1	10	44.497
020-TOE	10	25	38.304
020-TOE	25	42	24.258
021-TOE	0	22	29.413

Sample ID	Upper Depth (cm)	Lower Depth (cm)	Raw C ($kg \cdot m^{-3}$)
021-TOE	22	36	33.584
021-TOE	36	47	9.935
021-TOE	47	58	7.346
021-TOE	58	70	7.834
021-TOE	70	84	8.127
022-FOOT	0	9	39.658
022-FOOT	9	34	31.519
022-FOOT	34	53	26.672
022-FOOT	53	65	22.131
022-FOOT	65	73	14.448
023-FOOT	0	1	
023-FOOT	1	8	35.121
023-FOOT	8	17	15.682
023-FOOT	17	27	14.735
023-FOOT	27	40	15.659
023-FOOT	40	53	19.864
023-FOOT	53	77	33.907
023-FOOT	77	86	29.781
023-FOOT	87	100	25.099
023-FOOT	100	122	22.269
023-FOOT	122	147	9.916
023-FOOT	147	158	12.055
025-FOOT	0	10	41.638
025-FOOT	10	20	21.097
025-FOOT	20	35	19.59
025-FOOT	35	50	20.754
025-FOOT	50	61	18.307
026-BACK	0	8	38.546
026-BACK	8	24	12.502
026-BACK	24	36	7.606
026-BACK	36	48	5.334
026-BACK	48	56	5.453
027-SUM	0	10	29.345
027-SUM	10	27	18.189
027-SUM	27	44	9.742
027-SUM	44	52	8.708
027-SUM	52	73	
027-SUM	73	85	7.555
028-DEP	0	10	19.578
028-DEP	10	14	65.393
028-DEP	14	30	27.711
028-DEP	30	50	38.582
028-DEP	50	58	78.346
028-DEP	58	70	67.585
028-DEP	70	85	50.874
029-SUM	0	30	24.966
029-SUM	30	47	8.02
029-SUM	47	70	5.234
029-SUM	70	82	4.215
029-SUM	82	100	4.28
031-BD1	0	5	41.123
031-BD1	5	10	30.465
031-BD1	10	15	19.382
031-BD1	15	20	18.807
031-BD1	20	25	19.229
031-BD1	25	35	18.452
031-BD1	35	45	19.116
031-BD1	45	60	26.427
031-BD1	60	75	44.676
031-BD1	75	90	36.862
031-BD1	90	105	32.205
031-BD1	105	120	30.417
A1	0	10	68.473
A1	10	25	22.501
A1	25	40	36.027
A1	45	70	72.249

Sample ID	Upper Depth (cm)	Lower Depth (cm)	Raw C ($kg \cdot m^{-3}$)
A1	70	95	24.807
B2	0	10	105.003
B2	10	20	78.994
B2	20	35	27.254
B2	35	50	60.596
B2	50	65	87.728
B2	65	75	51.804
B2	75	90	34.445
B2	90	105	39.125
C3	0	5	60.995
C3	5	10	52.265
C3	10	15	62.484
C3	15	20	61.902
C3	20	25	67.049
C3	25	30	71.841
C3	30	40	52.525
C3	40	48	105.179
C3	48	58	84.613
C3	58	68	95.847
C3	68	78	93.954
C3	78	87	97.806
C3	87	97	
C3	97	107	98.693
C3	107	127	54.908
D4	0	11	47.44
D4	11	22	63.604
D4	22	37	54.142
D4	37	52	67.868
D4	52	67	93.688
D4	67	87	105.595
D4	87	100	117.837
E5	0	10	56.763
E5	10	25	45.261
E5	25	30	38.048
E5	30	40	39.213
E5	40	52	35.346
F6	0	10	80.465
F6	10	20	79.585
F6	20	30	69.513
F6	30	40	42.147
F6	40	60	27.647
F6	60	70	13.241
F6	70	88	8.403
G7	0	10	63.974
G7	10	22	40.071
G7	22	30	34.544
G7	30	45	54.197
I9	0	15	42.654
I9	15	22	34.114
J10	0	8	49.645
J10	8	22	33.914
L13	0	8	32.67
L13	8	22	24.886
L13	22	30	21.278
L13	30	35	17.772